RETROSPECTIVE ANALYSIS OF MINE SEISMICITY:
GLENCORE, KIDD MINE

by

Sandra V. L. Smith

Thesis submitted in partial fulfillment of the
requirements for the degree of Master of Applied Science (MASc)
in Natural Resources Engineering

Faculty of Graduate Studies
Laurentian University
Sudbury, Ontario

© Sandra V.L. Smith, 2017

THESIS DEFENCE COMMITTEE/COMITÉ DE SOUTENANCE DE THÈSE
Laurentian Université/Université Laurentienne
Faculty of Graduate Studies/Faculté des études supérieures

Title of Thesis Titre de la thèse	RETROSPECTIVE ANALYSIS OF MINE SEISMICITY GLENCORE, KIDD MINE		
Name of Candidate Nom du candidat	Smith, Sandra		
Degree Diplôme	Master of Science		
Department/Program Département/Programme	Natural Resources Engineering	Date of Defence Date de la soutenance	June 26, 2017

APPROVED/APPROUVÉ

Thesis Examiners/Examinateurs de thèse:

Dr. Marty Hudyma
(Supervisor/Directeur(trice) de thèse)

Dr. Shailendra Sharan
(Committee member/Membre du comité)

Dr Eugene Ben-Awuh
(Committee member/Membre du comité)

Dr. Brad Simser
(External Examiner/Examinateur externe)

Approved for the Faculty of Graduate Studies
Approuvé pour la Faculté des études supérieures
Dr. David Lesbarrères
Monsieur David Lesbarrères
Dean, Faculty of Graduate Studies
Doyen, Faculté des études supérieures

ACCESSIBILITY CLAUSE AND PERMISSION TO USE

I, **Sandra Smith**, hereby grant to Laurentian University and/or its agents the non-exclusive license to archive and make accessible my thesis, dissertation, or project report in whole or in part in all forms of media, now or for the duration of my copyright ownership. I retain all other ownership rights to the copyright of the thesis, dissertation or project report. I also reserve the right to use in future works (such as articles or books) all or part of this thesis, dissertation, or project report. I further agree that permission for copying of this thesis in any manner, in whole or in part, for scholarly purposes may be granted by the professor or professors who supervised my thesis work or, in their absence, by the Head of the Department in which my thesis work was done. It is understood that any copying or publication or use of this thesis or parts thereof for financial gain shall not be allowed without my written permission. It is also understood that this copy is being made available in this form by the authority of the copyright owner solely for the purpose of private study and research and may not be copied or reproduced except as permitted by the copyright laws without written authority from the copyright owner.

ABSTRACT

Understanding the rock mass response to underground mining is a significant benefit to assist with decisions aimed at maintaining safe access and controlling conditions in which incidents of rock mass failure may occur during excavation development. As Canadian mines get deeper, high stress conditions become more prevalent, often leading to dynamic rock mass failure. This failure results in recordable dynamic stress waves, also called mining induced seismic events. The occurrence of large seismic events has become commonplace in many Ontario hardrock mines.

This thesis investigates the mining-induced seismic events recorded in the deepest levels of Glencore's Kidd Mine, near Timmins, Ontario. The research focuses on mining-induced seismic events in Mine D, which is between 2000 and 3000 metres below surface. Spatial and temporal trends of large seismic events are investigated. Particular emphasis is placed on analysis of the variations in radiated seismic energy associated with large magnitude events.

Through analysis of seismic source parameters such as radiated seismic energy, a better understanding of dynamic rock mass failure in a mine is achieved. This improved understanding aids in managing the risks associated with deep mining in high stress conditions.

KEYWORDS

Seismicity, Deep underground mines, Deep hardrock mines, Ontario hardrock mines, Mining-induced seismicity, rock mass response to mining, seismic response to mining, mXrap analysis in deep hardrock mines, energy variations, apparent stress, spatial and temporal analysis.

ACKNOWLEDGEMENTS

The author wishes to thank the staff at Glencore's Kidd Mine for providing the data and time in support of my research. In particular, I wish to thank Mr. Greg Cooper, Mr. Norm Disley and Mr. Dave Counter, for their efforts in helping me understand the complexities of the Kidd Mine geology, mining, rock mechanics and seismic data.

I would also like to extend acknowledgement and thanks to my advisor, Dr. Marty Hudyma, for his steady guidance and encouragement during the evolution of this thesis.

The encouragement of family, friends and coworkers has been greatly appreciated and none more so than my daughter, Alison. Her kindness, patience and her ability to keep me anchored have been invaluable.

TABLE OF CONTENTS

LIST OF TABLES

LIST OF FIGURES

LIST OF SYMBOLS AND ABBREVIATIONS

σ_v , σ_z = vertical stress, compressive stress, taken as positive

σ_h = minor horizontal stress

σ_1 = major principal stress

σ_2 = intermediate principal stress

σ_3 = minor principal stress

σ_x = horizontal stress in x-direction

σ_y = horizontal stress in y-direction

σ_n = stress normal to e.g., fault plane

σ_{sc} = stress threshold

σ_{hper} = horizontal stress, perpendicular to the strike of the ore body

σ_{hpar} = horizontal stress, parallel to the strike of the ore body

ϵ = strain

τ = shear stress

ρ = rock density, kg/m^3 or t/m^3

γ = unit weight, N/m^3

z = depth below ground surface, m

$k = \sigma_h / \sigma_v$

ν = Poisson's ratio

E = Young´s modulus; or

E = Seismic Energy, radiated from the source (joules)

c = P- or S-wave velocity in the rock (m/s)

R = distance from the seismic source (m)

Jc = integral of the square velocity

Fc = the radiation pattern coefficient for either P- or S-wave

G = shear modulus (rigidity)

V = volume

F = force, N

μ = coefficient of friction

A = area

D = average shear displacement

d = distance

m = metres

Δ = focal depth

M_L = local magnitude

M_0 = seismic moment magnitude

M_N = Nuttli magnitude

ES, EP = seismic energy in S-, and P-wave respectively

N = number of events

a = constant

b = relation between small and large events in a certain time interval

ERR = Energy Release Rate

DI = damage initiation

Q = rock mass quality index

1.0 INTRODUCTION

Understanding rock mass damage and behaviour in underground mining is a significant benefit to assist with decisions aimed at maintaining safe access and controlling conditions in which incidents of rock mass failure may occur during excavation development. As mine development is increasingly deeper, localized rock mass response is more susceptible to the mining induced stress changes. Identifying rock mass behaviour resulting in high magnitude seismic events and possible interactions and trends can provide a basis for understanding the overall rock mass response as mining progresses; and to apply appropriate engineering design to increase safety in the development environment. In-situ rock mass strength, existing structure in the rock, depth, confinement, geometry of excavations and previous fracturing from adjacent development are contributing factors to the rock mass response.

High magnitude seismic events in abutments and related rock mass behaviour indicative of seismic trends are considered for review. Seismic system data from Glencore's Kidd Mine in Timmins, Northern Ontario, has provided the base case for this research. A site visit to the Kidd Mine's deeper development levels in areas affected by seismic events was conducted to provide visual context of the data study. The results of the seismic energy response, seismic event grouping and spatial and temporal relevance are discussed. A general discussion of seismicity review conducted at the Creighton Mine in Sudbury is included for comparison with a mine of similar depth and maturity.

Diederichs (2003) describes classifications for underground instability: structurally controlled, gravity driven fallout and stress controlled rock mass yield. Several research papers have identified the effect of stress, strain, confinement and of underlying mechanisms on rock mass yielding in hard, brittle rock. This thesis explores theory, research and results related to rock mass yielding, contributing factors and empirical observations.

1.1 Seismicity in Underground Mines

In a pre-mining state, a rock mass is at a stable stress state, subjected only to weathering and tectonic pressures. Underground mine development activities promote local changes in the stress state as rock is excavated, and at increasing depths, the stresses increase due to gravity loading. The quality of the rock mass, the presence of geological features, increasing depth and mining activity introduce localized failure and related seismic activity. The levels of energy radiated from seismic events are recorded during mining activity; and a focused spatial and temporal review can assist with identifying changing conditions and the relation of events with the corresponding rock mass response.

1.2 Stress Redistribution and Strain Softening

Figure represents the five regions of strain softening when a moderately jointed rock mass responds to stress loading and unloading (Cotesta *et al.,* 2014), represented as a relation of stress to strain. The yielding response occurs between the yield point and the peak. This can also be stated as the point at which the rock deformation is inelastic, will no longer return to its original state when the stress is removed; and the threshold beyond which yielding behaviour becomes brittle behaviour.

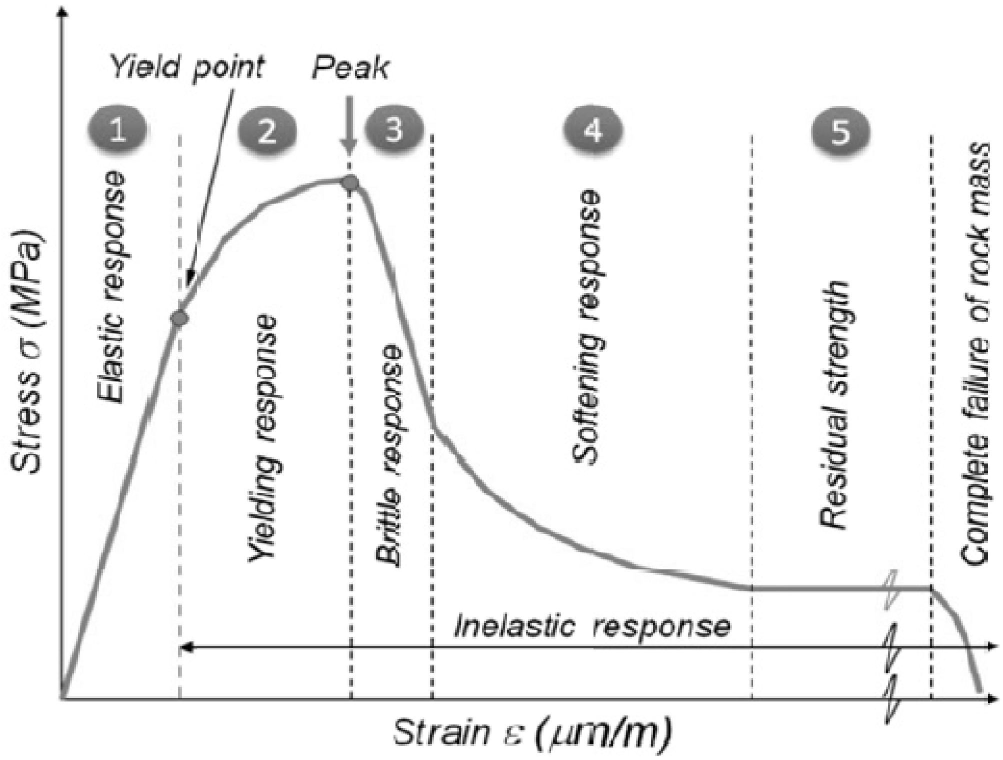

Figure 1: Five regions of strain softening response of a moderately jointed rock mass (Cotesta et al., 2014; after Andrieux et al., 2008).

Each seismic event provides insight into the relative level of stress in the rock mass and the amount of rock mass deformation associated with the event. Brown and Hudyma (2017) noted that increases in the seismic source parameter, apparent stress, are related to stress conditions in the rock mass. Seismic moment is proportional to rock mass deformation (Gibowicz and Lasocki, 2001).

The five regions of strain softening response may be identified using seismic data and the magnitude of events with corresponding apparent stress and rock mass behaviour described as follows:

- Region 1_ Small events, low apparent stress, elastic rock mass response;
- Region 2_ Large Events, high apparent stress, brittle response, possible rockbursting;
- Region 3_ Large events, high moment, lower apparent stress, rock mass softening;
- Region 4_ Smaller events, lower moment, low apparent stress, only residual strength remaining; and
- Region 5_ Few, very small events, rock mass failure.

1.3 Rock Mass Response

Correlations may be identified between the strain softening response of a rock mass and the relative seismic energy occurrence within each region of strain softening. Mining induced seismicity introduces changing conditions and trends in seismicity such as magnitude, spatial and temporal distributions and energy variations should correspond with the rock mass response.

In deep hard rock mines, the sudden release of stored energy in the rock will be seen as seismic waves. In locations of active mining and where the seismic event is of a high magnitude, the released energy may cause damage to openings. Geological structure, rock mass strength as well as excavation geometries will have an effect on the rock mass response and the severity of damage.

1.3.1 Strain

Stress re-distribution around mined excavations results in localized damage at the location of the energy release, such as strain related rockbursting in a stope or at a working face. Local stress re-distribution may affect pillars and the severity will differ depending on the state of the host rock, location, geometry, confinement and associated openings. If a pillar fails, the loss of support will cause a secondary re-distribution of stresses and may affect nearby pillars.

1.3.2 Structure

Mining activity may induce displacement or reduce confinement near existing faults, resulting in energy release. Failure through intact rock can also occur where stresses exceed the strength of the rock. Either case may cause a significant rock mass response from ejection of blocks to complete rock mass failure.

1.4 Seismic Monitoring and Data

As mining occurs at increasing depths and typical blasting procedures applied during development induce rock mass fracturing, along with increased stresses at depth in hard rock; the dynamic rock mass response to mining invariably includes more frequent, larger and potentially damaging seismic events.

Past knowledge of the rock mass behaviour and technological improvements are essential to planning future mining phases. Improvements in data modelling and monitoring capabilities as well as dynamic ground support, ventilation, environmental controls, automated production equipment and sophisticated communications are integrated into a system which enhances the technical staff's capabilities for development planning.

The mine seismic system is an important tool to understand and characterize the source, the magnitude and the probable mechanism of recorded seismic events. Understanding the events is a key requirement to proactively assessing hazards and damage potential.

Changes in the stress state can be used to identify potential, rock mass instability and trends over time can provide insight into the location, size and strength of seismic related hazards. Monitoring and reviewing energy radiated from seismic events in discrete locations can assist with identifying changing conditions and the rock mass response. An understanding of the past response to mining can be incorporated into future mine planning of extraction sequences, locations and volumes of stopes with the intention to reduce rehabilitation of ground support, uninterrupted mining and safe access.

1.5 Scope

The scope of the research presented includes the review of seismic records, in the database provided by Glencore's Kidd Mine operations located in Timmins, Ontario. The review includes a general mine history background and an understanding of the current mining depth, the current seismic system installed and the geological setting with location of known structures. The seismic data review will be undertaken using the mXrap seismic software (Harris and Wesseloo, 2015) to identify apparent stress and energy variation parameters that indicate hazard areas or pre-cursory behaviour leading to high magnitude and potentially damaging seismic events. The review will delineate areas interest with high magnitude events and will outline the behaviour and mechanism associated with the seismic events. This research uses the data provided and does not include calibration, stress modelling or any additional 3D modelling of the Kidd Mine data.

1.6 Problem Statement

Seismic events may be the result of mining activity such as stope and development blasting, or as a result of joint slip or rock fracturing resulting in energy released, often directly related to mining. Increased stresses, as mining progresses to greater depths, are a significant contributing factor to the occurrence of seismicity and the resulting damage. Mine seismic monitoring systems were developed to monitor seismicity and to provide tools to manage related rockburst hazards. Mine seismic systems record the acoustic energy ground motions and the results assist with characterizing the seismic events to determine the source, magnitude and the probable mechanism involved.

Recording and evaluating seismic source parameters using a variety of established methods provides practical methods to assess hazards and potential for damage as well as identifying higher risk areas where rockburst potential exists; and adds factual considerations to support design decisions for future underground development.

Glencore's Kidd Mine is currently operating at depths of 2 to 3 km and experiencing damaging seismic events. The seismic array of uniaxial and triaxial recorders has been updated as mining progresses and data capture is reliable with a state of the art instrumentation on a fibre optic system. A robust dynamic resistant ground support system was adopted for the deeper levels of the mine to combat increasingly difficult ground conditions.

The number of events recorded is significantly less compared to similar operations at similar depths (e.g. Vale's Creighton Mine, Agnico Eagle's LaRonde Mine) and trends are not relatable between operations. In spite of the significant effort to mitigate risk and damage, seismic events in high stress abutments and pillars continue to present challenges and require frequent rehabilitation.

A retrospective analysis of seismicity beginning at the early stages of Kidd Mine D development is an opportunity to gain an understanding of the mechanisms, spatial and temporal trends, instability and potential interactions of high magnitude seismic events. The results of the analysis may be an additional tool to pro-actively identify regions of increased seismic related hazard.

1.7 Research Approach

The approach to the analysis and development of this thesis is the evaluation of seismic data in order to determine spatial and temporal trends, precursory behaviour and potential interactions which may result in high magnitude or high damaging events. The data set under review is the operational data, provided by the engineering department of Kidd Mine, for the deeper levels from approximately 2000 m to 3000 m depth. A preliminary review of the entire data set will be conducted and a more focused review of recent years of mining as well as regions that may be identified with increased occurrence of high magnitude events.

1.8 Thesis Structure

Context and Objective

Chapter 1 outlines the context and objective of the Kidd Mine seismic data analysis.

Literature Review

Chapter 2 contains a literature review with background information related to seismicity in the context of underground mining, research on rock mass response to mining, rock strength and the effects of stress and strain as well as rock mass behaviour in the context of underground hard rock mining.

Background, Glencore's Kidd Mine

Chapter 3 presents a summary of Glencore's Kidd Mine development, geological setting, seismic system and an overview of the history of seismicity and geotechnical challenges of mining at increasing depths.

Methodology and Analysis

Chapter 4 describes the seismic data provided for Glencore's Kidd Mine D, the analysis approach using industry standard techniques to determine spatial, temporal and energy trends in underground mine seismicity. Individual seismic parameters and mechanism are described in context of the Kidd Mine D data, using mXrap software (Harris and Wesseloo, 2015). An analysis is conducted of areas with increased event rates or with increased occurrences of high magnitude events and potential trends and interactions based on the data, with a discussion of the effectiveness of the review to assist with determining future trends.

Conclusion

Chapter 5 includes a summary of the results of the analysis, key conclusions and recommendations for additional work. The author's contributions include the development of an analysis approach, the potential interaction of spatially distinct areas and the use of such an analysis for hazard assessment of future development. The recommendations suggest additional complementary research to further assess the applicability of a robust retrospective analysis and a prescriptive methodology.

2.0 LITERATURE REVIEW

The following sections describe an overview of past studies conducted by multiple researchers that have explored rock mass strength, contributing stresses, relative strain, yielding, effect of confinement, damage initiation, damage limits and the applicability in hard rock underground excavation and pillar design and applied terminology.

2.1 Terminology

The following terms are discussed throughout this paper; they are generally applied in engineering and materials sciences and presented here in the context of hard rock underground mining:

- **Breakout**: The formation of damage in a borehole or excavation which typically forms in a V-shaped notch perpendicular to the direction of the major principal stress.

- **Damage**: The strength reduction thresholds for rock mass damage are usually derived from upper and lower limits of damage initiation on laboratory test samples.

- **Deviatoric Stress**: The stress difference between the major principal stress, σ_1, and the minor principal stress, σ_3.

- **Elastic Modulus**: Two primary elastic moduli typically used in rock mass strength calculations:
  - **Young's Modulus (E):** also referred to as the elastic modulus, is the ratio of normal stress to strain and is given as $E = \sigma_1 / \epsilon$.

    Where:

    σ_1 is the major principal stress;

ϵ is the strain associated with sample loading

- **Shear Modulus:** is the tendency for a material to fail in shear under opposing applied forces and is expressed as a ratio of stress over strain, given as $\mu = (F / A) / (\Delta x / y)$.

  Where:

  F / A is the force over the cross sectional area; and

  $\Delta x / y$ is the horizontal displacement over the vertical height.

- **Empirical method**: A design approach which applies past knowledge, often for a large number of cases collected through experience or experiment, to design applications that have a similar context and design basis.

- **Failure**: The point at which the rock mass is permanently deformed and can no longer support increasing applied loads. Failure implies a significant loss of rock mass integrity in underground excavations where pillars and tunnels require some degree of rehabilitation to remain safe and serviceable.

- **Moment Magnitude/Seismic Moment**: A physical quantity, related to total energy released, to measure fault slip over a specified area of the fault surface. The Seismic Moment is typically used to determine size of a slip related event, expressed in Nm as: $M_0 = \mu A D$.

  Where:

  μ is the rigidity of the rock mass;

  A is the area of slip across the fault; and

  D is the average slip displacement

- **Poisson's Ratio**: The ratio of expansion to compression deformation, normal to the axis of the extension or compression when a material undergoes axial strain.

- **Rockburst**: The sudden, dynamic ejection of rock at boundary excavations under seismic strain, often causing damage. Rockburst potential increases with depth in good quality, brittle rock.

- **Strength**: As applied to the rock mass surrounding underground excavations; the strength is the ability to resist applied loads.

- **Seismic Event:** A sudden deformation within a volume of rock which generates detectable seismic waves.

- **Seismic Energy:** The energy released at the source of a seismic event; and measure as S-Waves and P-Waves, expressed as:

  $$E = 4\pi \rho c R^2 \frac{Jc}{Fc^2}$$ (Gibowicz and Lasocki, 2001).

  Where:

  E = radiated energy from the source (joules)

  ρ = density of the rock mass at the source (kg/m^3)

  c = P- or S-wave velocity in the rock (m/s)

  R = the distance from the seismic source (m)

  Jc = the integral of the square velocity

  Fc = the radiation pattern coefficient for either P- or S-wave

- **Seismic Parameters:** Used to quantify seismic events in terms of time, location, energy variation and seismic moment.

- **Seismic Waves:**

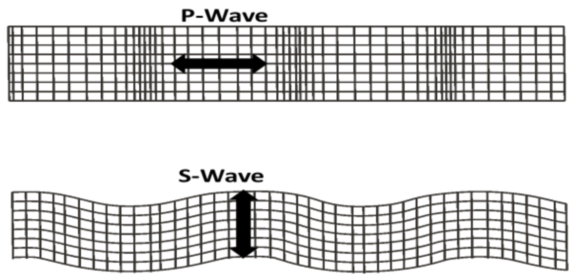

P-Wave, S-Wave, After Hudyma (2010)

P-Wave: A P wave, or compressional wave, is energy generated in a seismic body in a back and forth motion parallel to the direction of the P-Wave.

S-Wave: An S wave, or shear wave, is generated in a seismic body with energy applied perpendicular to, and along the length of the wave.

- **Strain**: Normalized deformation of a rock mass under applied stress. Three broad types of strain are elastic (recoverable change), ductile (permanent plastic change) and brittle (rupture).

- **Stress**: Load per unit area applied to the rock mass.

- **Theoretical / Analytical method**: Application of mathematical concepts with defined input parameters based on formulation that has been derived from, and proven in, practical applications.

- **Uniaxial Compressive Strength (UCS)**: A value of rock mass strength derived from laboratory testing of intact rock samples; measured in terms of the rock's ability to resist the load, applied to the long axis of the sample; units are in MPa.

- **Yield**: The yield strength of a material is measured at the point at which the stress applied to the material begins to deform plastically. Yielding is initiated due to damage to the rock mass fabric and results in a sudden change in the load bearing capacity of the rock; it does not necessarily result in failure and may continue to provide support.

- **Yield Point**: The upper limit of applied load where; before reaching the yield point the deformation is elastic and the material will return to its original state as the applied stress is removed; and beyond the yield point, the deformation is permanent (plastic) and non-reversible.

2.2 Rock Mass Yielding and Damage Limits

Understanding rock mass damage and behaviour in underground mining is a significant tool to assist with decisions aimed at maintaining safe access and controlling conditions in which incidents of rock mass failure may occur during excavation development. Identifying rock mass behaviour resulting in yielding ground and controlling the degree of yielding while still providing some level of support to the excavations can provide a basis for understanding the overall rock mass response as mining progresses. Identification of trends can provide supporting information for engineering decisions to increase safety in the development environment. In-situ rock mass strength, existing structure in the rock, depth of mining, confinement and geometry of excavations and previous fracturing from adjacent development are contributing factors to the rock mass response during mine development.

Diederichs (2003) describes two classifications for underground instability: structurally controlled, gravity driven fallout; and stress controlled rock mass yielding. Several researchers have contributed significant efforts to assist with understanding the effect of stress, strain, confinement and of underlying mechanisms on rock mass yielding in hard, brittle rock. This section explores founding theories, research and results related to rock mass yielding, damage limits, contributing factors, empirical observations and applicability to deep mining.

2.2.1 Theory and Research

The following sections describe an overview of past studies conducted by multiple researchers (e.g. Brace *et al.*,(1966), Castro *et al.*,(1995, 1997), Cotesta *et al.*,(2014), Diederichs (2003); (2007), Diedrichs *et al.*,(2004), Falmagne (2001), Hoek and Brown (1980), Kaiser *et al.*,(2000), Lunder *et al.*,(1994), Martin (1997), Martin and Maybee (2000) and others) that have explored rock mass strength in relation to contributing stresses, relative strain, yielding, effect of confinement, damage initiation, damage limits and the applicability in hard rock underground excavation and pillar design.

2.2.2 Stress and Strain

Strain discontinuities resulting in extension crack initiation are recognized as part of the primary damage process, controlled by internal tensile strength (Diederichs, 2007). The fracturing, even under compression, leads to visible extension fractures and subsequent spalling. Unsupported excavations under high anisotropic stresses can form V-shaped notch geometries as spalling occurs. The surrounding ground, once the stresses have been reduced or relieved, is often stable and may retain load bearing capacity. Variations of rock mass strength, cohesion and internal angle of friction will contribute to variations on rock mass response. A subsequent change in geometry or reduction in tangential stress around openings can release pre-fractured rock resulting in ground falls that are independent of seismicity in underground mines.

In conditions where the strain on excavations may be static, cracks that were initially subcritical may experience time dependent growth enhanced by environmental changes including humidity and temperature variations; promoting ongoing crack propagation resulting in rock mass fatigue, leading to spalling, ground falls and excavation or pillar damage (Diederichs, 2007). The graph in Figure 2 depicts the general non-linear relation of stress, strain, elastic and plastic deformation. Where the stress path bounds the excavation in low confinement areas, the extent of fracturing becomes sensitive to the amount of confinement. The directional trend of cracking is parallel to the major principal stress, σ1.

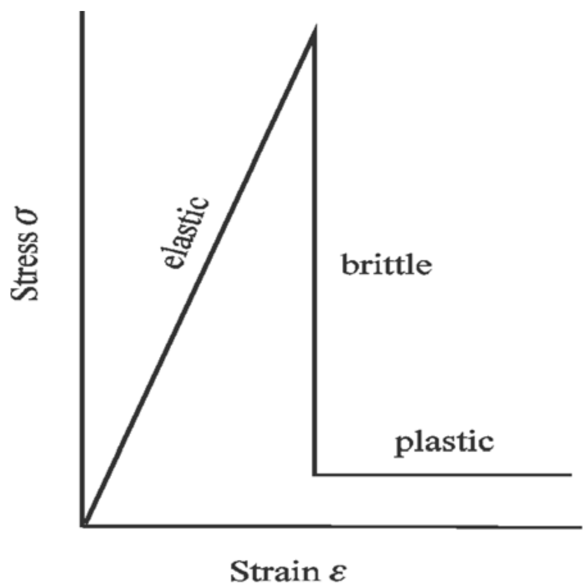

Figure 2: General relation of stress, strain and rock mass damage response (Hoek, 2000).

The major to minor principal boundary stress ratio, σ1/σ3, is often an indicator of the extent of fracturing. As σ3 approaches zero with reduced confinement; the crack length increases in the direction of the major principal stress, σ1. When the boundary stress ratio exceeds 10, σ1 is 10 times greater than σ3, the rock mass exhibits instability, and failure and spalling along weakness planes are more likely to occur.

Diederichs (2003) summarizes that crack initiation is dependent on deviatoric stress, is not sensitive to degree of confinement; and yield will result when a critical crack density and interaction is reached. Longer crack extensions serve to decrease the density of cracks needed for the onset of yield which occurs at a lower strength threshold.

Factors which affect the onset of rock mass yielding are primarily controlled by the intact rock in situ, as well as scale, pre-existing fractures, damage induced during excavation, crack-surface interaction and local tension. Such mechanisms can reduce in situ yield strength to a lower crack initiation threshold. Greater confining pressures in rock a short distance from the excavation opening will reduce the tendency to damage because fractures are primarily discontinuous and there is no kinematic displacement to promote block formation.

Castro *et al.,* (1997) summarized that some conditions in laboratory uniaxial and triaxial tests did not have an effect on the mode of damage initiation such as end-boundary conditions, stress path and rate of applied load. In high confinement regions, fracturing may form ahead of the stope face during development but experience shear displacement rather than yielding. Time dependent fracturing occurs at post peak deformation and is controlled by the state of the overall rock mass system. Castro *et al.,* (1997) also stated that the laboratory testing may not reliably estimate peak strength due to different loading conditions that cannot easily be reproduced.

2.2.3 In Situ Strength

The strength of the rock mass surrounding an excavation is related to several possible factors including pre-existing damage, low confinement, surface interaction, stress rotation and possible loss of effective confinement due to slabbing. Low confinement is a key condition which may enhance crack propagation. The composite strength envelope, proposed as a tool to complement support design and assist with identifying rock mass damage threshold, spalling limit and shear failure, is illustrated in the graph in Figure 3 - the transitional curve for in situ rock strength is plotted indicating the lower and upper bound strength limits (Diederichs and Kaiser, 2004).

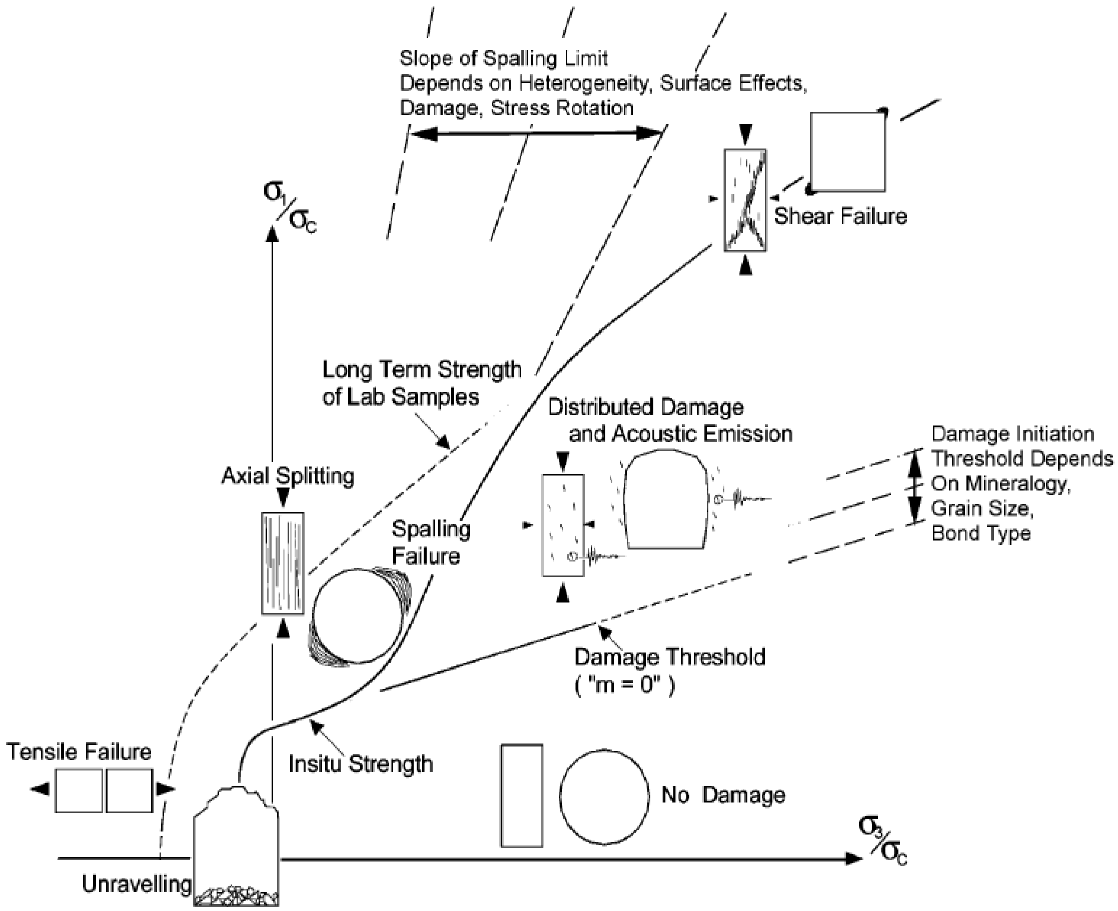

Figure 3: The composite in situ strength envelope for hard rock (solid curve) composed of segments corresponding to upper bound strength (high confinement), lower bound strength or damage initiation (low confinement) and the transition zone related to the spalling (Diederichs *et al.*, 2004).

Back analysis and case histories provide a basis to estimate strength where rock mass failure has occurred. Failure has been observed in the form of spalling or fracturing around tunnel openings and precipitated by the stress environment that causes the fracturing.

Martin (1997) discusses the stress relative to the uniaxial compressive strength of rock laboratory samples as a tool to identify tunnel stability; expressed as a ratio of the far-field maximum stress to the unconfined compressive strength of the rock; σ1/σc. The ratio can be used to indicate typical rock mass stability for different stresses, as observed in square tunnels in South Africa and modified from Hoek and Brown (1980):

- Stable, unsupported: σ1/σc ≤ 0.1
- Minor Spalling; light support required: σ1/σc = 0.2
- Severe Spalling; moderate support required: σ1/σc = 0.3
- Increased Spalling; heavy support required: σ1/σc = 0.4
- Stability may be difficult to achieve; extreme support required: σ1/σc = 0.5

The graph in Figure 4 (Martin and Maybee, 2000) illustrates the relation of the above list of stability ratios for square tunnels. These ratios do not reflect the maximum tangential stress at the tunnel boundary for different shaped (arched or circular) tunnels.

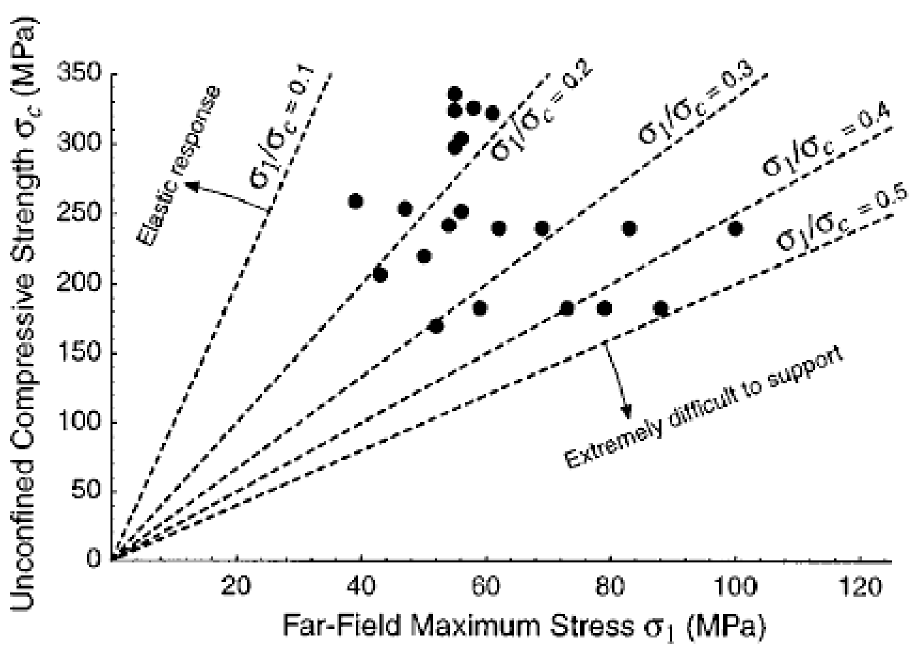

Figure 4: Empirical stability classification developed for square tunnels in South Africa, modified from Hoek and Brown (1980) after Martin *et al.* (1999).

Multiple factors affecting the rock mass in situ yield strength are discussed in the following sections.

2.2.4 Damage Threshold, Strength and Yield

Two distinct points of the rock mass damage threshold are considered the bounding region used to identify rock mass stability conditions:

- Damage Initiation is the Lower Bound Strength; and
- Onset of Crack Interaction is the Upper Bound Strength.

Yield is observed where the Hoek-Brown parameter for frictional strength, *m*, approaches zero as illustrated on the graph in Figure 5 (Diederichs, 1999; 2003).

Back analysis conducted during a study at the Creighton Mine (Diederichs, 1999; 2003) with damage zones determined by borehole cameras, indicated a lower bound limit for observed yield, where the Hoek-Brown (1980) criteria of $m = 0$ and $s = 0.25$. Figure 5 (Diederichs, 2003) illustrates the comparison of observations to the Hoek-Brown failure envelope.

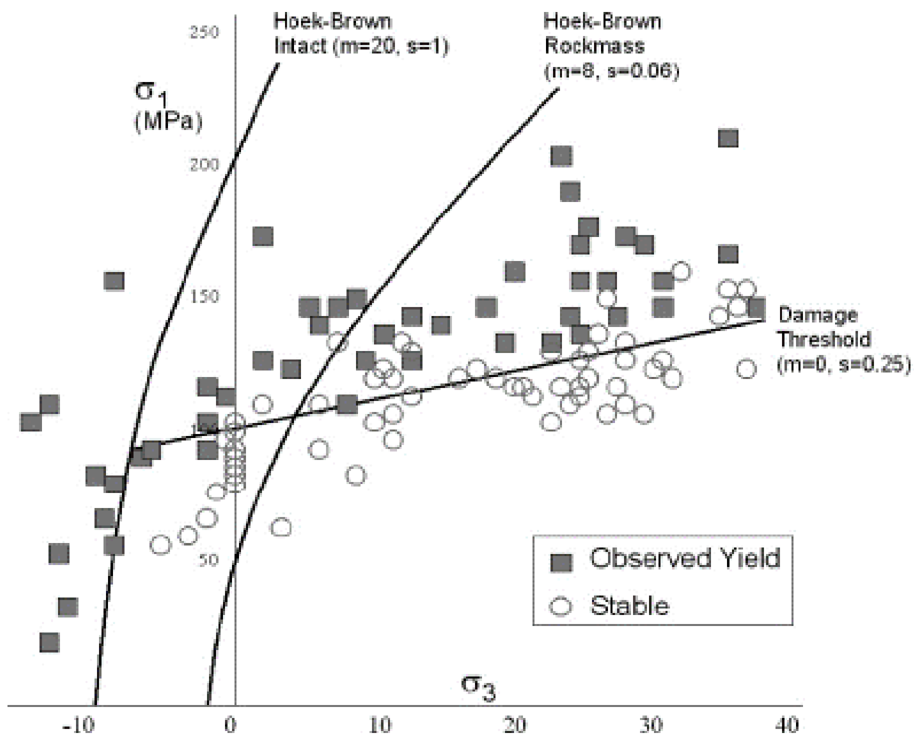

Figure 5: Comparison of yield observations with Hoek-Brown failure envelopes and with *m* = 0 damage threshold (Diederichs, 2003; after Diederichs, 1999).

Compressive damage and yield behaviour in hard rock are induced by strain acting normal to the direction of the principal stress, or maximum compression (Diederichs, 1999). The Lower Bound strength of a rock sample in a laboratory analysis is the point where damage initiation occurs. The Upper Bound strength is the point where crack propagation is measurably significant; after which the density leads to crack interaction and progressively leads to failure.

The in situ strength of the rock, the internal flaws and heterogeneity combined, correspond to a lower damage initiation threshold of the rock mass when under compressive loading.

Empirical observations of failure in massive, moderately jointed hard rock (Castro *et al.*, 1995) identified a failure initiation when the tangential stress at the excavation boundary is greater than 30% to 50% of the rock UCS strength measured from laboratory samples; with some sensitivity to confining stress. These values correlate well when compared to compressive strength values obtained from laboratory testing indicating that the damage initiation limit can be as low as one third in igneous rocks and up to one half for dense clastic sedimentary rock such as breccia and sandstone (Diederichs, 2007). A range of damage initiation stress thresholds and peak strength under time dependant loading was captured by Brace *et al.*,(1966) and described by Diederichs (2007), illustrated in Figure 6.

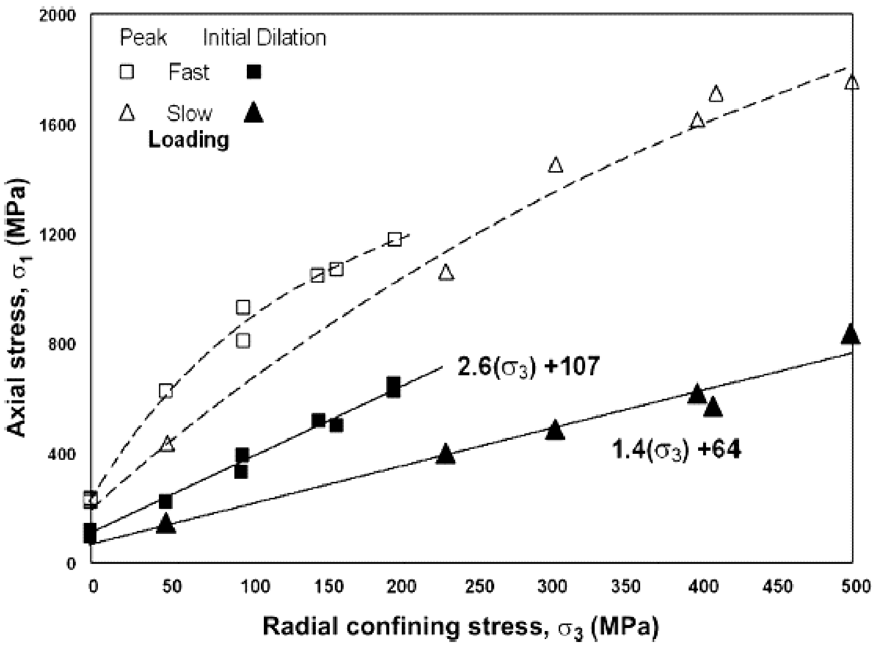

Figure 6: Test data showing the range of damage initiation thresholds in short and long term loading for Westerly Granite (after Diederichs, 2007).

Damage initiation is independent of existing fractures in the rock. Moderately jointed and massive rock has been studied and the findings concluded that extension fracturing around openings is related to low confining pressures combined with high stresses. The extension cracks will propagate in the direction of the maximum compressive stress (Castro *et al.*, 1997).

Castro (1996) and Castro *et al.*,(1997) presented a rock mass damage initiation (DI) criterion, expressed as $(\sigma 1 - \sigma 3) \cong \sigma_{sc.}$

Where:

- $\sigma 1$ and $\sigma 3$ are the local or induced major and minor principal stresses; and
- σ_{sc} is the stress threshold value at which stable crack growth commences for intact rock tested under uniaxial compression.

The stress threshold, σ_{sc}, was identified in the range of 25% to 40% of the strength of the host rock (σ_c). Castro (1996) applied the DI criterion to studies of rock mass behaviour in a deep mining environment, conducted at the Sudbury Neutrino Observatory (SNO Lab) in Sudbury, to assist with evaluating the effect of extension fracturing around mine excavations. Castro (1996; 1997) also conducted investigations, supported by observation of several Canadian hard rock mines, to support the view that the damage initiation within intact rock is primarily due to nucleation and propagation of extension fractures. Some of the observed characteristics of extension fractures (Castro, 1996) include:

- clean surfaces;
- no signs of shear displacement;
- nucleation is located in stress concentrators (i.e. pores, existing cracks and grain boundaries);
- formation at < 10° angle to the direction of the major principal induced stress; and
- highly sensitive to stress changes.

Breakouts occur in boreholes or excavations that are under high in situ stresses and are characterized by progressive failure of the opening by slabbing or spalling (Castro, 1996). Over time, the breakout process continues until it reaches a stable shape with V-shaped notches perpendicular to the direction of the major principal stresses and resulting in an overall elliptical geometry. The concentrations of stresses are highest at the tip of the V-shaped notch which encourages microcracks, mostly along grain boundaries in intact rock. As the microcracking progresses, a larger area is subjected to the cracking, which propagates radially, coalescing into fracturing, ultimately resulting in surface damage as thin slabs. Castro (1996) describes observations of breakouts at the Underground Research Lab (URL) in Lac du Bonnet, Manitoba, as well as deep tunnels in South Africa, originating as a band of stress in the roof or walls that formed a notch where stresses were concentrated and developed extension fractures, deepening the notch by localized buckling or shearing at the notch tip. Extension fractures developed in the walls from the notch tip in a direction sub-parallel to the walls. Slabbing resulted as the breakout progressed along the walls.

Castro *et al.,* (1997) state that extension cracks nucleate under compressive stress as the extensional strain exceeds a critical value. And, while damage initiation is a stress sensitive phenomenon, the subsequent crack growth and interaction is dependent on the strain or deformation of the openings. (Diederichs, 2007).

The stresses that induce crack damage are proportional to the local principal stress difference, or deviatoric stress, near the excavations. Castro *et al.,* (1997) also state that the major principal stress, σ_1, typically exceeds the minor principal stress, σ_3, by six to ten times in order to initiate extension cracks.

Castro *et al.,* (1997) conducted back analysis of field observations in South African tunnels and confirmed that, under the observed conditions, damage initiation starts when the principal stress, σ_1, is approximately 0.2 times the compressive strength of the host rock (σ_c) and that stable crack growth occurs when the maximum tangential stress surrounding excavations is 0.25 to 0.4 times σ_c.

Diederichs (2007) modelled the empirical relation between damage initiation and yield strength, monitored the crack accumulation during testing and the lateral strain response in a crystalline rock sample. The instantaneous ratio between incremental lateral and vertical strain was measured in the laboratory testing and provides an identification of the onset of systematic cracking, as illustrated in Figure 7.

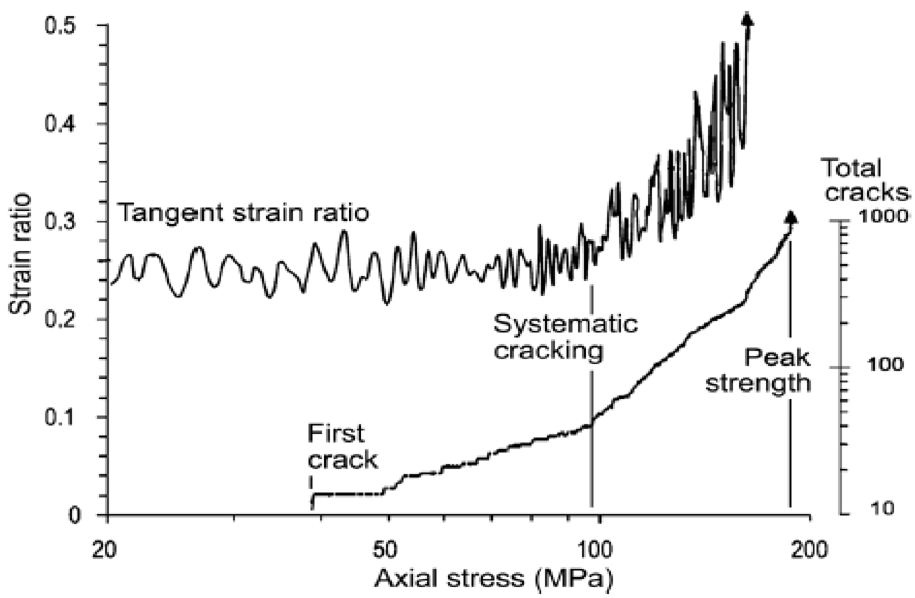

Figure 7: Relation between tangential stress ratio and crack initiation and accumulation in numerical simulations. The systematic crack initiation threshold can be distinguished from crack initiation (after Diederichs, 2007).

A second method of simulating the crack accumulation curve is with acoustical emission to detect the onset of damage. Early acoustic detection of in situ damage does not provide measurable strain; and other factors may introduce variability in identifying damage initiation. The stress threshold where significant strain is identified on the axial stress-strain plot defines the beginning of yield, or the yield point, in a rock mass.

The yield strength identified from laboratory samples coincides with the upper bound strength of the in situ rock, while the lower bound strength is considered the threshold of systematic damage, as opposed to the crack initiation threshold.

2.2.5 Rock Mass Damage

Damage accumulation and crack interaction contribute to rock mass yielding and subsequent failure. Castro *et al.*, (1997) states that the onset of damage is primarily controlled by the properties of the intact rock and laboratory tests on intact rock can provide information to assist with assessing the onset of damage.

A critical crack density, once attained and with further interaction, will result in subsequent damage. If the process continues to a point where sufficient crack density is reached, yielding and subsequent failure will occur. Any pre-existing crack damage in the rock mass contributes to a drop in yield strength (Martin, 1997).

Crack initiation is dependent on deviatoric stress and is not as sensitive to confinement. Yielding occurs when a critical crack density and interaction is reached. Longer crack extensions decrease the onset of yield which occurs at a lower strength threshold.

Studies and back analyses have been conducted that indicate the range of rock mass yielding typically occurs between 0.3 to 0.5 times the UCS of laboratory samples, which is closely related to the DI (Castro *et al.*, 1997): damage initiation starts when $\sigma 1$, is approximately 0.2 times the compressive strength of the host rock σc, and crack growth occurs at a maximum tangential stress of 0.25 to 0.4 times σc.

Falmagne (2001) conducted studies at the Underground research Centre (URL) in Manitoba which described rock mass degradation using seismic monitoring. The review outlined the use of a Cluster Index (CI) and a corresponding Degradation Index (DI). These indicators were developed using seismicity records with cumulative volume and energy variations. Falmagne (2001) observed that a sudden drop in DI indicates new events are occurring within a concentrated area with increased fracture interaction and coalescence leading to rock mass degradation and potential overbreak. A low DI indicates a change in rock mass properties, which, if the DI is below a certain threshold, will experience yielding but will not have sufficient interaction to propagate rock mass failure. Falmagne (2001) summarized that the seismic event clustering can delimit zones of rock mass yielding and the degradation may be used to quantify the degree of yielding.

2.2.6 Confinement

An increase in confinement around an excavation or pillar distributes the loads, reduces the effect of stresses and increases support capacity of the rock. Conversely, a loss of confinement in a fractured rock mass may induce relaxation and gravity driven failure where structure is present.

The early stage process is dependent on the initial intact rock mass conditions, and the ongoing damage, under compressive loading, reduces the tensile strength of the rock (Castro *et al.*, 1997).

Lunder *et al.* (1994) identified confinement as a key element to the strength of pillars and predicted failure; where geometry alone was the typical approach to pillar stability design in previous assessments. Pillar stability calculations using a width to height ratio as well as a confinement factor to determine rock strength relations for underground mine pillar design accounted for final pillar shapes. Increasing confinement, tested on laboratory specimens, is directly associated with increasing strength and the association is directly applicable to pillars and the rock mass resistance to applied stresses.

Poisson's ratio can be measured in laboratory testing and gives an indication of the instantaneous ratio between lateral and vertical strain; providing a means to monitor crack accumulation and strain response. Acoustic emissions may also identify the onset of damage initiation, which may not be apparent in strain measurements (Diederichs, 2007). Diederichs (2007) states that the systematic damage threshold is an appropriate indicator of in situ spall strength.

The relation of UCS*/UCS has been widely used as a guideline to predict failure in deep underground openings. Diederichs (2007) attempted to validate the use of the relation. A best fit trend of several empirical observations of failure radius correlated reasonably well to elastic modelling predictions with some variation and is expressed as σ_{max} / UCS*.

Where:

- σ_{max} is the maximum tangential boundary stress; and
- UCS* has been obtained by acoustic emission measurement, radial strain data or empirical methods.

Empirical observations identified that damage in various hard rock laboratory samples initiated at a UCS* (the lower bound rock mass strength) range from 0.2 to 0.5 times the standard UCS strength tests; and the boundary stress ratio > 10 indicates fracturing to the point of instability and likely spalling and failure in an excavation.

Stress rotation, which occurs as damage is being created, increases crack growth and density, decreasing the strength of the excavation. Crack length is directly related to yield and strength reduction, as the greater extension promotes earlier interaction fracturing.

Strength reduction mechanisms in excavations do not apply directly to laboratory samples due to the geometry. The laboratory sample is subject to internal confinement and is radially constrained, limiting the extension of fractures, therefore the laboratory sample fails by a sequence of non-extending micro cracks that reach a density where the cracks will interact (Diederichs, 2007). In an excavation, the cracks can propagate and extend in length, resulting in earlier interaction and ultimate spalling. Figure 8 illustrates a compilation of theory and experimental investigations highlighting the difference between laboratory samples and excavation boundaries, and delineates:

- In situ yield envelope (solid line, 2D);
- Transition from yield threshold at high confinement, to crack initiation threshold;
- Difference between laboratory testing and in situ wall conditions.

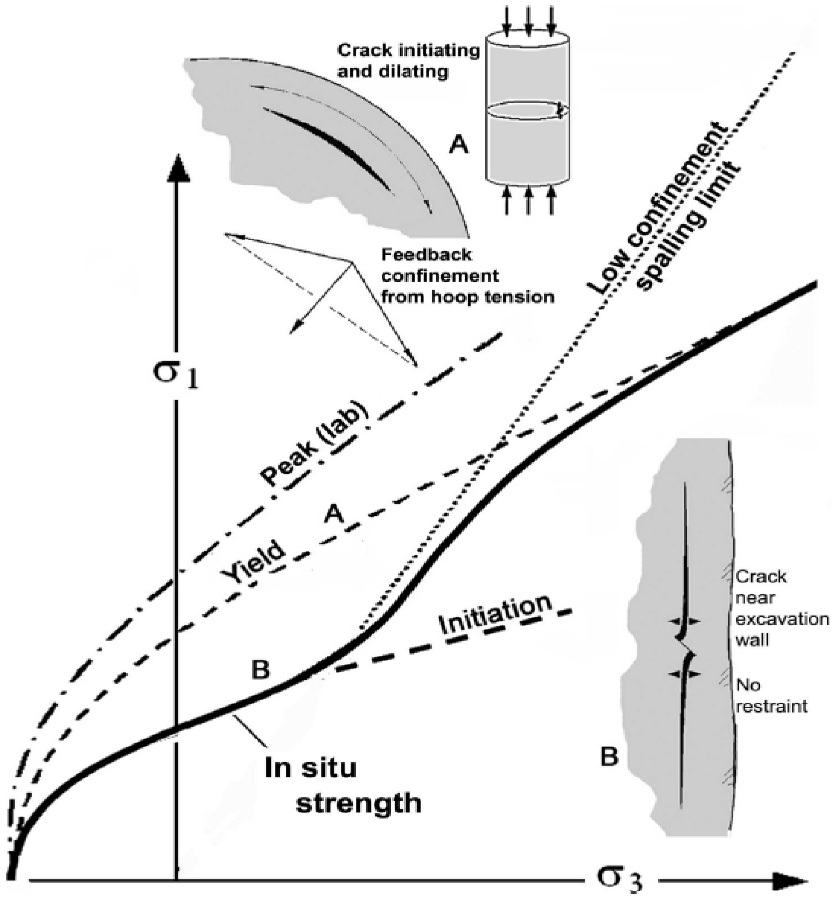

Figure 8: Synthesis of theoretical and experimental investigations (after Diederichs, 2007).

2.2.7 Spalling Limit

Excavation damage and spalling may occur as the ratio of minor to major stress, $\sigma 3/\sigma 1$, is in the range 10 to 20. Spalling is associated with the lower bound damage initiation and the upper bound crack interaction threshold, resulting in a composite stress path limit, identified in Figure ***8*** (Diederichs, 2007).

Confinement can provide load distribution, reducing the effect of stresses and increasing support capacity. Loss of confinement induces relaxation and is conducive to potential gravity driven failure where rock mass structure is present.

2.3 Creighton Mine Case Study

Vale Canada's Creighton Mine in Greater Sudbury is one of the deepest mines in Canada; and the environment is a hard brittle rock mass under high stress with significant seismic activity. The studies conducted at Creighton describe events similar to those experienced at Kidd Mine. During late 2014, Creighton was actively mining at the 8070 Level (2460 m) concurrently with a main access ramp under development down to the 8200 Level (2500 m). The resource is open at depth with potential for a deeper mining horizon. The deep mine planning requires a strategic approach with a specific review of methods that can lead to a better understanding of the rock mass response and to apply mine design strategies accordingly. Understanding the behaviour of the rock mass response under high stress conditions at Creighton is key to mitigating safety risks.

Studies conducted at Creighton have focused on the two major types of seismic mechanisms which are associated with deep hard rock mining: the first one is related to stress redistribution and rock mass fracturing; and the second is related to shearing and fault-slip events.
The focus of the Creighton case study by Cotesta *et al.* (2014) and summarized in this section was of stress redistribution as a result of the rock mass response due to mining.

The regions of rock under review were areas under development which had been exposed to mining induced stresses, subsequently yielded and reached residual strength. These areas become seismically quiet and a measurement of the volumetric fracturing provides a basis for assessing the extent of rock mass yielding.

2.3.1 Yielded Regions

Yielding in the rock mass causes stresses to be shed further away from mine development areas. Monitoring data in the far-field rock around the developed areas show an increase in stresses and seismic activity in these outer regions. Cotesta *et al.* (2014) demonstrate these relations, illustrated as radial zones in Figure 9, showing the yielded rock mass surrounding the mined stopes, the stress horizons and the corresponding areas of seismicity.

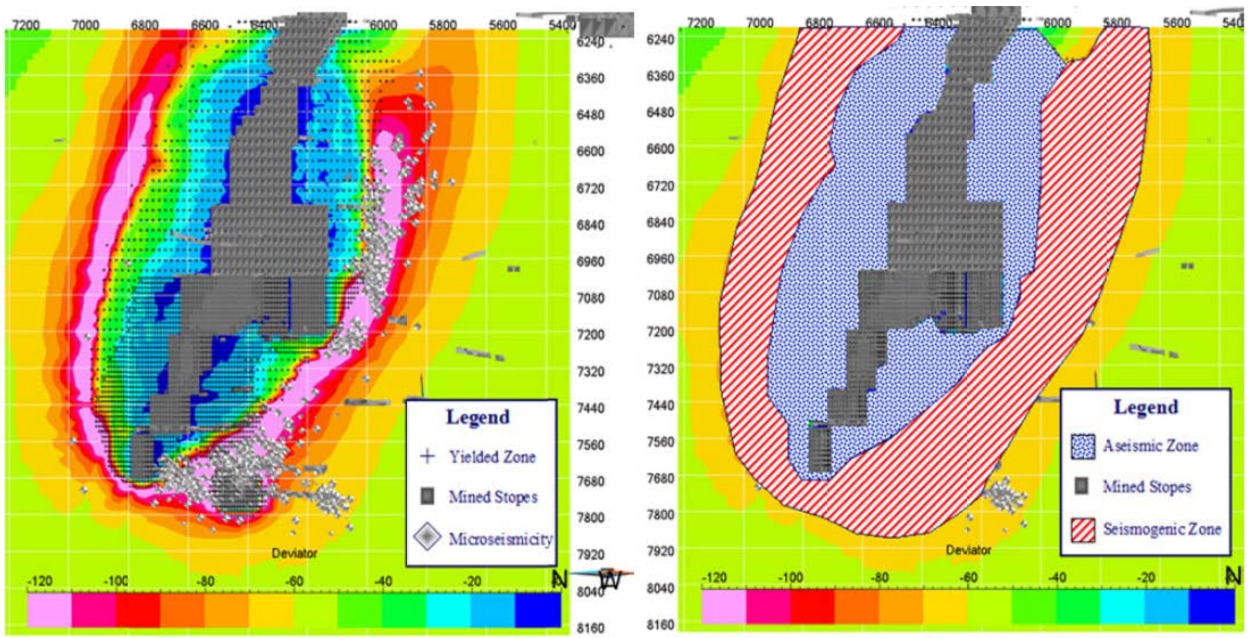

(a) (b)

Figure 9: a) cross-section through Creighton Mine from a depth of 1,902 m to 2,487 m showing modelled stresses, yield, voids and microseismic spheres; b) corresponding aseismic and seismogenic zones (after Cotesta *et al.*, 2014).

Cotesta *et al.*, (2014) developed calibration models with an effort to observe a correlation of the amount of microseismic events as they corresponded to stress levels. A reduction of seismic events in the yielded regions was observed while the regions outside of these yielded zones exhibited seismicity and higher deviatoric stress levels.

2.3.2 Stress Observations

The Creighton studies relate the amount of damage observed in underground excavations to the magnitude of the major principal stress, the major and minor principal stress ratio, deviatoric and tangential stresses, the Hoek-Brown damage threshold where $m = 0$, the effect of confinement, depth of fracturing, and excavation and pillar geometry. Compared to the laboratory testing for rock mass UCS, the in situ strength of the rock varies according to the local conditions; including rock mass, fracturing and geometry. As many of these parameters should be included where information is available to attain the most comprehensive study and gain a more complete understanding of the rock mass yielding potential. Stresses at the excavation boundary are reduced when the rock mass reaches a yielded state, and potentially experiences reduced effects from mining induced seismicity and rockbursting.

The seismic data review and stress observations were applied to overall stress hazard maps. Cotesta *et al.* (2014) applied the study to long-range mine planning and risk mitigation in probable hazard areas in the deep mining. The study noted that seismic system records captured localized events related to structure, however, areas not well covered by the sensor array may not be well represented when identifying potential hazard areas.

2.4 Apparent Stress, Energy Variations and Rock Mass Response to Mining

Mine seismic systems record acoustic energy waveforms emitted from uniaxial or triaxial sensors, typically installed in the perimeter of mine development; and the results assist with characterizing the seismic events to determine the source, magnitude and the probable mechanism involved.

Recording and evaluating seismic source parameters using established industry criteria provides practical methods to assess hazards and potential for damage as well as indicating locations of rockburst potential, and increases the basis for design support decisions for underground development.

While absolute stress cannot be directly interpreted from seismic waveforms, a change in the stress state can be used to identify potential instability. Seismic source parameters and energy variations can be used to identify risk related to stress drop and related rock mass behaviour. Trends over time can provide insight into the seismic hazards including location, size and strength of the source.

The following sections further discuss the apparent stress and energy relations with rock mass response.

2.4.1 Frequency-Magnitude Relation

Analysis of the relation of the frequency and the magnitude of seismic events collected from a stable seismic system can provide a measure in a power-law relation of the power exponent, named the b-value. The b-value, identified in the graph in Figure 10, is expressed as:

$$\text{Log } N = a - b\, m$$

Where:

- N = the Number of events greater than or equal to magnitude m,
- m = the event magnitude,
- a = the relation of the number of events in a data population, and
- b = the power law exponent.

The b-value in a large population typically approaches 1.0 and variations from unity indicate the predominant mechanism: a higher b-value indicates non-shearing mechanism while a lower b-value indicates a higher tendency of shearing mechanism. The ratio of a/b, plotted as the intersection of the data with the x-axis, provides an estimation of the probability of future large events. Previous mine studies have concluded that the a/b value is conservative and typically estimates events higher than what is actually experienced.

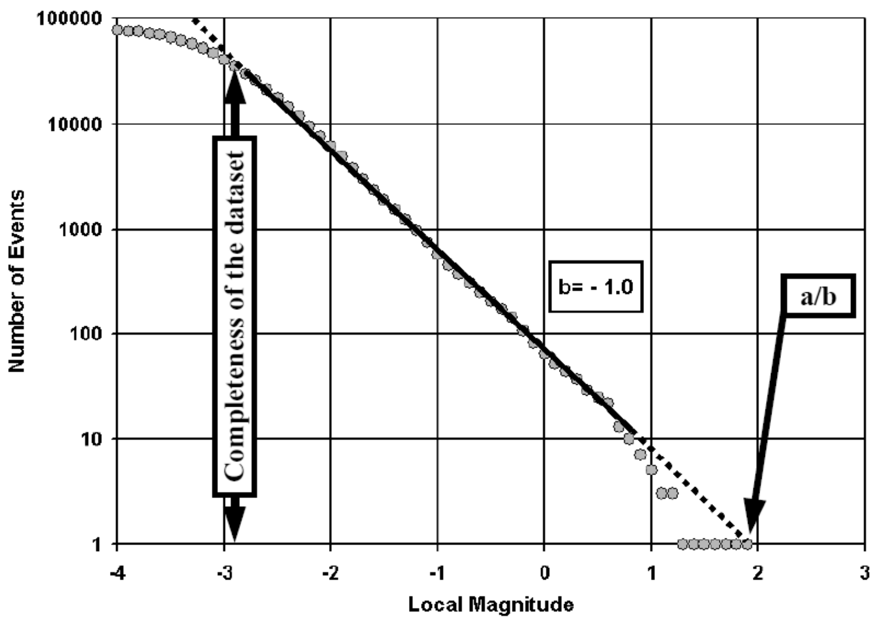

Figure 10: A typical Gutenberg-Richter frequency-magnitude relation for a large population of data (Hudyma, 2010).

2.4.2 S:P Energy Ratio

The ratio of the Shear Wave (S-Wave) to the Compressional Wave (P-Wave), or the S:P energy ratio, can provide an indication of overall relation with possible fault-slip mechanism is present, with the s-wave to p-wave energy ratio greater than 10 (Cichowicz *et al.*, 1990), or conversely, volumetric rock mass fracturing will be represented with an s-wave to p-wave energy ratio in the range of 1 to 3 (Urbancic *et al.*, 1992).

2.4.3 Apparent Stress

The following presents a summary of apparent stress and apparent stress time history (ASTH) as a seismic source parameter and analysis technique with a review of the theory and application of apparent stress to mine seismic monitoring system data.

Research conducted by Wyss and Brune (1968) for earthquake activity proposed a definition of apparent stress (σa) as a measurement of stress change, or seismic energy (E) as it relates to the seismic moment (Mo), taking into account the stiffness of the rock (G), the shear modulus of rigidity (stiffness of the rock). The relation is summarized in the following equation:

$$\sigma a = G\ x\ \frac{E}{Mo}\ ;$$

The seismic moment is defined as a measure of the strength of a double couple shear dislocation event from a seismic source (Brady and Brown, 2006). According to Brady and Brown (2006), the seismic moment in a mine setting is not readily available since the slip area of the discontinuity cannot easily be obtained, but can be derived from mine seismic system data.

Seismic energy is measured by the radiated seismic waveforms released at the source. The energy typically increases with seismic moment (Mendecki and van Aswegen, 2001). The following definition is provided (Mendecki and van Aswegen, 2001) and illustrated in Figure 11.

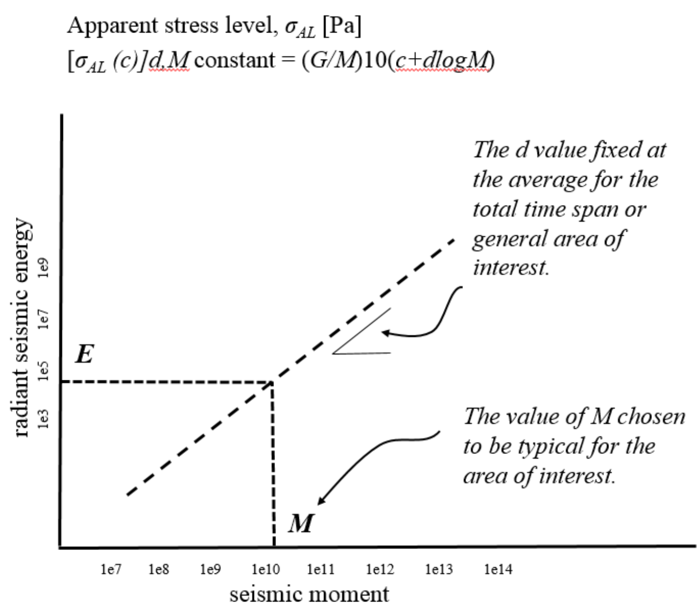

"For a given slope of the E-M relation, the constant c would indicate the level of stress (from all events in the data set). σ_{AL} is a useful engineering parameter for the comparison of stress variation in space or time. By choosing the fixed M_{AS} the average for the data set, σ_{AL} would be equivalent to the average apparent stress." (Mendecki and van Aswegen, 2001).

Figure 11: Apparent Stress Level σ_{AL} (after Mendecki and van Aswegen, 2001).

Apparent stress has been termed a model-independent seismic source parameter in that it is not bounded by specific geological or geophysical event triggers. Apparent stress provides an indication of related stress increase due to fracturing propagated as a result of mining induced seismicity, an indication of potential stress release and associated seismic hazard (Hudyma, 2010).

Earthquake energy radiation studies linked the significance of apparent stress with shear stresses causing fault slip (Choy and McGarr, 2002). When applying this to earthquake studies, the focus was on structures along tectonic plates and oceanic ridges with locally intense deformation and a high apparent stress was associated with strong rock and high levels of deviatoric stress. Further study relating the magnitude of apparent stress with potential damaging earthquake events was conducted (Choy and Kirby, 2004) and, incorporating established international seismographic networks, attempted to use apparent stress to improve evaluation of hazards and to determine the structural mechanism involved in tectonic plate subduction processes. The study also attempts to associate the maturity of faults with apparent stress and associated events. The generalized view is that the older more mature faults have less apparent stress, causing less regional damage along the fault, possibly due to a contact surface that has been subject to geological processes and has lower frictional properties. Where high apparent stresses were recorded in past earthquakes, especially with younger faults, there were highly damaging results. These observations suggest that mature faults and low apparent stresses associated with high seismic energy during mining advance will impact the rock mass in a more subtle manner with less associated damage. The rock mass is impacted to the extent that a fracture zone develops, the rock mass undergoes relaxation and maintains support capacity with a reduced risk of rockbursting. Parallels may be drawn to the effects of destress blasting on the rock mass during development where careful planning pre-fractures the rock and reduces the level of stresses to advance the mining front with reduced risks, especially where a high stiffness contrast may be present, such as with intrusive dykes.

The international seismographic network introduced additional observations and methods to forecast the potential of strong events. Observations of apparent stress in seismic events, the temporal and spatial distribution and relative strength (Qin and Qian, 2006) were evaluated with stresses before and after earthquakes in the Yunnan province of China. The study found that the distribution of high apparent stress was located around the locations of two high magnitude earthquakes.

Senatorski (2007) discusses the scaling relation of apparent stress using theoretical models of earthquakes based on a single fault plane. The study includes comparison to various source parameters related to apparent stress including energy, moment, material strength, slip velocity and rupture area. The trend seen in the results confirms and explains the relations studied in different data sets. A minimum apparent stress is related to uniform fault rupture propagation, and an increase in apparent stress is associated with increasing seismic moment. The scaling relation identified that characteristics of both small and large events for typical earthquakes are thought to be similar and that a minimum apparent stress is needed to propagate the rupture process.

2.4.4 Apparent Stress Time History

Apparent Stress Time History (ASTH) is a measurement of apparent stress above a specified threshold over a period of time with a trailing time period (Hudyma, 2010). The threshold of high apparent stress is determined on a local mine basis and typically represents the upper 10-20% of events, to be used as a starting point until sufficient analysis has been completed to calibrate the data. A reasonable trailing time period is three to seven days (Mikula *et al.*, 2008) which will smooth the data over periods of less activity (such as weekends) while still presenting sufficient detail for analysis. Trends will indicate whether the ASTH increases over time as this could indicate elevated seismic hazard risk.

The variations of high apparent stress over a period of time during mine development can be analysed to determine trends and develop an understanding of the effects of mining induced seismicity and to identify zones of higher apparent stress and possibly large damaging events. The amount of energy in a large seismic event is often higher as stress increases and the apparent stress is directly affected. Large events often occur after stope blasting. Conversely, seismicity on mine faults does not typically exhibit stress changes, therefore the energy radiated is low and will not register a high apparent stress.

Seismic data analysis focused on ASTH can provide short term hazard assessment with a reasonably successful identification of location, timing and magnitude. Therefore, as the frequency of ASTH events increases, the likelihood of a large event within a relatively short period of time also increases. Seismic source activity not related to mine blasting may be due to shearing along faults and if multiple events of ASTH are recorded when blasting is not occurring; the stress change could be due to rock mass response along a geological feature.

2.4.5 Energy-Moment Relation

An Energy-Moment relation can be plotted representing the log of total radiated seismic energy and the log of average seismic moment. The resulting slope of the line in a typical energy-moment relation is generally around 1.2 to 1.6. Any marked variations or distinct populations provide an indication of potential errors in a data set or potentially unreliable data recording. A typical energy-moment relation is shown in the plot in Figure 12 (after Hudyma, 2010).

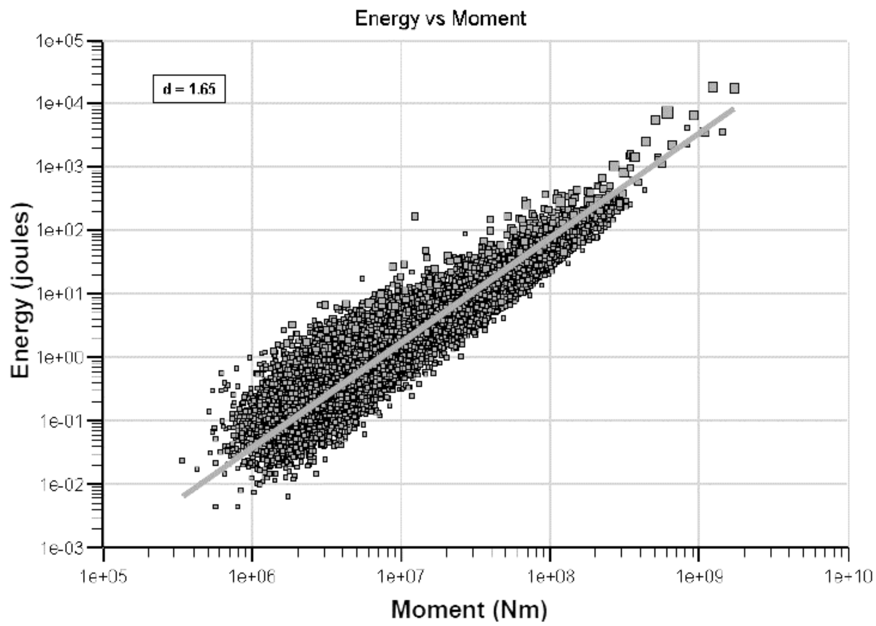

Figure 12: Typical Energy-Moment relation of a seismic data set (after Hudyma, 2010).

2.4.6 Energy Index

The Energy Index (EI) is generally defined as the relative amount of energy released for a population of seismic events compared to the amount of energy expected. Mendecki *et al.*, (2007) define the EI with the following relation:

$$EI = \frac{E}{\bar{E}(P)} = \frac{E}{10^{d \log P + c}} = 10^{-c} \frac{E}{P^d}$$

Where;

- E is the radiated seismic energy of an event, $E(P)$ is the average energy radiated by events;
- P is the observed potency; and
- $d = 1.0$ is proportional to the apparent stress.

The EI reflects the relative stresses at the source of the seismic event and considered proportional to the apparent stress (Mendecki *et al.*, 2007). A graph depicting the relation of the EI concept is illustrated in Figure 13.

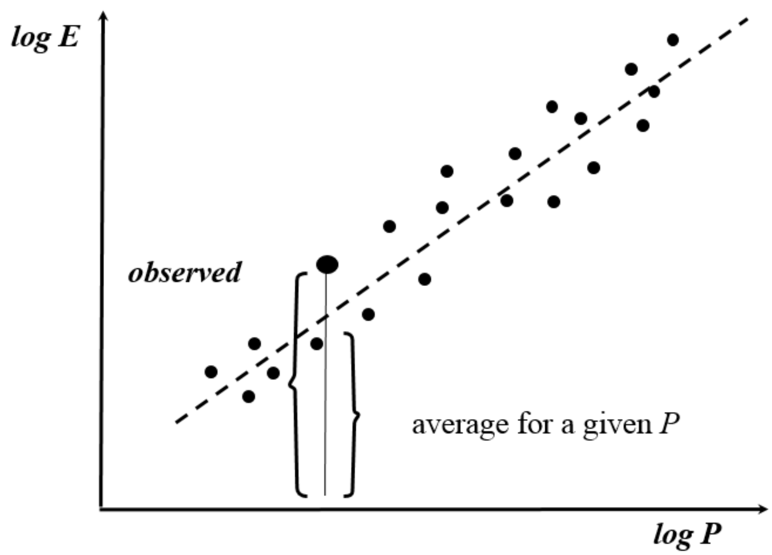

Figure 13: Energy Index concept, after Mendecki *et al.*, (2007).

While the EI is not considered a predictor for damaging seismic events, it may be used to identify potential areas of rock mass instability. A trend of seismicity may be evaluated from the entire data set to delineate potential energy trends during future mining; and is related to the occurrence of smaller events that typically dominate a data set. A logarithmic relation of seismic energy and seismic moment can be graphed to provide visual identification of atypical events and assist in identifying regions experiencing potential instability. When areas are accumulating stresses, such as pillar and stope abutments, the EI will indicate a value greater than one; as the stresses increase and the structure begins to yield, the value will decrease to less than one (Hudyma, 2010). The relation of energy recorded in seismic events can be plotted on a chart to display the expected energy and the actual energy recorded.

2.4.1 Cumulative Apparent Volume

Cumulative Apparent Volume (CAV) estimates the volume of rock mass deformation for a given seismic event. Instability analyses can be conducted by plotting the CAV in relation to the log(EI) in a time history chart; the resulting changes in the CAV indicate where significant changes in energy and associated stress increase and decrease are occurring related to a seismic event.

2.4.2 Application to Underground Mine Development

As with earthquake studies, apparent stress in an underground mine environment and the associated changes in seismic energy and moment are indicators of potentially large and damaging seismic events. While originally assessed as discrete events, the changes of apparent stress over time have been considered an important tool to assist with the identification and evaluation of trends.

The seismic energy analysis using a ratio of expected energy to energy released, or the energy index (EI), for large events is similar to the apparent stress. The primary difference between the two parameters is the number of small versus large events: EI population of events is predominantly composed of relatively small magnitude while a high apparent stress population is related to larger magnitude events with higher stress levels.

The intensity of damage resulting from seismic events is reflected in the amount of energy released and can be measured with stress related source parameters including apparent stress, static stress drop and dynamic stress drop. Other elements that influence the potential damage from a seismic event (Ortlepp *et al.*, 2007) include:

- The location relative to the event source;

- the excavation size;
- rock mass properties;
- pre-existing fracturing; and
- the stress in the intact rock beyond the fractured zone.

An explanation of burst fracture, (Ortlepp, 1997), identifies the source mechanism of large seismic events, associated with large stress drops and high apparent stress, and indicates that spontaneous shear rupture in a high stress abutment in a deep mine can propagate quickly toward a stope and has the potential for intense damage. Ortlepp refers to the mechanism as a 'man-made' fault; and the resulting damage also depends on the proximity of the rupture front to the open excavation. If the rupture daylights into the stope, the potential for damage is very high as the confinement is reduced or absent. An example of a mining induced burst fracture under high apparent stress conditions is illustrated by Ortlepp (1997), shown in Figure 14.

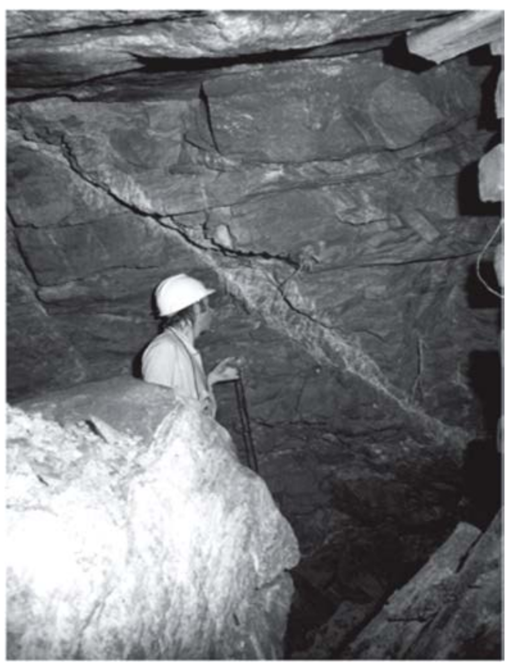

Figure 14: View northward of easterly-dipping burst fracture about 7 metres below worked-out area some 30m behind westerly advancing B4W longwall face (Ortlepp, 1997) p.58.

2.4.3 Evaluation of Mine Hazards

Incorporating apparent stress as part of an evaluation of mine hazards improves the assessment of large events with a higher risk of potential damage (Hudyma, 2010). Studies have been conducted (Spottiswoode *et al.*, 2008; Ortlepp *et al.*, 2007) which determined a relation between the level of change in apparent stress and the change of energy released during seismic events. Spottiswoode *et al.*, (2008) termed the energy release rate (ERR) and, in a case study of two deep gold mines in South Africa identified a direct relation between ERR and apparent stress.

A case study to associate bulk strength of the rock mass to peak ground motion using the apparent stress source parameter (McGarr, 2001) was conducted and the author proposed a relation of apparent stress to shear stress acting on a fault during a fault slip seismic event. The study evaluated soft and strong rock and summarized that the soft rock events did not exhibit high magnitudes, while the strong rocks had higher peak ground motions, even with minimal fault movement, and the strong rock events were more likely to be high magnitude and damaging events.

Gibowicz and Lasocki (2001), describe previous studies of rockburst hazard potential by analysing source parameter relations. In a study by Alcott (1998), variations of seismic energy, seismic moment and apparent stress identified elevated risk were applied to ground control decisions. Data collected was calibrated relative to observed damage at Brunswick Mine and variations were assessed to identify trends in seismically active areas and elevated risk. In a second study of a South African gold mine, by Glazer (1997), an apparent stress index was established to determine stress values above and below the average for the mine seismic events recorded. Large damaging events occurred in areas where the apparent stress index was high even if the seismic event was located outside the damaged areas. The index could be used as an indicator to adjust ground support for areas with a high apparent stress index. A third study conducted by Król (1998) at a copper mine in Poland identified a relation between source parameters and geological structure, mining conditions, seismic activity and rockburst hazards.

2.4.4 Re-Entry Protocol

While seismicity in mining is not easily controlled, there is a distinct advantage to be able to understand the rock mass response and the level of stress, energy release and subsequent magnitude of events and the associated potential level of damage. Armed with sufficient knowledge based on back analysis and time history, assessment of events can provide a reasonable re-entry protocol for hazard areas in a mine.

Magnitude and apparent stress time history can be applied to improve management of personnel activities in high stress environments and can identify areas that are potentially susceptible to elevated stress. The cause and effect relation over time, if carefully recorded and monitored, will assist with determining high risk areas as well as areas that have returned to background levels of seismicity. Where mine seismicity levels remain high for longer periods indicates that the rock mass is continuing to adjust to the effect of blasting and these may be seen in energy variations of the seismic data. Areas where seismicity and apparent stress return to background levels in a relatively short amount of time may indicate that there is a lower probability of a significant large event. (Mikula *et al.*, 2008).

Re-entry analysis using apparent stress, magnitude-time and energy index evaluations is carried out on a continual basis as event rates and trends are recorded and processed. The return to background levels of seismicity after blasting can be measured and the typical time of seismic decay can provide the estimate of time for safe re-entry. Some back analysis is usually required to gain an understanding of the rock mass response in context of the actual mine development activities in place.

Documentation by Mikula *et al.*, (2008) provided for a software program developed by the Australian Centre for Geomechanics (ACG) to analyse seismic risk, Mine Seismicity Risk Analysis Program, currently distributed under the name *mXrap* (Harrison and Wesseloo, 2015), applies several industry analysis techniques.

Rock mass failure is induced over time and is not typically an instantaneous process. As such, careful review of seismic data can identify the gradual process caused by mining, stress and geological features. The rate of occurrence as well as the level of seismicity can add insightful tools to assist with keeping personnel safe from potentially higher risk areas.

Mine geometry changes following a blast will result in stresses readjusting around the opening and recording the energy variations will identify the time period of stress readjustment (Mikula *et al.*, 2008).

While identifying the apparent stress frequency, magnitude and energy changes within a system is a useful guide to determine re-entry protocol, it should not be the only assessment in place. The mine geology, excavation geometries, structural features, mining methods and other seismic source interpretation tools and mine development parameters should be used to provide context and confidence in the interpretation of the rock mass response to mining.

2.4.5 Magnitude Scales and Seismic Hazard

Local mine seismicity and relative hazards vary and as such, each mine has a local measure of the potential hazard based on experience. The likelihood of occurrence of large events may be assessed through a review of past seismicity. A significant outcome of seismic data monitoring and review is to assess the probable location of hazards with some degree of confidence. The review should include verification of the data set for consistent and auditable event records, collected over a period of time.

The magnitude of events provides a relative measure of the strength of an event from measured displacement at a given frequency. More commonly known magnitude scales that have been developed include the Richter Magnitude (Richter, 1935), developed primarily to describe earthquake events based in California; the Nuttli Magnitude scale (Nuttli, 1973), commonly used in Eastern Canada to provide a measure of earthquakes and seismic events; and a Moment Magnitude scale (Hanks and Kanamori, 1979) which is a measure of the seismic moment and is best associated with the size of a fault slip event.

The term Local Magnitude (M_L) has been widely used to describe a magnitude scale calibrated from moment magnitude of events recorded on a local seismic monitoring system, typical in underground mining, and is applied to quantify events within that localized system. As a general guide, Hudyma (2010) provides a qualitative description of seismic activity relative to the Richter magnitude scale, as listed in Table 1.

The Kidd Mine seismic system, as described in Section 3.6, records significant events with a triaxial magnitude greater than M_L = -1.0 and large events greater than M_L = 0. Earthquakes Canada (2017) records Nuttli Magnitude for events that are detected on its regional system and Kidd Mine report large events that are mine blast related. The triaxial magnitude recorded on the mXrap system is reported in Local Magnitude, M_L; and Kidd Mine reports the M_L + 1.5 as equivalent to Nuttli Magnitude (M_N) (Disley, 2014).

Table 1: Qualitative description of seismicity relative to the Approximate Magnitude Scales Richter (Hudyma, 2010) and Local Magnitude (M_L)

Approximate Local Magnitude (M_L)	Approximate Richter Magnitude	Qualitative Description (Hudyma, 2010)
-4.0	-3.0	• Small bangs or bumps heard nearby. Typically, these events are only heard relatively close to the source of the event. • This level of seismic noise is normal following development blasts in stressed ground. • Events are audible but the vibration is likely too small to be felt. • Not detectable by most microseismic monitoring systems.
-3.0	-2.0	• Ground shaking felt close to the event. • Felt as good thumps or rumbles. May be felt remotely from the source of the event (more than 100 metres away). • Often detectable by a microseismic monitoring system.
-2.0	-1.0	• Often felt by many workers throughout the mine. • Should be detectable by a seismic monitoring system. • Significant ground shaking felt close to the event. • Similar vibration to a distant underground secondary blast.
-1.0	0.0	• Vibration felt and heard throughout the mine. • Bump may be felt on surface (hundreds of metres away), but may not be audible on surface. • Vibrations felt on surface similar to those generated by a development round.
0.0	1.0	• Felt and heard very clearly on surface. • Vibrations felt on surface similar to a large production blast. • Events may be detected by regional seismological sensors located a few hundreds of kilometres away.
1.0	2.0	• Vibration felt on surface is greater than large production blasts. • The Geological Survey of Canada can usually detect events of this size.
2.0	3.0	• Event is detected by earthquake monitors throughout the province.

3.0 KIDD MINE

Glencore's Kidd Mine currently extends to a depth of approximately 3 km and is the deepest active base metal mine in the world. Located approximately 27 km north of Timmins in northern Ontario, has been actively mining for over 50 years with initial operations by open pit starting in 1966 until 1976. The current life of mine using underground open stope development is expected to continue until 2021. A schematic of the Kidd Mine open pit and underground is shown in a longitudinal section in Figure 15.

3.1 Background

Underground sublevel open stope mining with consolidated backfill, was started with the first shaft development in 1969 for the upper levels of the No. 1 Mine. A second shaft was developed and No. 2 Mine continued was from the 2800 Level to 4000 Level. A third winze shaft was developed as mining advanced with No. 3 Mine to the 6800 Level. No. 4 shaft was commissioned for the deeper phase of mining, Mine D (also referred to as No. 4 Mine), is currently at the 9600 Level, approximately 3000 m below surface, with a spill pocket below the 9600 Level shaft station and ramp access from a main ramp adit at surface.

Mining at these depths continues to provide challenges for the mine's technical staff. A general layout of the lower mine development of No. 3 Mine and Mine D is illustrated in Figure 15, and a representation of seismic events in Mine D, from January 2012 to September 2016, is shown in Figure 20.

Counter (2014) describes the incremental development of the mine to increasing depths. The knowledge of the rock mass behaviour at each phase of mining, and the improvements to various technology and equipment over time provided additional planning tools for the next phase of development. Among the more notable improvements over time are the mine's modelling and monitoring capabilities, ground support systems for dynamic loading, ventilation and environmental controls, remote and automated production equipment and fibre optics communications. Implementation of the fibre optics system has enabled real time monitoring of rock mass deformation during development cycles and provides additional tools to the ground control staff.

The research and review described in this paper has been made possible with access to the Kidd Mine data and the Kidd staff have generously provided their time and insight. The mine has been actively promoting research efforts over the years and shares significant results with industry. As the ground control and planning team acquire increased knowledge of rock mass behaviour increases, it is applied to develop methods and tools for a proactive approach in dealing with the multiple challenges.

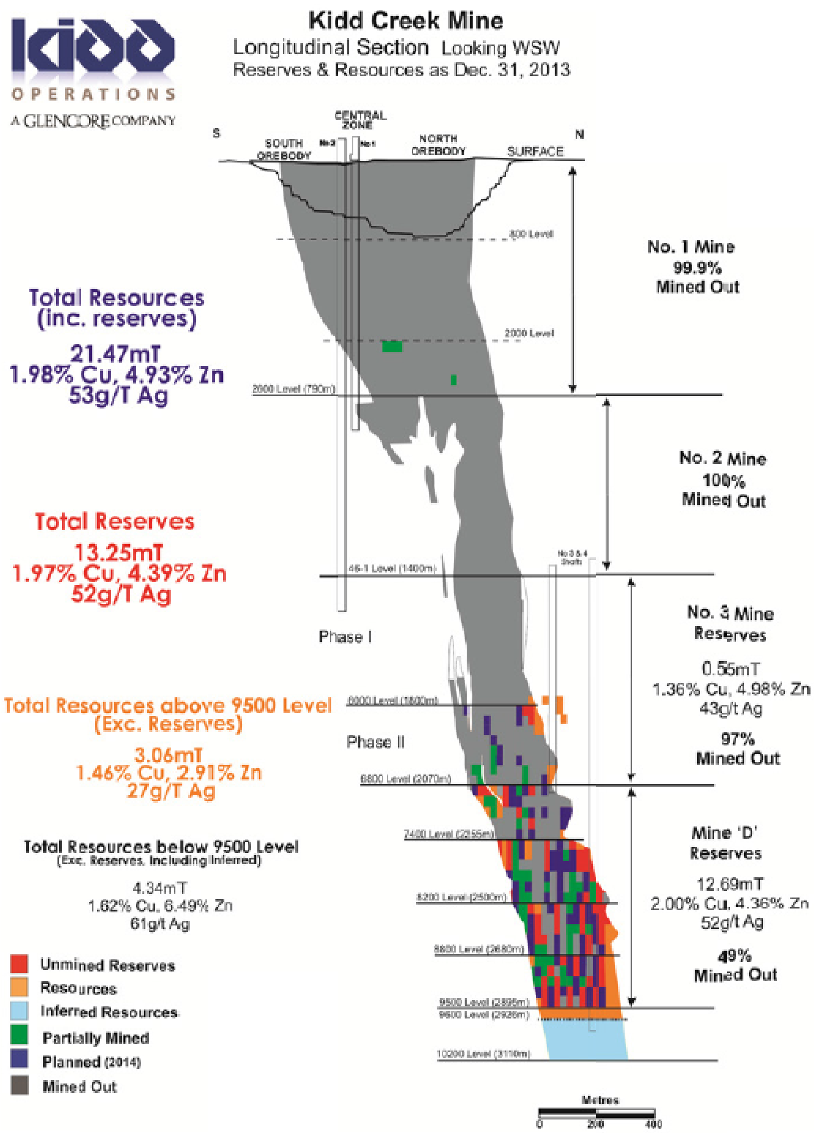

Figure 15: Kidd Creek long section, showing extent of historical mining from surface to 9600 Level and reserves as at December 2013 (Counter, 2014).

3.2 In Situ Stress

Various stress test methods have been conducted at Kidd Mine to determine the in situ stresses in the host rocks. Measurements were conducted during preproduction development to obtain the field stresses before experiencing changes due to the effect of mining. No recent stress tests were available for the lower Mine D, Block 4 stoping area, therefore the extrapolated stresses are considered conservative.

The major principal stress is generally sub-horizontal in an east-west direction near surface, and gradually rotating to northeast-southwest direction with depth; is generally within 15 degrees of normal to major structures and to the strike of the orebody.

The intermediate principal stress is also sub-horizontal, generally trending in a north-south direction near surface and gradually to a northwest-southeast direction with depth, and is generally parallel to the strike of the orebody.

The minor principal stress is sub-vertical, and is due to gravitational loading. A Kidd Mine geotechnical evaluation report states that, at an estimated 4 km depth, the virgin stress field would be isotropic or hydrostatic (Counter, 2009).

The stress ratios showing the correlation with increasing depth and deeper level stresses were extrapolated, as illustrated in the graph in Figure 16. Stress measurements taken on the 80 L (approximately 2400 m below surface) estimate the virgin stress field (vertical, horizontal perpendicular and horizontal parallel to strike of orebody) as follows (Counter, 2009):

- σv = 66.2 MPa;
- $\sigma hper$ = 71.1 MPa; and
- $\sigma hpar$ = 71.1 MPa.

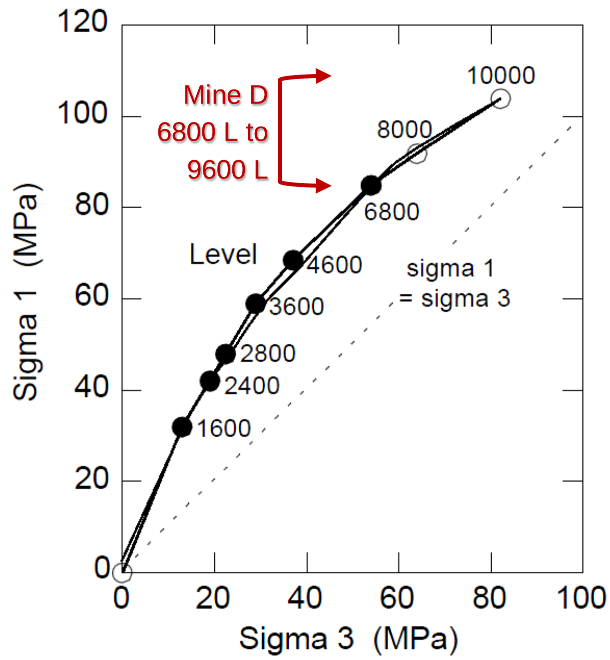

Figure 16: Plot of the stress ratios with increasing depth at Kidd Mine (after Counter, 2009). Current Mine D between 6800 Level and 9600 Level; estimated Sigma 1 from 80 to 100 MPa, Sigma 3 from 56 to 72 MPa.

The major to minor principal boundary stress ratio, $\sigma1/\sigma3$ for Kidd Mine D approaches 1.0 at current depths for the overall lower mine development and is not a key element for crack initiation causing widespread rock mass instability that may contribute to general failure or spalling along weakness planes.

Factors affecting rock mass yielding in Mine D may be primarily controlled by pre-existing rock mass structural features, mining induced damage, crack-surface interaction and local tension. Abutments with greater confining pressures and discontinuous fracturing will exhibit less damage, while pillars may experience more instances of rock mass damage.

3.3 General Geology

The ore is hosted in a felsic metavolcanic unit with distinct rock units that have undergone alteration, complex folding and faulting. Major structures have been mapped and are continuous for up to several hundreds of metres. Discrete joint sets are present in each of the different lithological units. The complexity of the fault zones is generally illustrated in Figure 17. Within the host metavolcanic unit, there are distinct lithological boundaries, local mine nomenclature for the main rock units are rhyolite, massive sulphide, and a mixed rhyolite fragmental zone with similar characteristics as the massive sulphide. Intrusives include gabbroic sills, andesite-diorite, and ultramafic rocks. The west hanging wall rocks consist of a metasedimentary greywacke, a quartz porphyritic felsic unit, and pillowed mafic metavolcanic flows. The rock strengths for these units, described in local terminology, and the Q' rock mass classification undertaken at the mine and reported in an internal geotechnical document, are listed in Table 2 (Counter, 2009).

Table 2: Uniaxial compressive strengths (σ_c) and corresponding Q' Rock Mass Classification (after Counter, 2009).

Rock Unit	σ_c (MPa)	Q'
Greywacke	160	15
Massive Sulphide	150	23
Andesite-Diorite	130	10
Rhyolite	110	10
Talc-Carbonate	65	8

3.3.1 Faults and Structure

Several cross-cutting fault systems have been interpreted during development, as displayed in Figure 17. The number of faults illustrated suggest that a portion of seismic activity in the mine is related to fault slip or shear mechanism. The seismic events occurring in peripheral areas is an indication of rock mass behaviour, yielding in response to mining activities, similar to the results obtained in a study conducted at the Creighton Mine by Cotesta *et al.*,(2014), and discussed in Section 2.3.

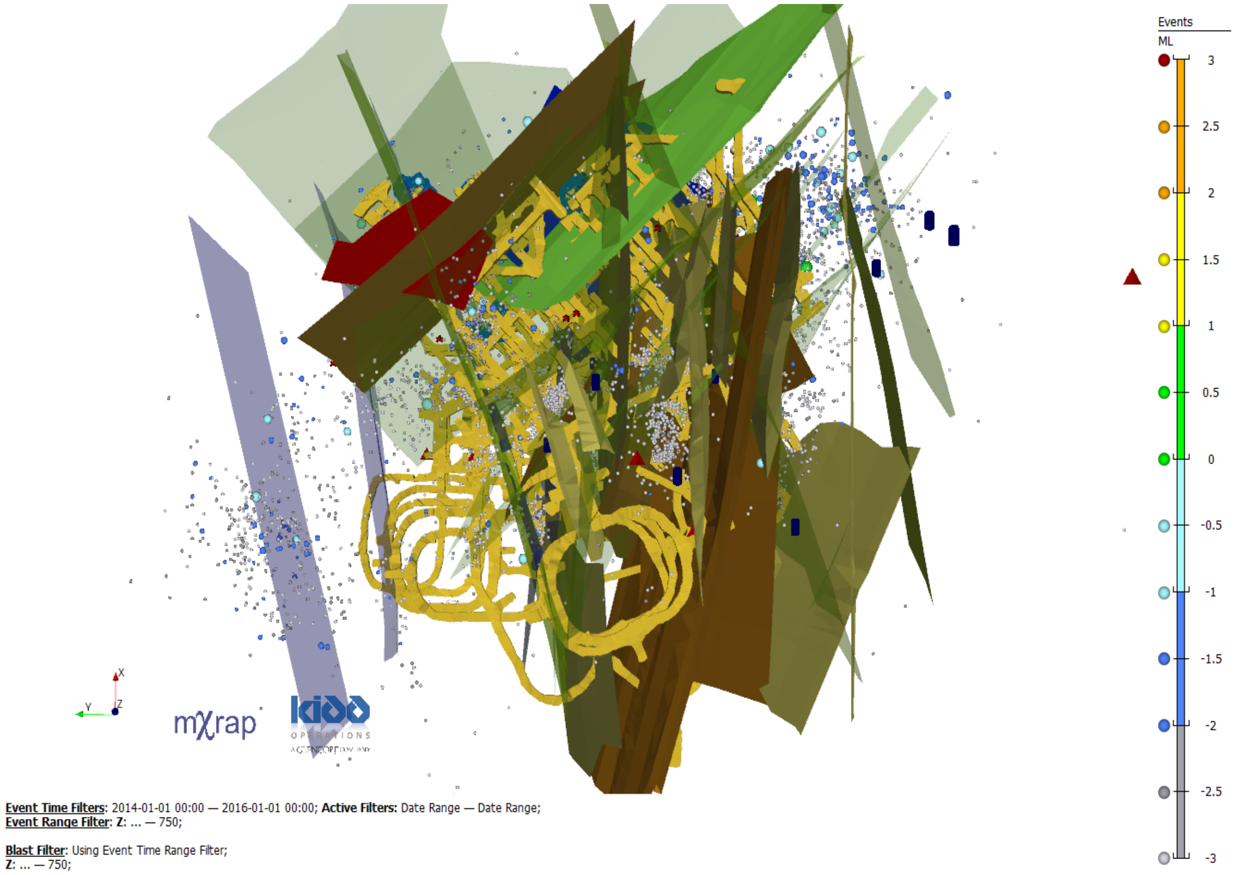

Figure 17: Plan View of Lower Mine D, Block 4 area showing observed fault systems.

3.4 Effect of Seismicity

Several areas of Mine D have experienced different degrees of damage related to seismicity. Table 3 displays a set of photos of the Kidd Mine D Block 4 area, taken during a site visit in February, 2015, depicting areas that have experienced sufficient stresses to cause rock mass deformation and damage to the ground support along drift walls and pillars.

Ground support upgrades, as described by Counter (2014) were implemented in select areas of the mine following damaging seismic events. The upgrades include robust dynamic load support systems with 1.8 m by 3 m welded wire mesh sheets with 4.82 mm wire (6 gauge WWM), reinforced with 7.77 mm wire mesh straps (0 gauge WWM) and modified cone bolts. The upgraded supports were installed near major geological structures and the areas of previous seismic activity in the southern abutment areas. Subsequent upgrades following damaging seismic events included friction stabilizer bolts, expandable bolts in select areas, closer spacing of the modified cone bolts and straps and shotcrete in heavily damaged areas. Intersections had additional support installed including expandable friction bolts, cable bolts with mesh strapping as well as specialized support in areas of extensive damage. A sample image of robust ground support system installed to repair a damaged crosscut at the 71-84XC intersection is shown in Figure 18 (Counter, 2014). Recent mining on the 9600 Level requires short development rounds to reduce the risk of rockbursting and re-support, however, the areas are frequently re-supported due to damage following seismic events.

Figure 18: 71-01 Dr South at 71-84 XC Intersection, facing south, after repair. Rupture plane located at embayment on right. Temporary post out of field of view on left. Note use of 4.5 mm chain link fence and 4.82 mm WWM over shotcrete, with various tendons. (Counter, 2014).

Table 3: Mine D Site Visit Photos, February 2015

February 2015	Mine D Block 4 Area, Cross Cuts and Pillars with Damage
Cross cut wall, damage to ground support, rock bulking and loose blocks along floor.	
Loose blocks ejected in cross cut below screen along drift and pillar, damage to screen near floor.	
Veining and rock fracturing localized near quartz veins.	

February 2015	Mine D Block 4 Area, Cross Cuts and Pillars with Damage
Ground support damage and rock fracturing.	
Loose broken rock in cross cut along lower portion of rib, bagging in mesh.	

3.5 Kidd Mine Geotechnical Reviews

Two internal ground inspection reports (Counter *et al.*, 2009a, 2009b), with observations conducted during a review of seismic events in No. 3 Mine, describe a relatively reduced occurrence of seismicity in Mine D when compared to activity experienced in No. 3 Mine. The past seismic activity in No. 3 Mine and the higher stresses in the lower elevations indicated that pillar panels in the Mine D areas have the potential to emit significant seismicity with yielding. Evidence of pillar yielding above 7500 Level generated large numbers of small seismic events (with low ground motion), however, no similar evidence of energy release was noted with pillar yielding in lower Mine D.

Counter (2009a) reports that the Mine D seismic system has greater sensitivity than the upper levels and the authors examined possible reasons for the difference in the mining areas, such as:

- Possible strain energy release coincident with development blasting may have resulted in a ‘loss’ of seismic data;
- Pre-conditioning of the rock mass may be occurring due to overloading and subsequently storing energy plastically and later experiencing fault displacement once the stored energy has built up.
- Subsequent energy build up could be repeated, potentially causing multiple occurrences of fault slip along the same geological features.

3.6 Kidd Seismic System

The following section discusses the evaluation of the Kidd Mine seismic data with a focus on energy and stress variations indicating potential rock mass yielding or instability. Understanding the history of seismic response to mining has provided tools to the engineering team to proactively adjust mine planning and development strategies at the Kidd Mine.

The first seismic sensors at Kidd Mine were installed in the 1980s using an MP250 based system, originally intended to monitor No. 1 and No. 2 Mines, then expanded in the early 1990s to monitor development in No. 3 Mine. The early system technology was limited and no longer in service, however, some of the sensors are still in place and connected to the updated system. A full waveform system was installed in 1997 and included a 48 channel ESG Hyperion system in No. 3 Mine, later updated to a 64 channel system with 24 uniaxial and 11 triaxial accelerometers. Following rock mass movement in the mine footwall and the effect on data transmission, additional recorders have been installed to record events from the lower part of No.3 Mine and below. A newer system installed in conjunction with the Mine D development includes sensors brought into service by 2007-2008 and signals are sent via fibre optics to a dedicated computer for analysis on surface (Counter, 2009). Continued development at depth has included ongoing seismic system upgrades with two arrays installed to cover from the 6000 to the 9600 Levels, including triaxial and uniaxial accelerometers and geophones.

Generally, the uniaxial sensors provide reliable distance and location of events recorded and the triaxial sensors record the event magnitude, the location vector and the source parameters. Industry standards over time have considered that a reliable seismic system will have at least three to four triaxial sensors for a relatively small mining area and a representative balance on uniaxial sensors in an array. Ideally, each event will be recorded on at least two triaxial sensors. The location of the array is preferentially installed in footwall development near active mining areas to capture the location and magnitude of events as correctly as possible. Some limitations of event location may be experienced due to excavation geometries creating raypath obstructions which may modify the signal. The Kidd Mine array includes 50 active sensors, displayed in Figure 19; of these, four triaxial and five uniaxial sensors are preferentially located within the lower Mine D area to improve data capture and increase confidence in the representation of events in the data set. Events in Kidd's Mine D seismic record have been captured on a minimum of 3 and up to 20 sensors.

The Kidd Mine seismic data has been maintained and calibrated over the life of the system with events sorted into clusters and named according to the mining areas; these include the:

- Lower area of No. 3 Mine; and
- Mine D development; with subset areas delineating Blocks 1 to 4.

The Kidd Mine seismic system reports event strength as Local Magnitude (M_L), calibrated from events on the local seismic system, and is applied to quantify events within that localized system. Mine personnel selected the local magnitude scale as it presents the data in a consistent and reliable manner.

Disley (2014) reports that significant events are recorded with a triaxial magnitude greater than -1.0 and a large event greater than 0.0. Disley (2014) uses Nuttli Magnitude (M_N) to describe the large events. The local system triaxial magnitude, M_L, reported with the ESG seismic system, plus 1.5 is applied to report the approximate equivalent M_N.

The data review for this study includes the entire database of seismic events from 2006 to 2016 with a focus on the latter period of mining in the subset of data encompassing just under a 5-year period from January 1, 2012 to September 20, 2016, representing mining activity at depths of 2 to 3 km in the Kidd Mine D, areas (6800 Level/2070 m to 9600 Level/3000 m), as shown in Figure 20.

Kidd Mine underground development has experienced several incidents of mine wide instabilities and, in recent years, several active mining areas with high levels of seismic activity which prompted additional efforts to understand the seismic rock mass response to develop mitigation measures.

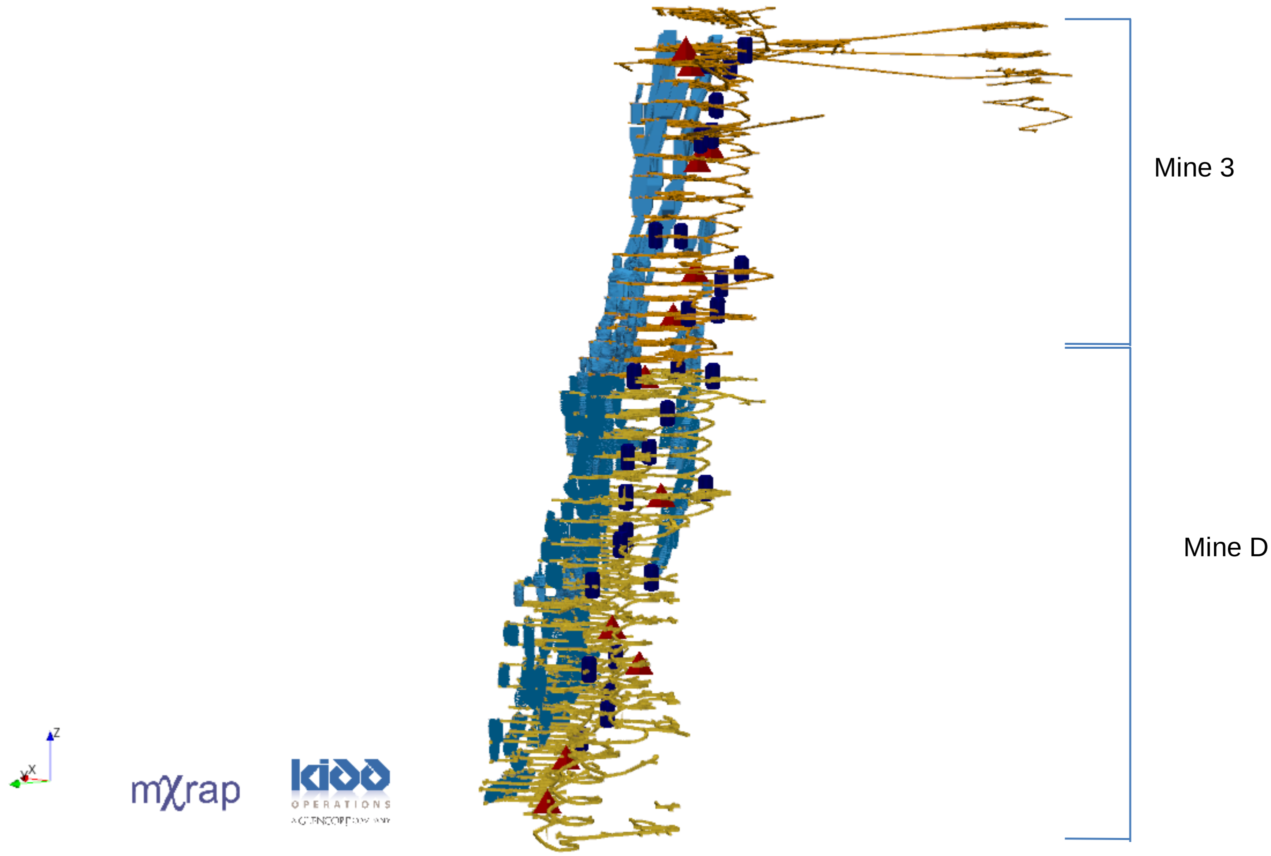

Figure 19: Overview of Kidd Mine 3 and Mine D general arrangement showing locations of the active uniaxial (dark blue cylinders) and triaxial sensors (red triangles), September 2016.

The seismic database provided by Kidd Mine for the purpose of this study includes events up to September, 2016. The data includes events recorded on 50 active seismic sensors installed in the mine:

- 15 active triaxial sensors; and
- 35 uniaxial sensors.

Mine D stope blocks are grouped by levels from Block 1 at 6800 Level to Block 4, currently extracting ore at 9500 Level, and are delineated from the upper limit at 1260 m elevation (2070 m below surface) to the lower level drawpoints at 2430 m elevation. Mining development is advancing on 9600 Level as of the writing of this thesis.

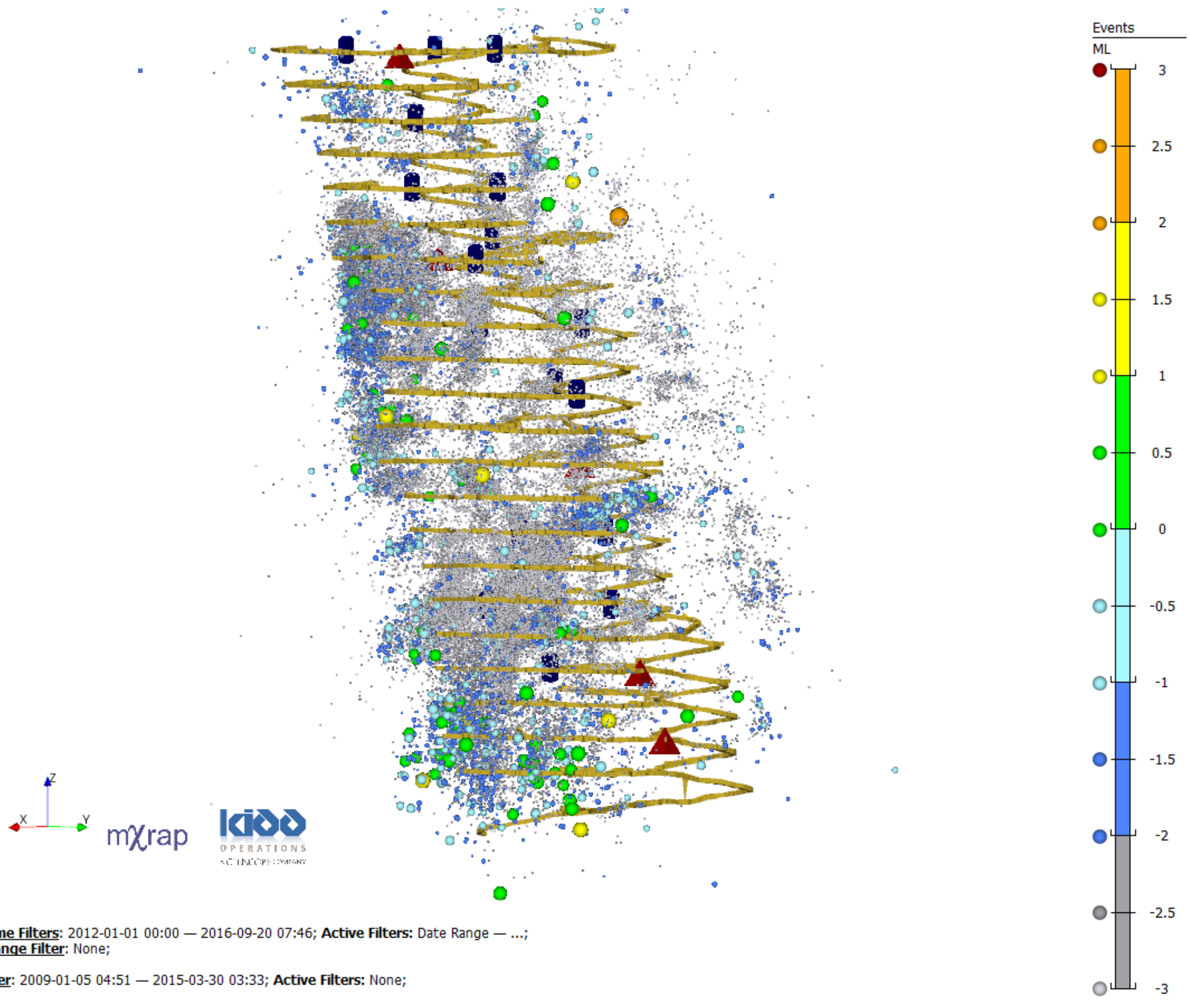

Figure 20: Kidd Mine D showing seismic events recorded between January 2012 and September 2016.

4.0 RETROSPECTIVE SEISMIC ANALYSIS

The data subset selected includes events from January 2006 to January 2016, to review relatively recent mining activity and the effects of mine development on pillars and abutments in the lower Mine D area.

The data was studied for spatial and temporal regions of seismic clustering and energy variations which provides evidence of anticipated rock mass behaviour, based on Disley (2014), including stress concentrations in pillars and abutments, slip on geological features and potential rock mass yielding.

Disley (2014) describes high levels of seismicity with significant reduction in apparent stress and an increase in apparent volume. These two primary factors combined indicate reduced strain energy being stored in the rock mass with a corresponding increase in volume leading to more displacement with each seismic event. The subsequent seismic events indicated failure planes across a pillar which did not correlate to any known fault planes or contact zones. Underground observations confirmed rock mass relaxation with evidence of water seeping through joints, loosening blocks and rock mass deformation.

Preliminary analysis included a review of data behaviour to identify the general composition of the seismic response. The overall data set for the entire mine appears to be consistent, well behaved and identifying areas with stress concentrations, occurrences of slip or yielding is expected upon closer examination of the targeted subset.

4.1 Frequency-Magnitude Relation

The data collection is stable and well behaved over the 2006 to 2016 period reviewed for events in Kidd Mine D. A possible bi-modal data relation is evident, suggesting a second mechanism for larger events. The data collection is depicted in the Frequency-Magnitude chart in Figure 21, and summarized as:

- Linear over > 2 magnitudes (each level of magnitude is depicted by grid spacing).
- The minimum magnitude sensitivity of approximately -2.3 M_L over approximately 10.7 years indicates with 98% of recorded events lower than local magnitude M_L 0.
- Second mechanism, possibly fault-slip, for larger events.

The maximum expected event size is 2.1 M_L with 60% probability of occurrence: indicated as the a/b value at the x-axis intercept and accepted in industry as a slight overestimate. Table 4 summarizes the Frequency-Magnitude values obtained from the chart.

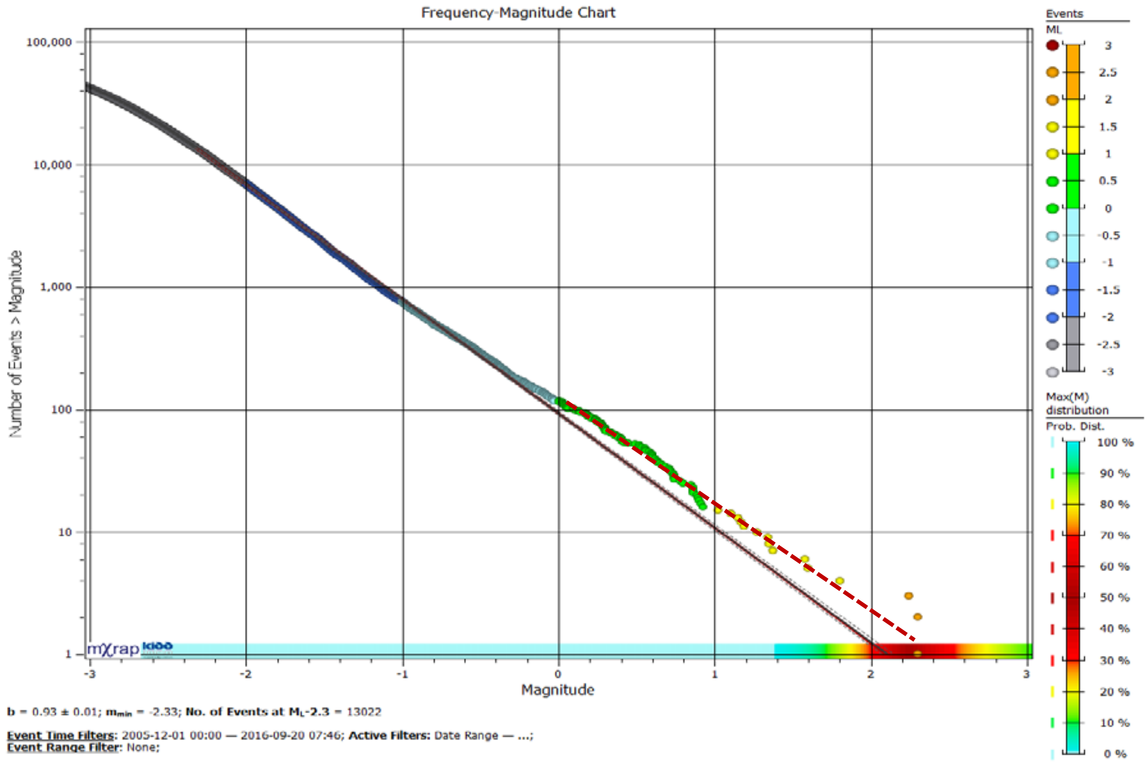

Figure 21: Kidd Mine D, Frequency-Magnitude chart: Events from 2006 to 2016.

Table 4: Frequency-Magnitude Chart Summary

b-value	0.93
Max. Expected Event Size, a/b	2.1
M_{min}	-2.3
Range of linear magnitude	-2.5 to -0.1 magnitude

The normal variation of the b-value is between 0.6 and 2.0 (Hudyma, 2010). A b-value of 0.93, from the Mine D database up to September 2016, suggests that a significant number of events are associated with fault slip (higher b-value) but the majority may be due to non-shearing mechanisms (lower b-value). Multiple events experienced in the lower levels of Mine D are consistent with the b-value interpretation and may be associated with persistent fault systems mapped in the development drives as well as non-shearing behaviour associated with large mine blasts.

4.2 S:P Energy Ratio

The ratio of the Shear Wave (S-Wave) to the Compressional Wave (P-Wave), or the S:P energy ratio, can provide the basis for understanding seismic source mechanism. A higher proportion of S-wave energy is an indication of fault slip events. The Kidd data reviewed and represented in the S:P Energy Ratio chart in Figure 22. All recorded mine events from 2006 to 2016 are shown in grey while the subset of select data, from January 2012 to September 2016, is displayed in colours according to the corresponding local magnitude legend. The trends for the overall data and the subset are very similar and indicates that there are no significant changes of seismic source mechanism in the later years of mining; the seismic system sensitivity and the magnitude of recorded events over time has remained consistent. Approximately 37% of the data subset of events have an S:P energy ratio greater than 10, indicating events with shear related mechanism and the remaining majority of events recorded at approximately 63% are not associated with shearing.

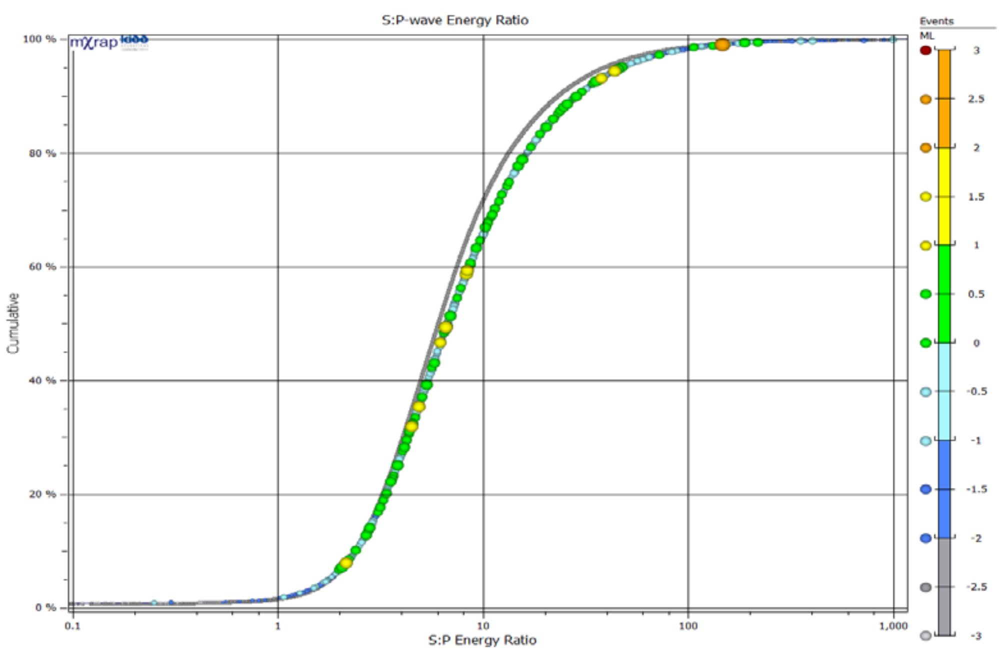

Figure 22: Shear and Compression Wave (S:P-Wave) Energy Ratio of Kidd Mine D. January 2006 to September 2016 (grey) compared to January 2012 to September 2016 (coloured by magnitude).

4.3 Magnitude-Time History

The Kidd Mine seismic data system has evolved and upgrades have been applied over time. A snapshot of the data, reflecting some of these changes, is depicted in the magnitude-time graph in Figure 23 of all Mine D events from 2006 to 2016. Proportionally, fewer events are displayed from the beginning of Mine D development, with density of events increasing gradually up to 2012; an obvious change is seen in 2013, where the lower limit of magnitude events recorded indicates a change of sensitivity – this period coincides with system updates and connection to a fibre optic system for data collection and processing. A second factor affecting the event rates likely coincides with increased mining activity with large scale blasting of stopes. The slope of the line representing the cumulative number of events also reflects these changes.

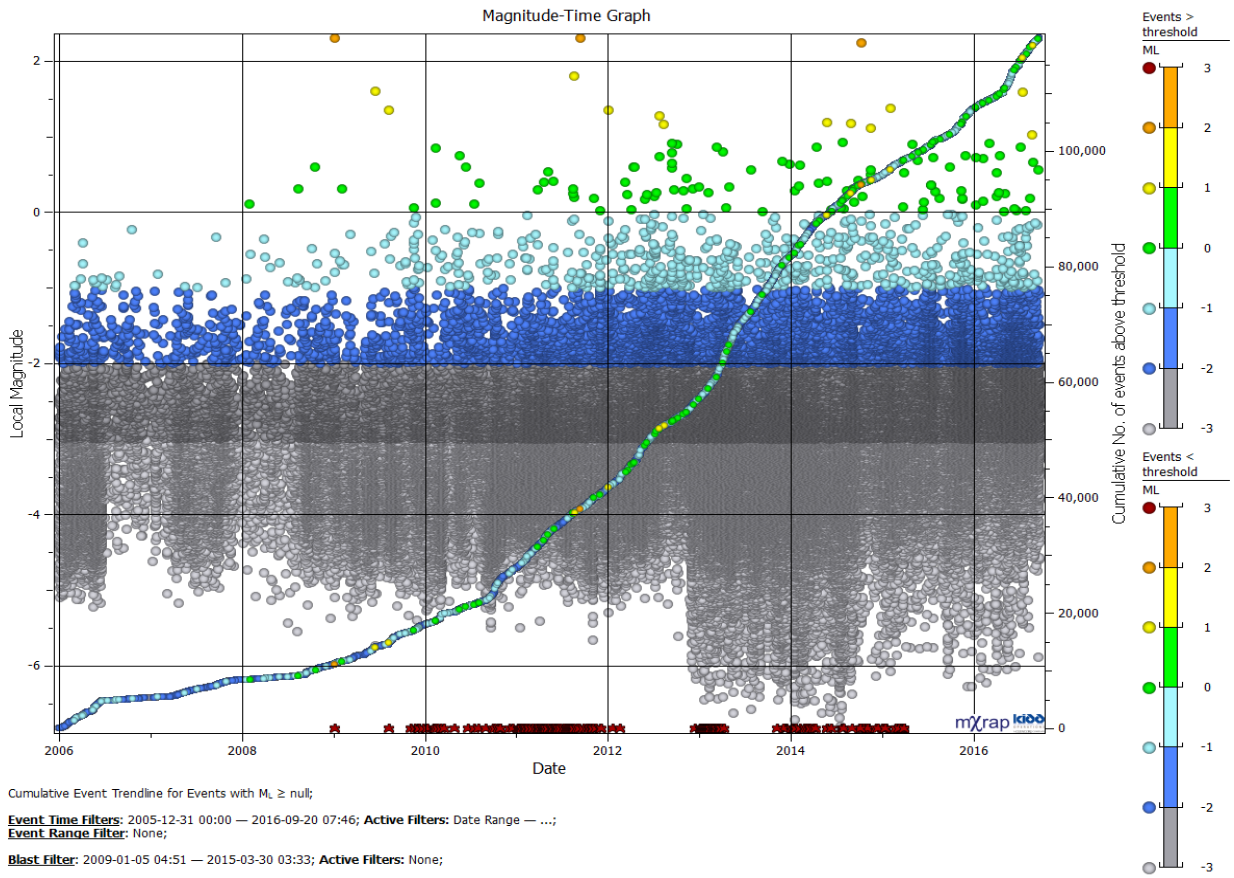

Figure 23: Magnitude-Time graph - All Mine D seismic events from 2006 to 2016.

A review of the events recorded distributes approximately 35% of the Mine D events from 2006 to the end of 2011 and the remaining 65% occur from 2012 to the final date of September 2016. The higher density of events occurs after a seismic system update and as the mine matures. As the data density is more conducive to displaying and analyzing trends, further review will focus primarily on the later years.

4.4 Apparent Stress

The higher magnitude events associated with periods of low apparent stress are an indicator of relaxation in the rock mass and typically reduced stresses within discrete areas such as pillars and stope abutments. The following graphs in Figure 24 illustrate the variations in apparent stress frequency during the Mine D development.

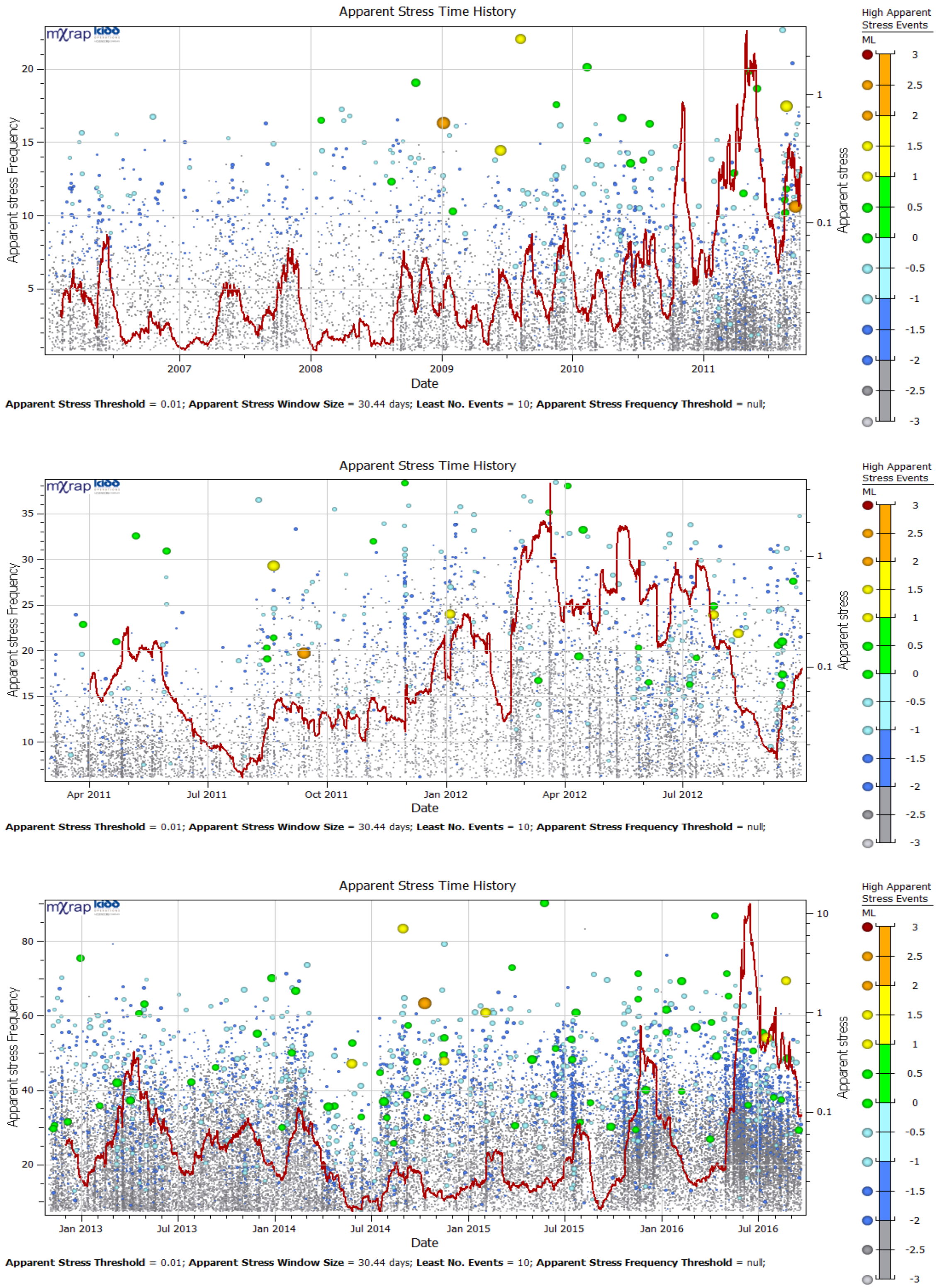

Figure 24: Kidd Mine D seismic data showing the Apparent Stress (AS) and AS frequency for (Top) January 2006 to October 2011; (Centre) March 2011 to October 2012; and (Bottom) November 2012 to September 2016.

4.5 Energy-Moment Relation

The chart in Figure 25 represents the relation of the Kidd Mine D data from January 2012 to September 2016; the subset of the log of total radiated seismic energy and the log of average seismic moment recorded in the database. The slope of the line in a typical energy-moment relation is generally around 1.2 to 1.6 and the data trend serves to determine the overall reliability of the recorded data. The Kidd data follows a trend line with a slope of 1.45 with no marked changes of the overall population of events and can be considered well behaved. Some of the events do not fit the overall trend: these represent less than 1% of the event population, they are a low magnitude, (< ML -3.0) and are not considered significant for the purpose of this study.

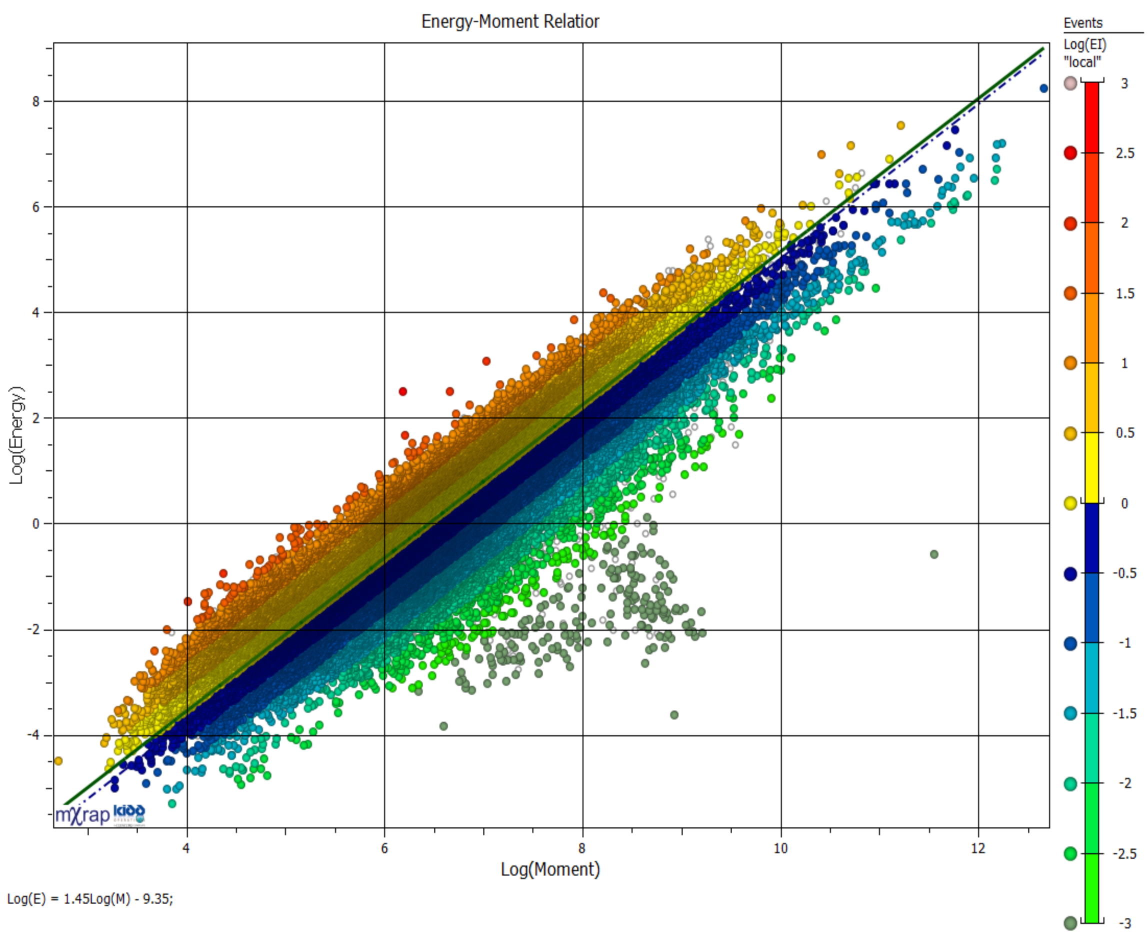

Figure 25: Kidd Mine D, Energy-Moment Relation. Events from January 2012 to September 2016, events displayed according to the log(EI) legend.

4.6 Energy Index and Cumulative Apparent Volume

The following examines the Energy Index (EI) and the Cumulative Apparent Volume (CAV); these are used to understand the changes in energy in the seismic events recorded in Mine D, and can be useful as indicators of potential instability.

The EI relation between energy observed and energy expected (Eo / Ee) is depicted with the rock mass deformation over time, represented by the CAV. The log(EI) / CAV chart can be a useful tool to investigate stress accumulation and potential strain deformation within specific areas or associated with geological features. As mining induced stresses are redistributed around excavations and localized stresses increase, the log(EI) tends to fluctuate in response to the changing conditions with a typically low CAV response. Instances of rock mass failure will be expressed as a decrease in log(EI) and local stresses; and a large failure will be seen with a sudden changed to the CAV. The EI may be used to identify potential areas of rock mass instability. Areas where the log(EI) is greater than 0 are accumulating stresses and the rock mass is undergoing fracturing as the log(EI) value decreases to less than 0.

The graphs depicted in Figure 26 show periods with a clear relation between the log(EI) and CAV in which individual rapid energy drops are associated with the relatively significant increase in apparent volume; while other periods indicate rapid energy drops with relatively static volumes. The overall data for Mine D indicates continual increase of CAV with significant rate changes in brief, distinct periods of time. Significant CAV changes indicating large scale failure are not typical: the sharp change of CAV in the centre graph in Figure 26, where the CAV shifts by four magnitudes may reflect an artifact of seismic system updates rather than actual rock mass failure events due to mining.

The nature of the CAV magnitude change cannot be explained strictly with an overview of the data. Areas of interest for subsequent review of instability reflected in the energy variations are further described in Section 4. Changes in the mining rate may be assumed strictly on the basis of the data, although additional information is needed to explain unusual occurrences. The general trend shows a decrease in log(EI) / CAV fluctuations toward the end of the period (2015-2016).

The increased CAV in the Kidd Mine D data indicates an increase in fracturing in the rock mass, along with a spatial record of seismic activity in the far-field rock mass outside of the development mining areas combine to indicate that the rock mass in the abutment is experiencing yielding and may be influenced by geological features. The confinement in the far-field rock mass provides support, however, the stope and pillar abutment areas with reduced confinement, or newly developed openings, may be sufficiently fractured to induce gravity fall of loose blocks and relatively shallow deformation.

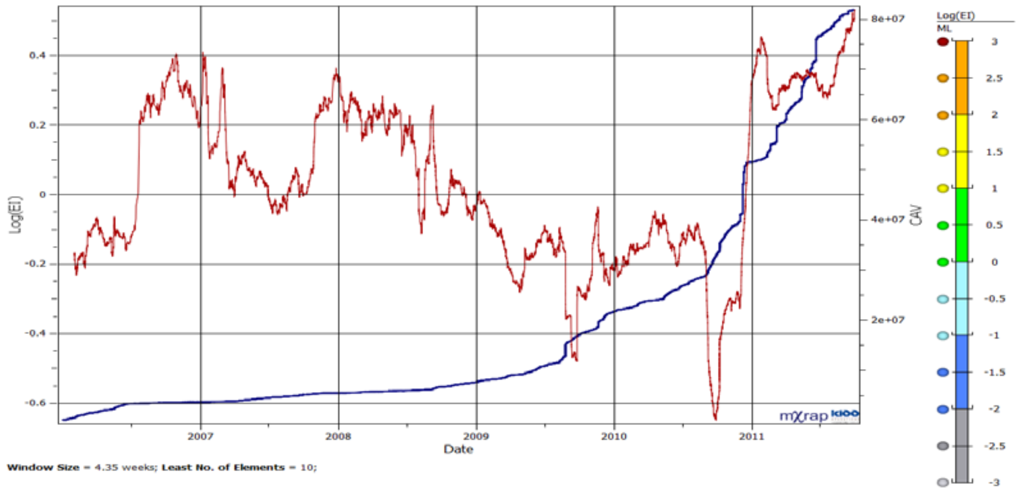

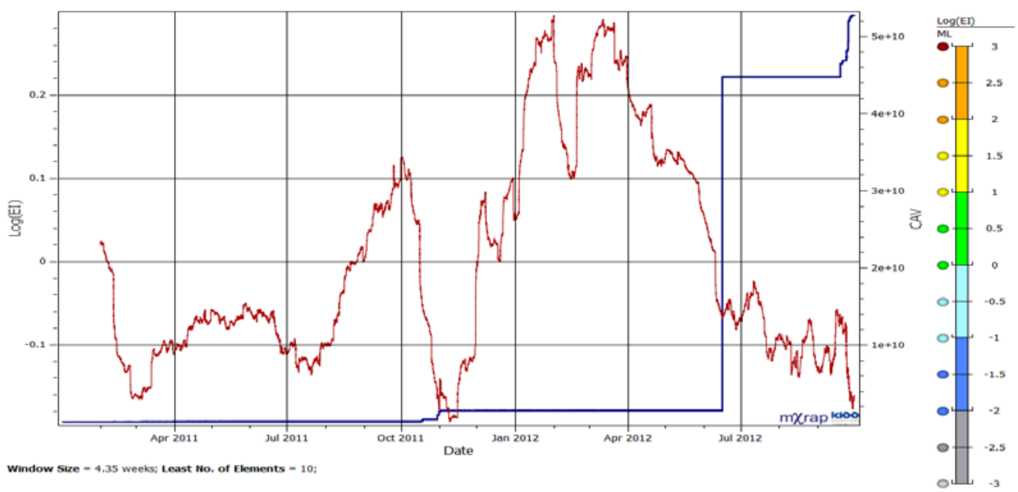

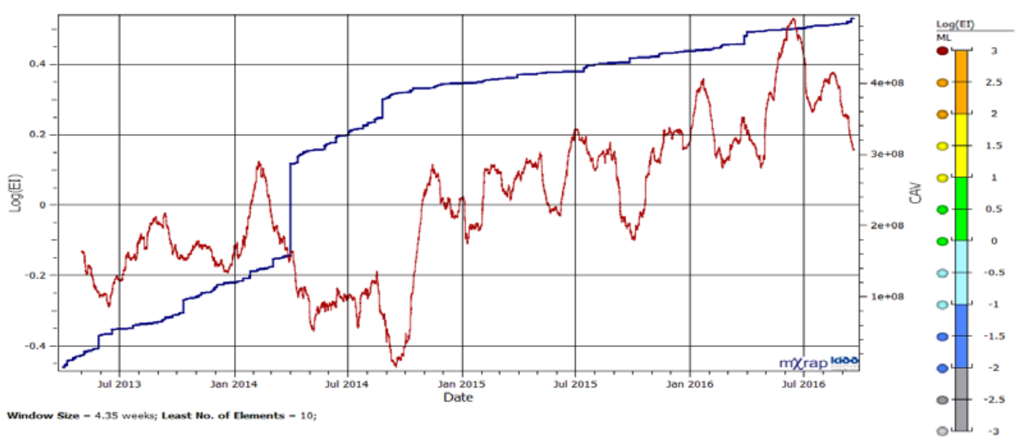

Figure 26: Kidd Mine D seismic data showing the Energy Index (log(EI)) relative to the Cumulative Apparent Volume (CAV) for: (Top) January 2006 to October 2011; (Centre) March 2011 to October 2012; and (Bottom) November 2012 to September 2016.

4.7 Mining Induced Seismicity

In general, underground mining related seismicity occurs as a result of development activity. Significant increases in event frequency can be correlated to excavation blasting; energy fluctuations signify stress increases and large seismic related deformation may be associated with pre-existing geological structures.

The geometry of excavations affects seismic response and includes the size of the individual excavations (stopes, drifts, etc.), spacing between levels, drift dimension, stopes and other related infrastructure and their locations relative to one another. The geological structures and their spatial relation with the geometry has a significant role in the layout of the mine development and impact the intensity and frequency of seismicity. Atypical seismic activity may be associated with a combination of high stress and weak geological features, and seismicity may increase with a decrease in confinement related to development. Stress related seismicity tends to occur directly after blasting while stresses are redistributed.

Three primary modes of seismicity typically occur during development and can be described as:

- Stress driven seismicity: Stresses increase as mining progresses deeper due to gravity loading and the stresses typically concentrate around excavation openings. Highly stressed rock will fail under conditions where the stresses exceed the rock strength. Stronger rock mass is associated with rockbursting and sudden failures are seen as seismic energy variations.
- Fault related seismicity: The location, persistence and type of faults in the mining footprint directly affect the seismic response. High energy release occurring near faults indicate a likely fault-slip mechanism.

- Pillar and abutment related seismicity: Blasting for large openings such as stopes causes stress redistribution and accumulation around pillars and abutments.

High magnitude events in hardrock mines are more likely to cause damage to excavations, while smaller events may cause smaller localized damage or no damage to excavation boundaries. This review identifies the location of high magnitude events and explores the associated seismic occurrences, potential spatial groupings and their location relative to existing excavations or geological structure. The relative location and time of the large events provides clues as to the mechanism and whether future mining may be located in potential hazard areas.

Spatial filtering in discrete areas of Mine D, with the identification of high magnitude events and spatial clustering of events depicted relative to the stope and level development shown in Figure 27. Far-field seismic events that are not directly related to stope development blasts can be seen extending beyond the periphery of the rock mass, away from the primary development.

The seismic event records in the far-field areas away from active mining are similar to results of studies conducted at Creighton (Cotesta *et al.,* 2014) where stress redistribution and rock mass fracturing, shearing, fault-slip events and yielding behaviour is identified as stresses are shed away from the development. Increased stresses and seismic activity is recorded in these outer regions, and the effects may be seen in pillars and abutments. Discussion of the Creighton Mine review by Cotesta *et al.,* (2014) is presented in Section 2.3

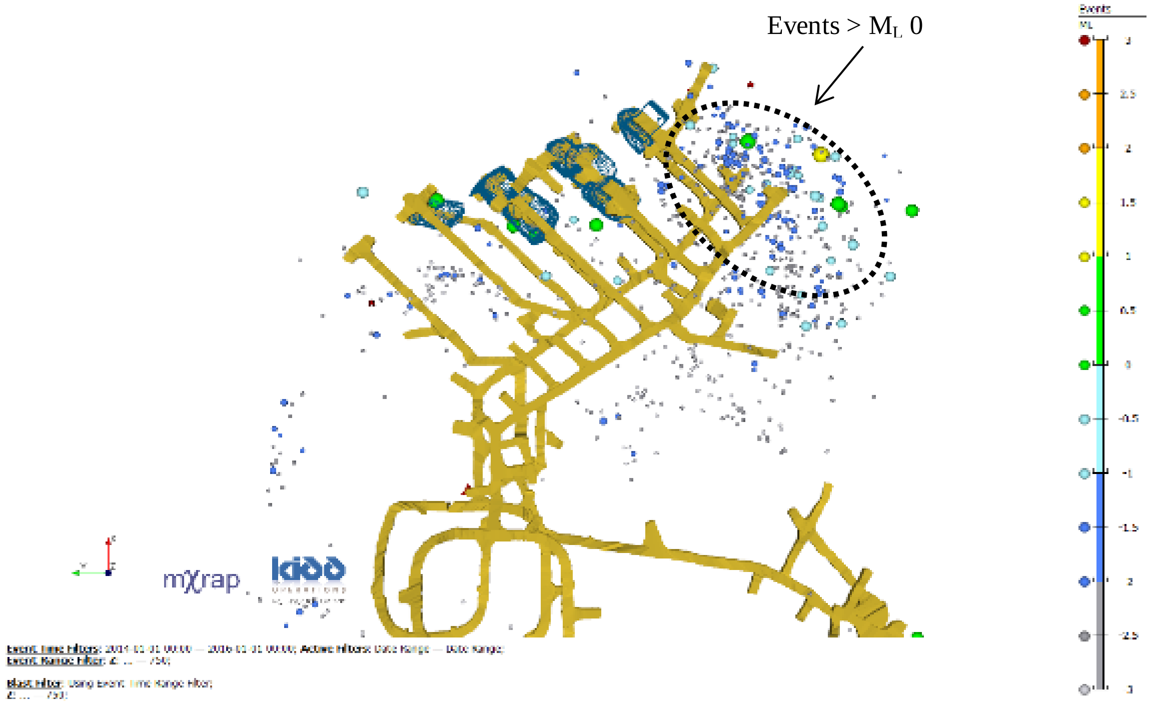

a) Plan View

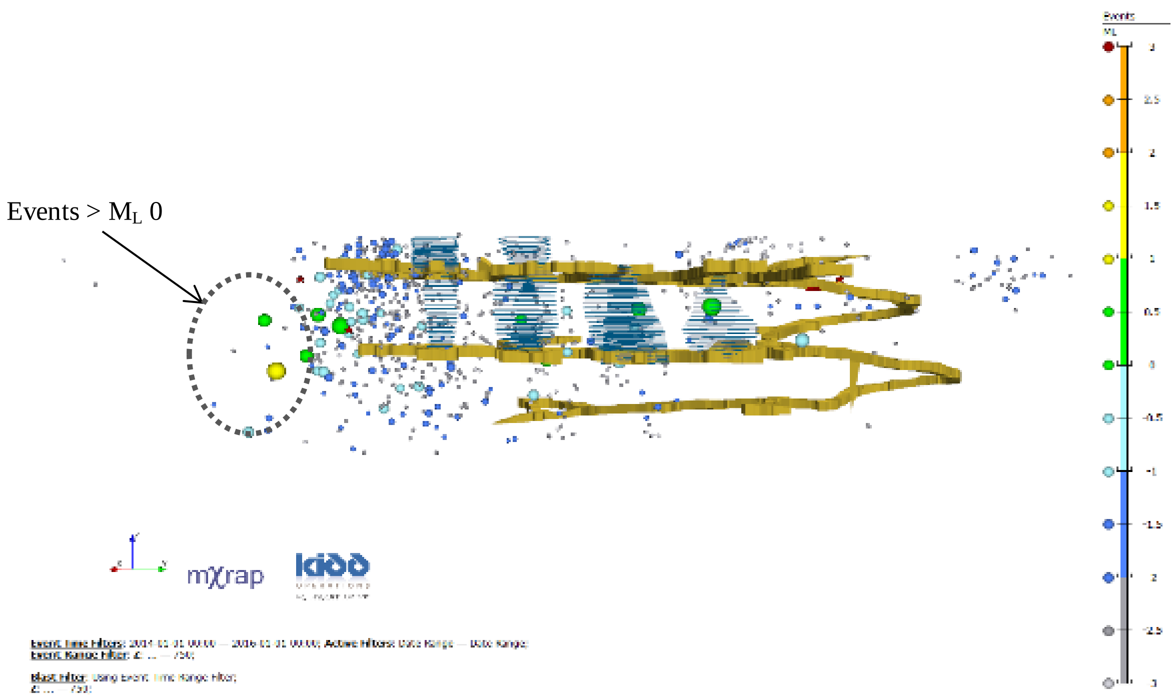

b) Isometric View, Looking West

Figure 27: Lower Mine D, Block 4, 9400, 9500 and 9600 Level with stopes and seismic events, a) Plan View and b) Isometric View, Looking West, depicted in Local Magnitude, M_N. Multiple events are recorded with > M_N 0 in far-field rock mass.

4.7.1 Summary of Events

A temporal and spatial review of seismic activity in Mine D was conducted to understand the frequency distribution in different production areas. A higher proportion of events, approximately 65%, occur in the later years of Mine D development from approximately 2012 to the end of the data set in September 2016. A general distribution of events is outlined monthly from January 2012 to September 2016 in Figure 28.

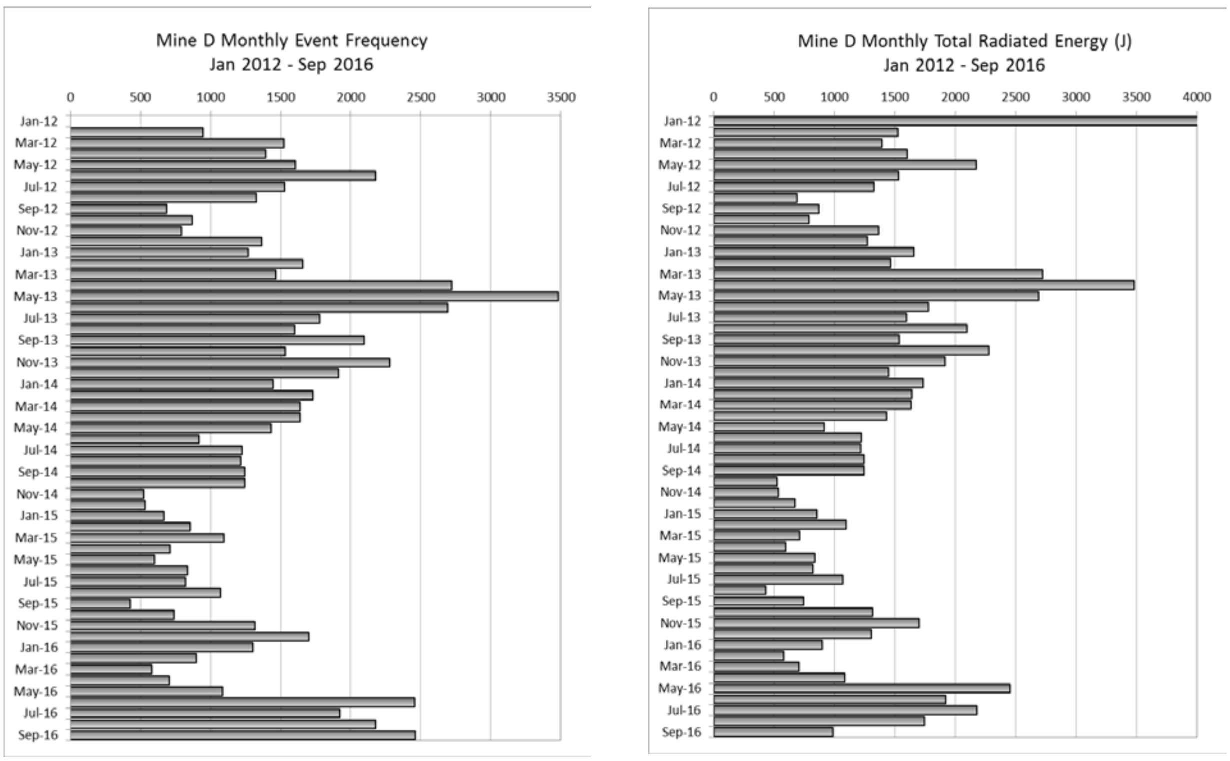

Figure 28: Mine D monthly event distribution from January 2012 to September 2016.

The event rate and energy release generally follow the same monthly distribution and observe similar behaviour. Typical extraction rate increases would result in event rate increases, however, the large number of events occurring in 2013 and in 2016, are likely representative of the proportion of fault or stope blast seismicity in the population. Mine D general arrangement, identifying seismic event distribution in mining Blocks 1 to 4, with a simplified representation of mine levels and corresponding metres below surface is shown in Figure 29.

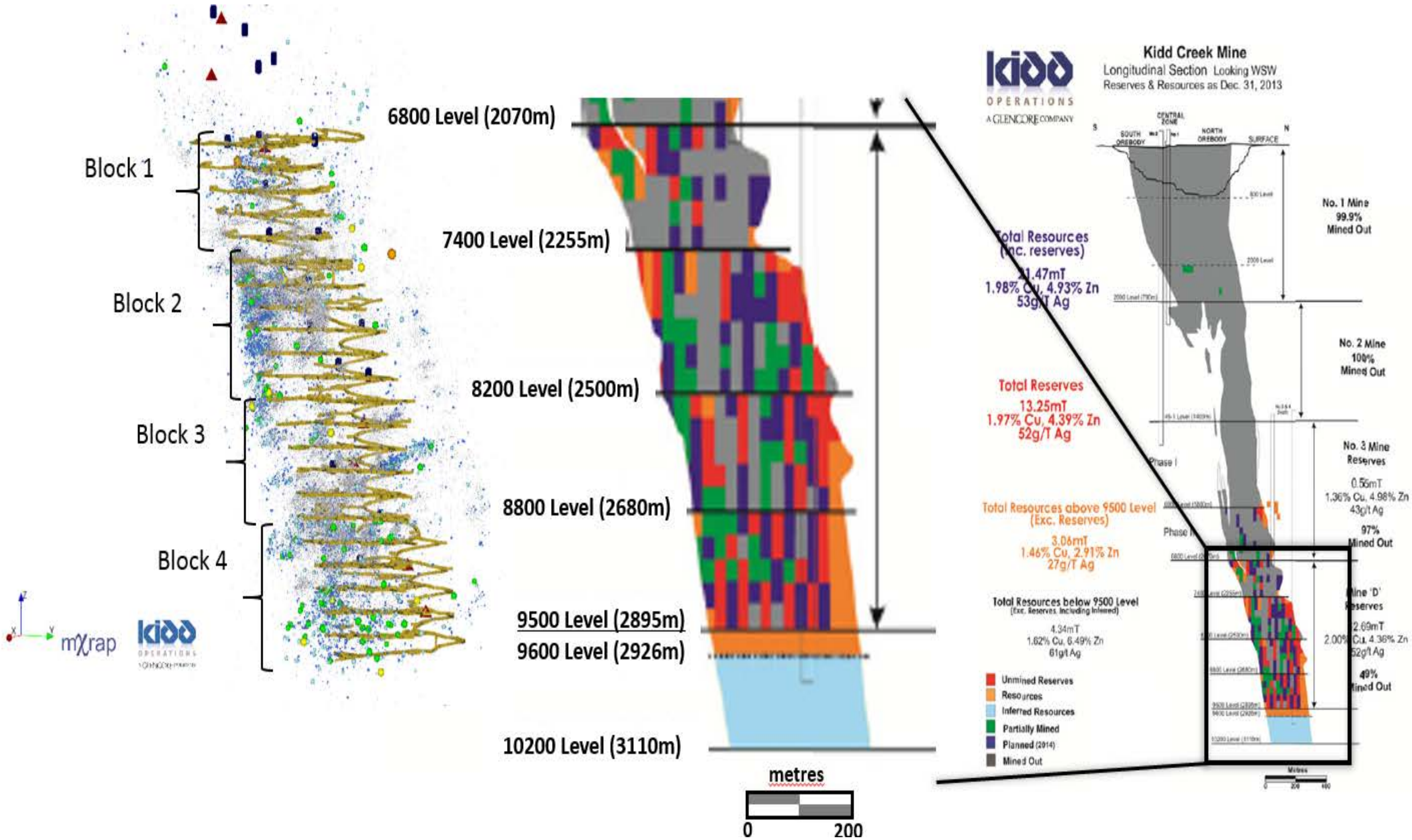

Figure 29: Kidd Mine D (Left) Seismic event distribution, mining Blocks 1 to 4; and (Right) Simplified representation of levels and metres below surface relative to the overall layout of the entire Kidd Mine.

Seismic events can often be related directly to blasting. A graphical distribution of event frequency by level is shown in the graph in Figure 30 (Left), with a comparison to frequency of inferred blasts, distributed by levels (Right). The occurrence of high frequency events and blasts depicts a good correlation, underlining the direct relation of mining induced seismicity. A graphical display of all seismic events indicates where blasting is occurring and the locations of large events indicate where rock mass is failing.

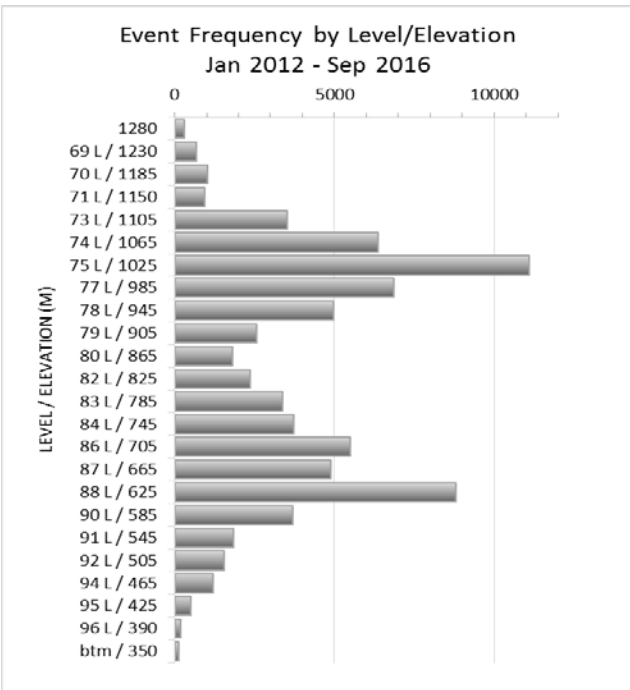

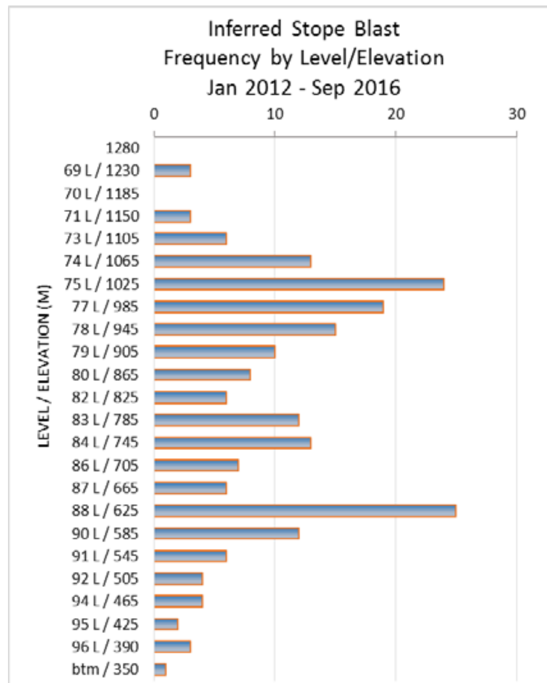

Figure 30: (Left) Distribution of Events in Mine D by Level and metres below surface. (Right) Distribution of significant blasts, by level and metres below surface.

Significant blasts, such as stope blasts, will exhibit a marked increase in event frequency, localized around blast time within a narrow time frame, and represented by a stepped increase in the cumulative events when plotted. Identifying each of these occurrences can be useful to infer blasts from seismic data. An example of higher event rates in a magnitude-time chart is depicted in Figure 31: two dates are outlined; July 17, 2015, with a marked increase; and July 23, 2015, exhibits a moderate event rate increase which may be due to a smaller blast volume. The seismic data in the period of January 2012 to September 2016 contains 202 distinctive event rate increases; approximately 95% of these can be associated with blasting, and the remaining 5% are less obvious and may be associated with blasting or with other seismic events not related to production.

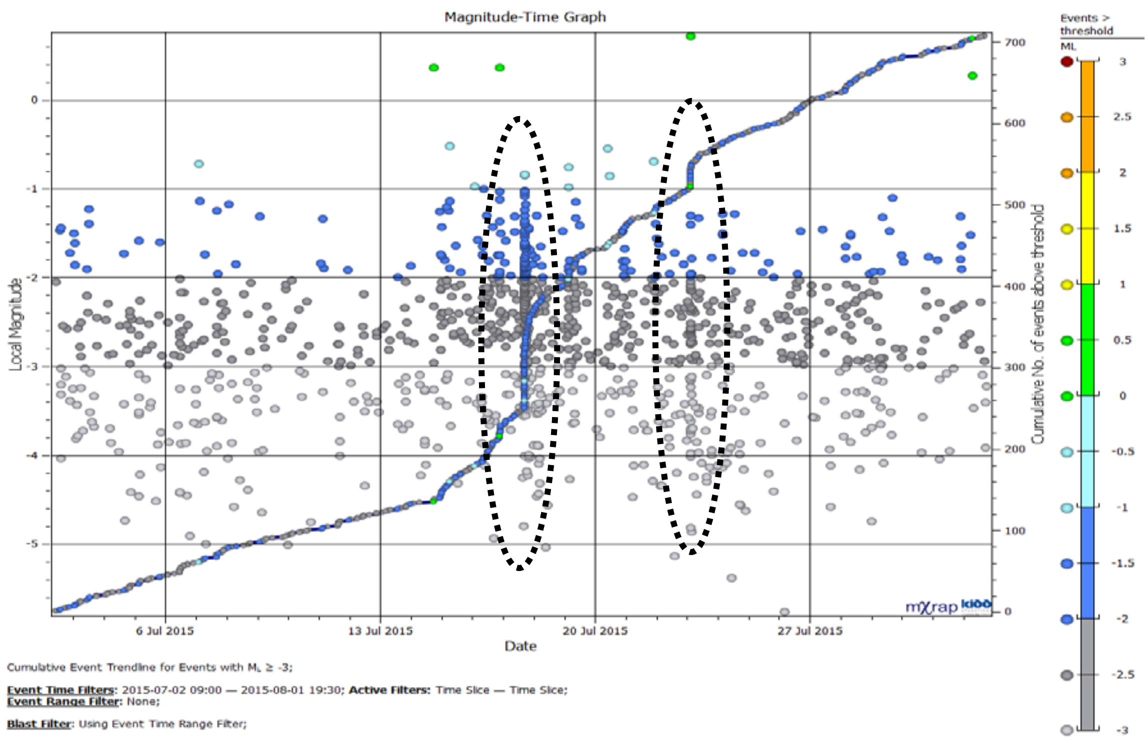

Figure 31: Example of typical event rate increase seen in data as a result of stope blasts with accompanying stepped increase in cumulative events, plotted as a blue line; High event rates outlined on July 17 and July 23, 2015.

4.8 Large Events

Seismic events recorded with a magnitude greater than $M_L = 0$ will be considered high magnitude events. Understanding the spatial and temporal occurrences of the high magnitude events provides a starting point for locating potential interactions of the effect of blasting, geometry and structure. There are fewer than 1% of events, from January 2012 to September 2016, that are high magnitude; these are identified on a monthly occurrence in Figure 32, by level in Figure 33 and displayed in relation to the Mine D levels in Figure 34.

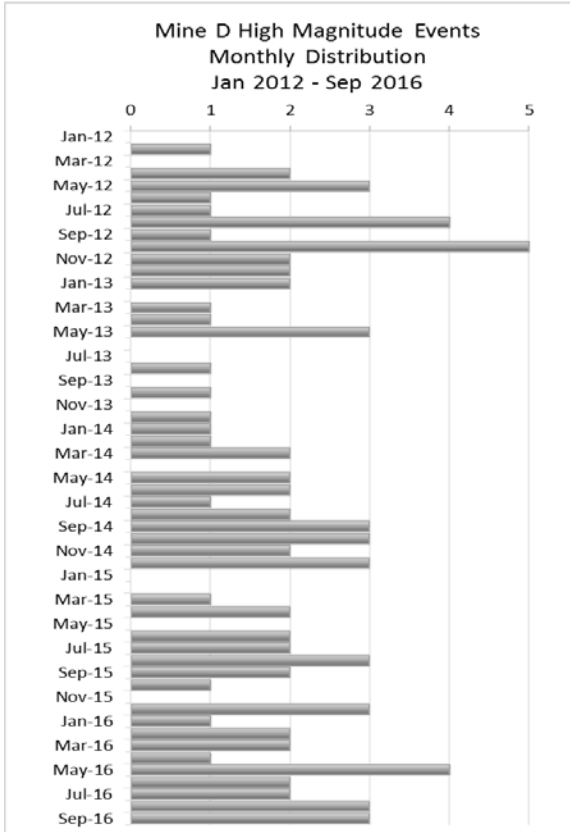

Figure 32: Mine D High Magnitude events - monthly distribution from January 2012 to September 2016.

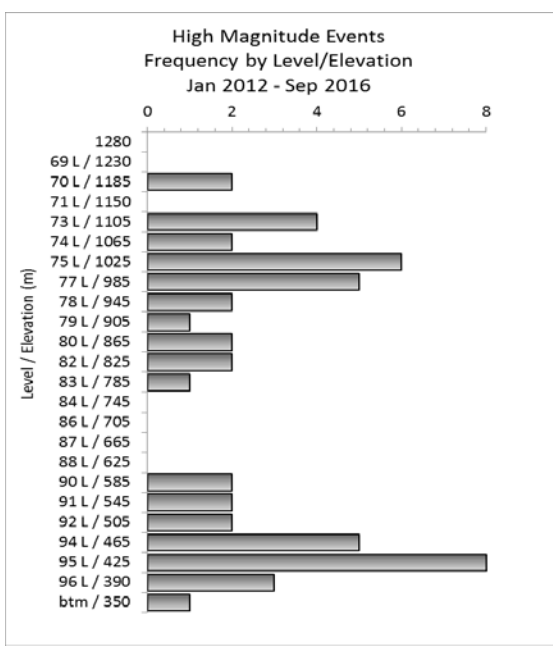

Figure 33: Mine D high Magnitude events, distribution by level, January 2012 to September 2016.

There are ten high magnitude events, occurring from January 2012 to September 2016, recorded with a local magnitude greater than or equal to M_L 1.0; four of these occur during periods of blasting, as inferred from the data; and the remaining six occur outside of blast times. The M_L 1.0 and greater events are listed in Table 5.

Table 5: Events with M_L >= 1.0; January 2012 to September 2016

Inferred Blast (Y/N)	**Date - Time**	**Level / Elevation (m)**	**M_L**
N	Aug/23/2016 13:28	btm / 350	1.02
N	Jul/16/2016 4:46	82 L / 825	1.58
N	Feb/3/2015 5:27	75 L / 1025	1.38
N	Nov/18/2014 4:41	92 L / 505	1.11
Y	Oct/11/2014 3:43	74 L / 1065	2.24
Y	Aug/30/2014 5:52	75 L / 1025	1.17
N	May/26/2014 3:52	95 L / 425	1.19
N	Aug/13/2012 6:11	92 L / 505	1.15
Y	Jul/25/2012 3:50	82 L / 825	1.27
Y	Jan/4/2012 4:49	83 L / 785	1.34

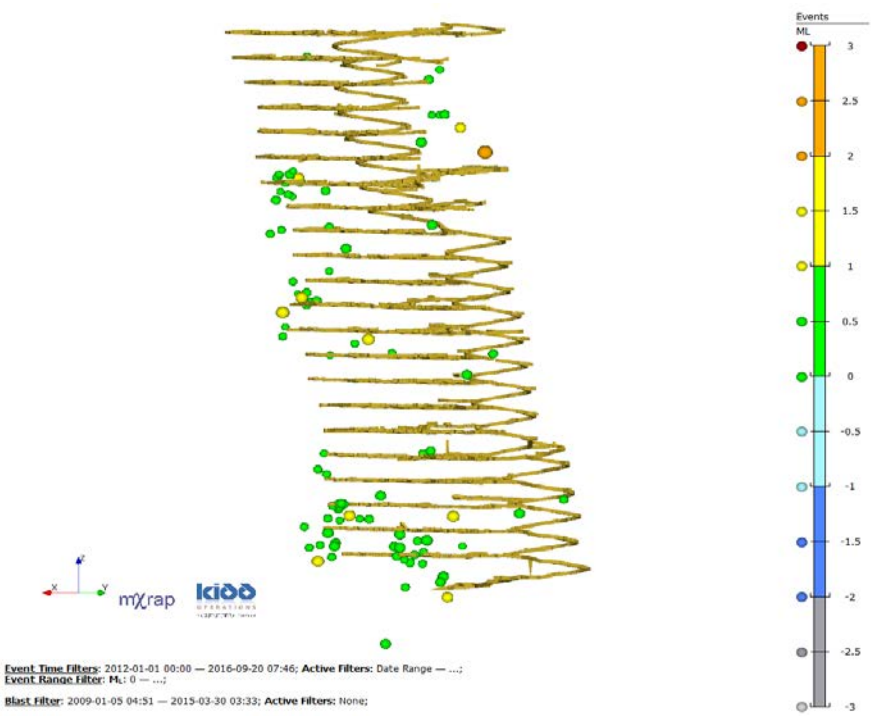

Figure 34: Mine D, High magnitude events from January 2012, to September 2016: Green symbols (M_L 0 to 0.99); Yellow and Orange (M_L 1.0 to 2.24).

4.9 Areas of Interest

Three seismic regions of interest were selected for additional review, these are generally outlined in Figure 35, and are based on the following observations:

- spatial grouping of events;
- grouping of events in the area;
- occurrence of high magnitude events within a grouping; and
- location relative to active mining.

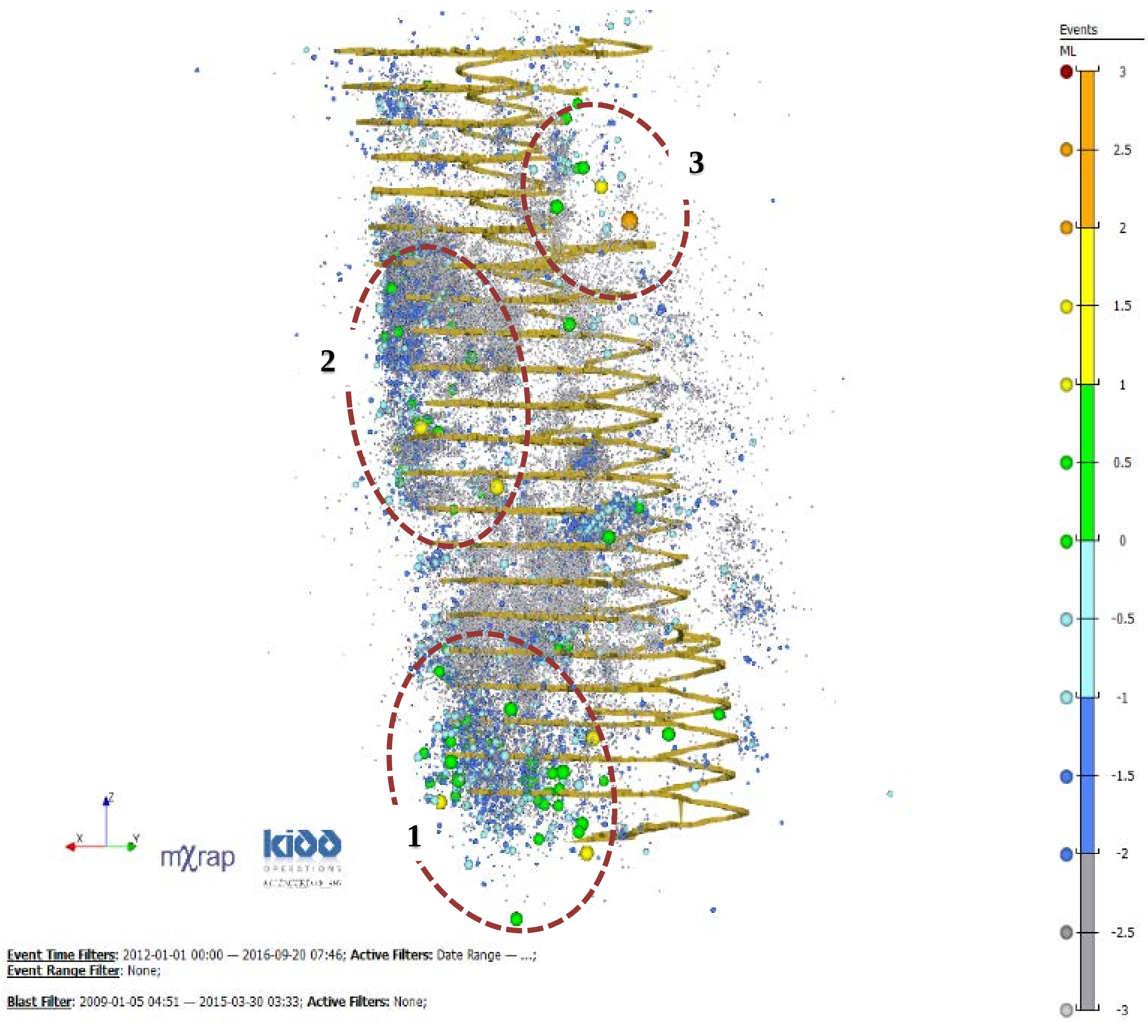

Figure 35: Mine D January 2012 to September 2016 seismic events; three outlined areas selected for review.

The large events occurring in selected areas of the mine are considered for potential hazard and damage to excavations. The variations of stress loading due to mining, rock mass properties and geological structures will create variable conditions for rock mass failure. Failure can occur in a gradual, yielding manner, or in a sudden, unstable manner, both will result in energy release.

The sudden release of energy in an unstable manner is typically associated with large events. Large seismic events that cause physical damage to excavations may result in minor rock spalling or more significant, catastrophic rock mass fracturing, with potential for extensive damage or destruction of excavations.

Temporal, spatial and seismic parameters for each area were reviewed to identify potential similarities or constraints that may be in place due to geological structures as well as the distance from existing excavations. Seismic events are not limited to areas of active stope blasting and may be an artefact of stresses migrating as development advances or may be as a result of movement along structure. Table 6 lists the large events, greater than M_L 0, in each of the three areas selected. The event mechanism listed is based on the S:P energy ratio, with S:P > 10 considered shearing events (Hudyma, 2010).

Table 6: Kidd Mine Large Event Summary, by Area of Interest

Area	Date	Time	M_L	log EI	AS (MPa)	S:P	Mechanism	Distance from Existing Exca-vations	Within 24 hrs of Mine Blast (Y/N)
1	Jul/6/2012	16:51	0.21	-0.5	0.1	5.7	Yielding	> 50 m	Y
	Feb/5/2013	7:46	0.25	-0.6	0.1	2.8	Yielding	> 50 m	N
	May/26/2014	3:52	1.19	-0.4	0.3	2.1	Yielding	> 50 m	Y
	Aug/14/2014	10:42	0.28	-1.0	0.1	4.8	Yielding	> 50 m	N
	Oct/14/2014	17:48	0.21	-0.8	0.1	2.2	Yielding	> 50 m	N
	Sep/26/2015	18:20	0.59	-1.0	0.1	2.8	Yielding	< 50 m	N
Average				**-0.72**	**0.12**	**3.4**			

Area	Date	Time	M_L	log EI	AS (MPa)	S:P	Mechanism	Distance from Existing Exca-vations	Within 24 hrs of Mine Blast (Y/N)
2	Dec/25/2013	23:21	0.63	0.9	2.2	47	Shear	< 50 m	N
	Jun/13/2014	12:57	0.03	-0.2	0.1	13	Shear	< 50 m	N
	Feb/3/2015	5:27	1.38	0.2	1.0	8.4	Yielding	< 50 m	N
	Mar/24/2015	4:34	0.06	1.3	2.8	7.5	Yielding	< 50 m	Y
	Jul/16/2015	21:39	0.36	0.1	0.3	4.5	Yielding	< 50 m	N
	Nov/18/2015	12:32	0.18	1.4	2.4	131	Shear	< 50 m	N
	Jan/10/2016	1:55	0.09	0.5	0.6	11.9	Shear	< 50 m	Y
	Jan/10/2016	8:48	0.72	0.5	1.1	6.6	Yielding	< 50 m	N
	May/2/2016	1:35	0	1.4	2.5	72.2	Shear	< 50 m	Y
	May/6/2016	23:16	0.24	1.0	1.5	19.1	Shear	< 50 m	N
	Jun/11/2016	5:27	0.04	-0.2	0.1	13.3	Shear	< 50 m	Y
	Jul/8/2016	11:43	0.86	0.2	0.6	15.6	Shear	< 50 m	N
	Jul/29/2016	13:25	0.02	-0.1	0.1	4.7	Yielding	< 50 m	Y
	Aug/25/2016	18:07	0.65	0.1	0.4	6.6	Yielding	< 50 m	Y
Average				**0.51**	**1.13**	**25.9**			
3	Oct/11/2014	3:43	2.24	0.02	1.2	147	Shear	> 50 m	N
	Jul/26/2014	14:26	0.92	-0.7	0.1	35.6	Shear	< 50 m	Y
	Aug/30/2014	5:52	1.17	1.25	7.1	43.7	Shear	< 50 m	Y
	Jun/14/2015	23:29	0.13	0.3	0.4	15.7	Shear	< 50 m	N
	Jul/23/2015	2:37	0.72	0.5	1.0	25.9	Shear	< 50 m	Y
	Dec/1/2015	15:23	0.74	-0.2	0.2	14.9	Shear	< 50 m	N
	Apr/4/2016	10:22	0.21	0.6	0.8	30.3	Shear	< 50 m	N
Average				**0.19**	**1.54**	**44.7**			

4.9.1 Area 1

The events in Area 1 are shown in sectional view, Figure 36(a), and in plan view Figure 36(b). The area of interest encompasses levels 9100 to 9600, however, the large magnitude events are constrained between 9400 and 9500 levels (dashed outline). In plan view, the large events are spatially constrained and occur between 30 and 80 metres from mine development and between 75 and 120 metres from open stopes. The large distances of events from open stopes is a contraindication of rock mass failures into mine excavations. Two mine faults, seen in the plan view, may be coincident with the large events.

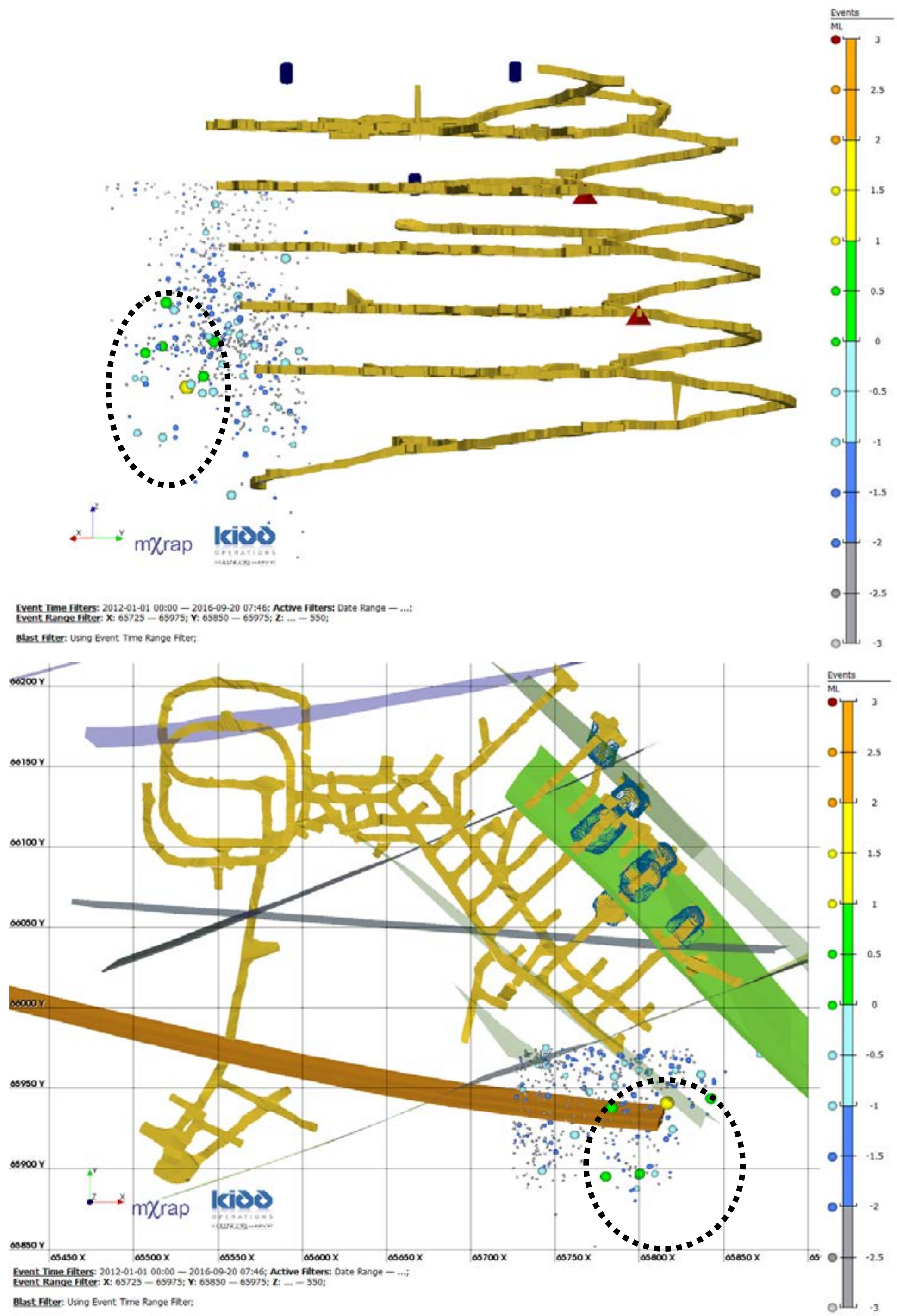

(a)

(b)

Figure 36: Area 1, 9100 to 9600 Levels, Seismic event distribution;
(a) Section View, looking North West;
(b) Plan View with faults and mined stopes on 9400 to 9600 Levels.

4.9.1.1 Frequency-Magnitude and S:P Energy Ratio

The Frequency-Magnitude relation of the Area 1 population, indicates well-behaved data, as shown in the graph in Figure 37(a):

- the b-value of 0.7 is reasonable, indicating a large portion of events with shearing source mechanism;
- the lower event sensitivity of -2.3 M_L is consistent;
- the data is linear over approximately 3 magnitudes; and
- the maximum expected event size of 1.2 $M_{L,}$ the a/b value at the x-axis intercept, is similar to the largest recorded event.

The S:P Energy Ratio trend indicates fewer shearing events (20%) in Area 1, shown in Figure 37(b), indicate stress-driven fracturing. The high magnitude events all have an S:P energy ratio less than 3, indicating a rock mass fracturing.

The b-value of the population suggests a shearing mechanism while the S:P energy ratio indicates likely rock mass fracturing occurring with the large events. This contradiction may be due to fault-slip occurring under high confinement, in abutment areas away from active mining.

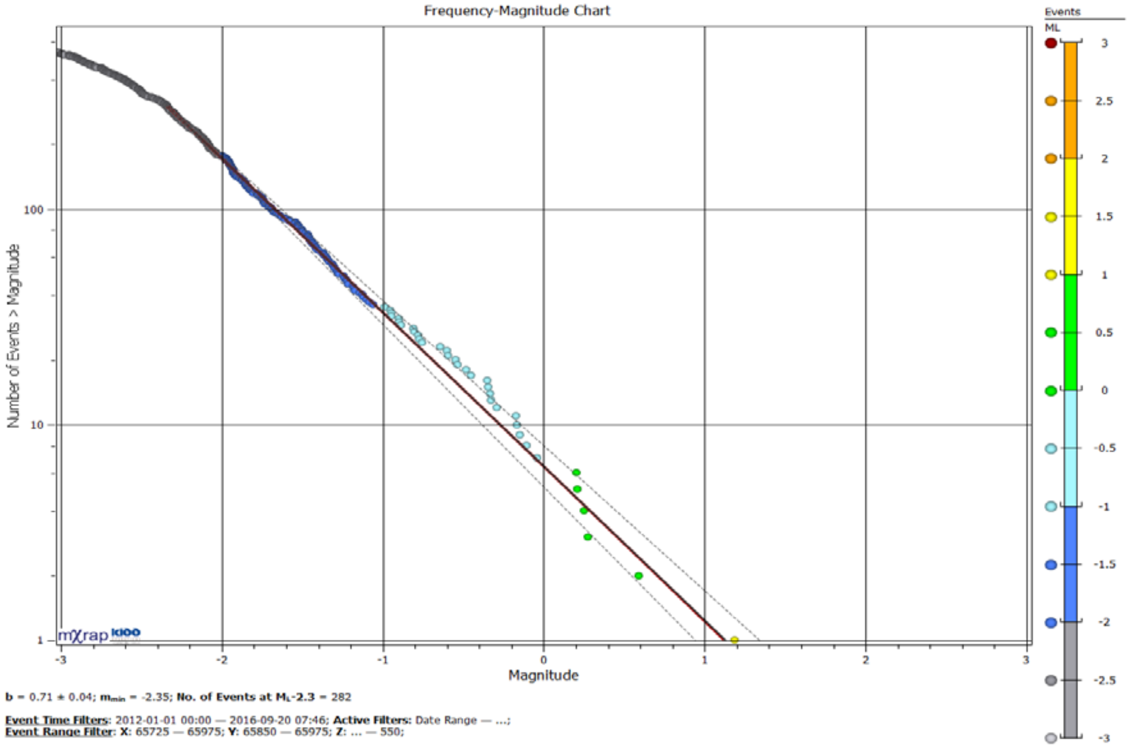

(a)

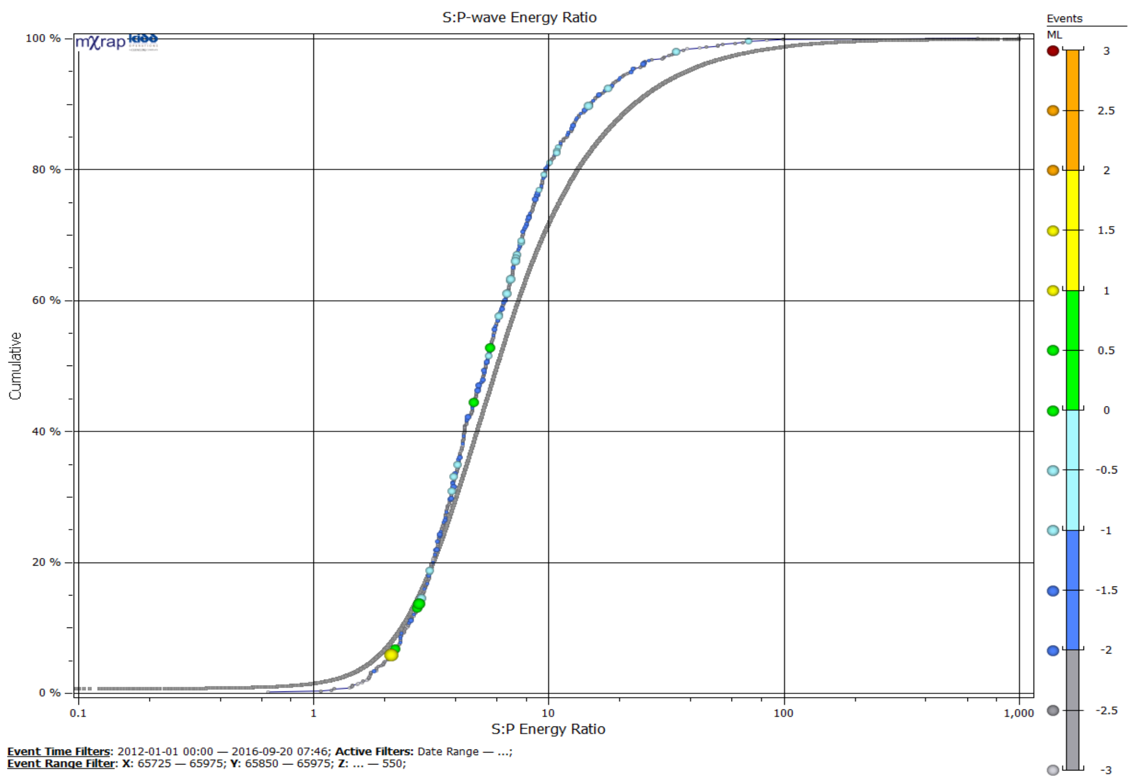

(b)

Figure 37: Area 1: (a) Frequency - Magnitude chart; (b) S:P Energy Ratio.

4.9.1.2 Magnitude-Time History

The Magnitude-Time History of Area 1 Figure 38, shows increased event rates corresponding with periods of increased Apparent Stress. This correlation is typical of large blasts.

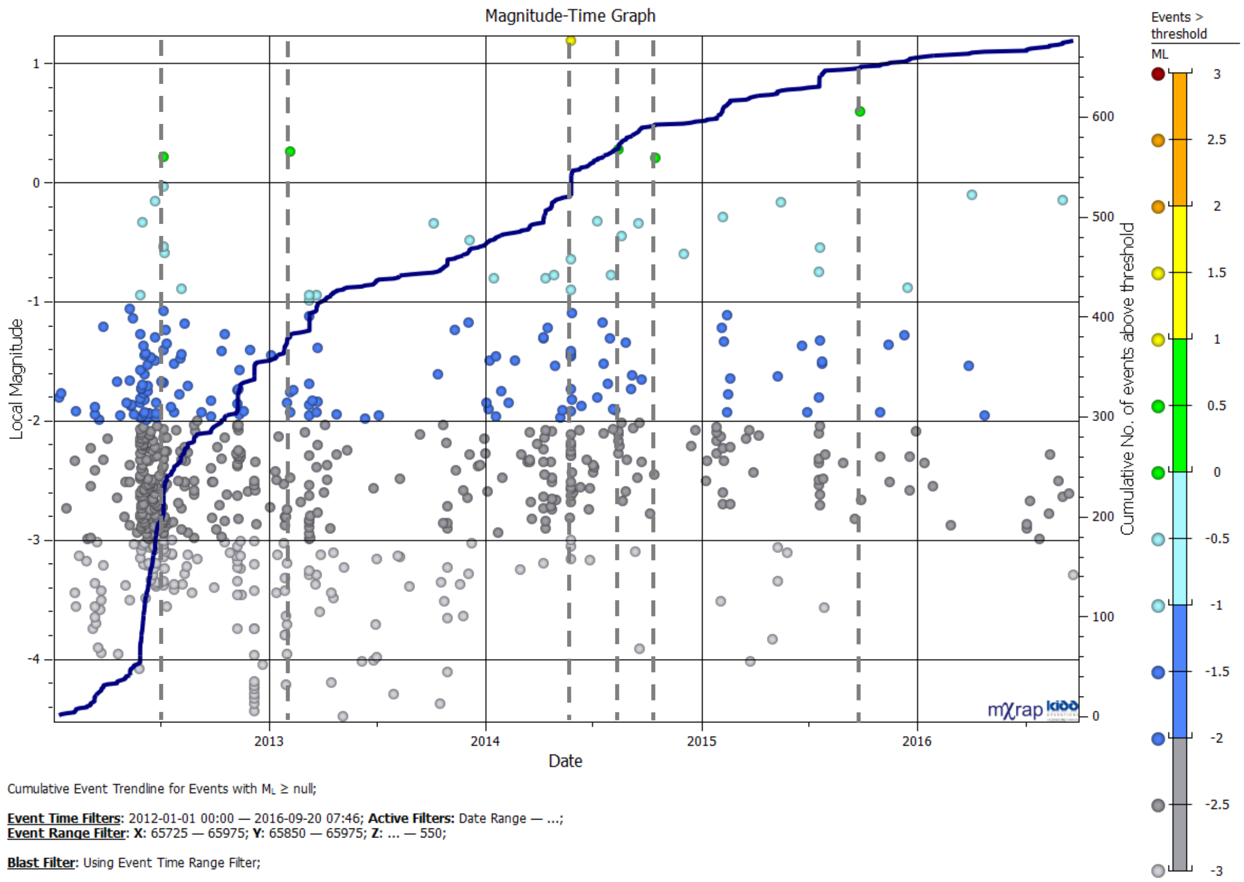

Figure 38: Magnitude-Time History of Area 1.

Observations noted in the Magnitude-Time History chart for Area 1 include:

- The first large event, in July 2012, occurs after a significant increase in seismic event rate, inferred as a series of stope blasts starting in early June 2012;
- The third large event, in May 2014, coincides with a small step in seismic event rate, indicating a large blast; and

- The other four high magnitude events (2, 4, 5, 6) occur outside of the timing of significant seismic responses to stope blasts.

Although the group of large events is well concentrated spatially, the timing of the events is not well correlated with stoping activities in the mine.

4.9.1.3 Apparent Stress

A peak of AS in this area is observed in mid-2012, while the later time period shows a reduced stress and frequency of AS events by 2015-16, illustrated in Figure 39. High magnitude events occur regularly in this time period.

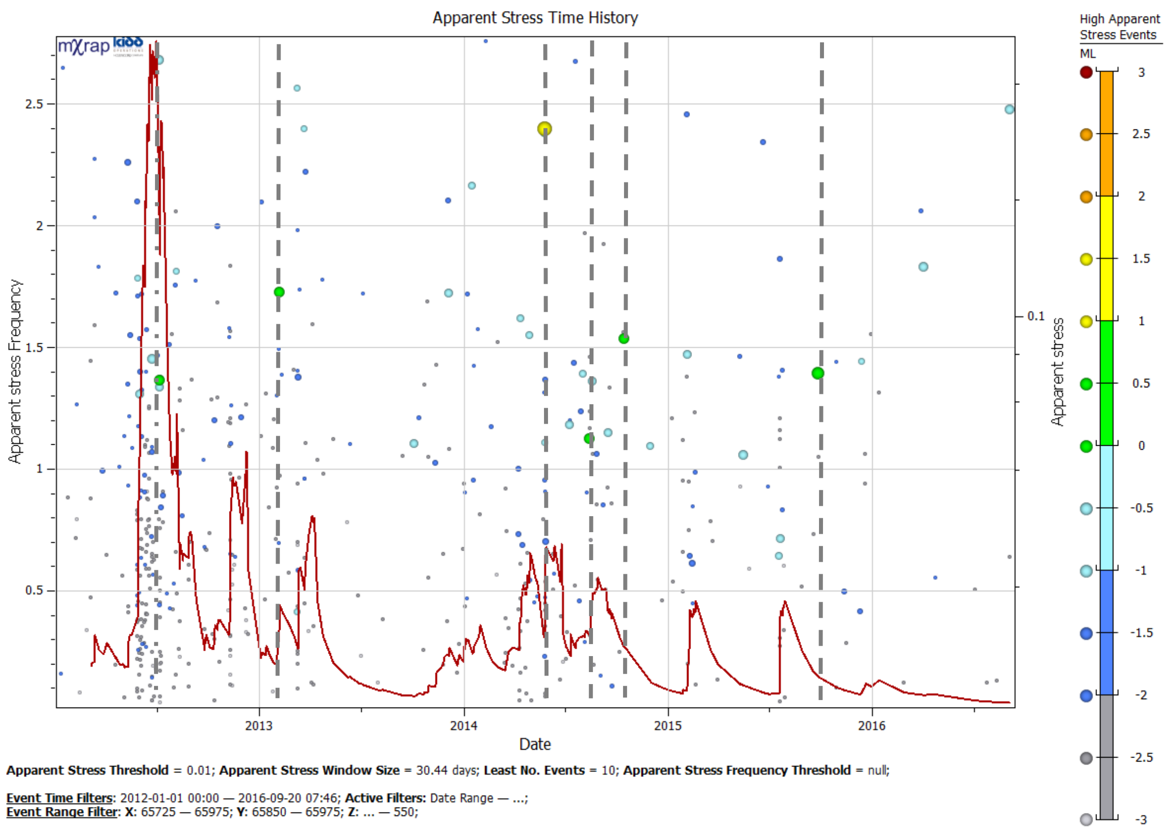

Figure 39: Apparent Stress Frequency Chart of Area 1 data subset.

Observations noted in the Apparent Stress Frequency chart for Area 1 include:

- The first large event, in July 2012, occurs well after the peak in Apparent Stress Frequency for the population, similar to the magnitude time history;
- Large events 2 to 6 occur at a low point in the Apparent Stress Frequency; and
- Large events 1 to 4 directly result in increases in the Apparent Stress Frequency.

The peaks in Apparent Stress Frequency correlate very strongly with increases in event rate seen in the magnitude time history chart, however the large events do not correlate with peaks associated with stope blasting. Local stress redistributions, indicated by increases in Apparent Stress Frequency and associated rock mass fracturing, correlate with the first four large events.

4.9.1.4 Energy Index and Cumulative Apparent Volume

An Instability Analysis of Area 1 (Energy Index, Cumulative Apparent Volume) is shown in Figure 40.

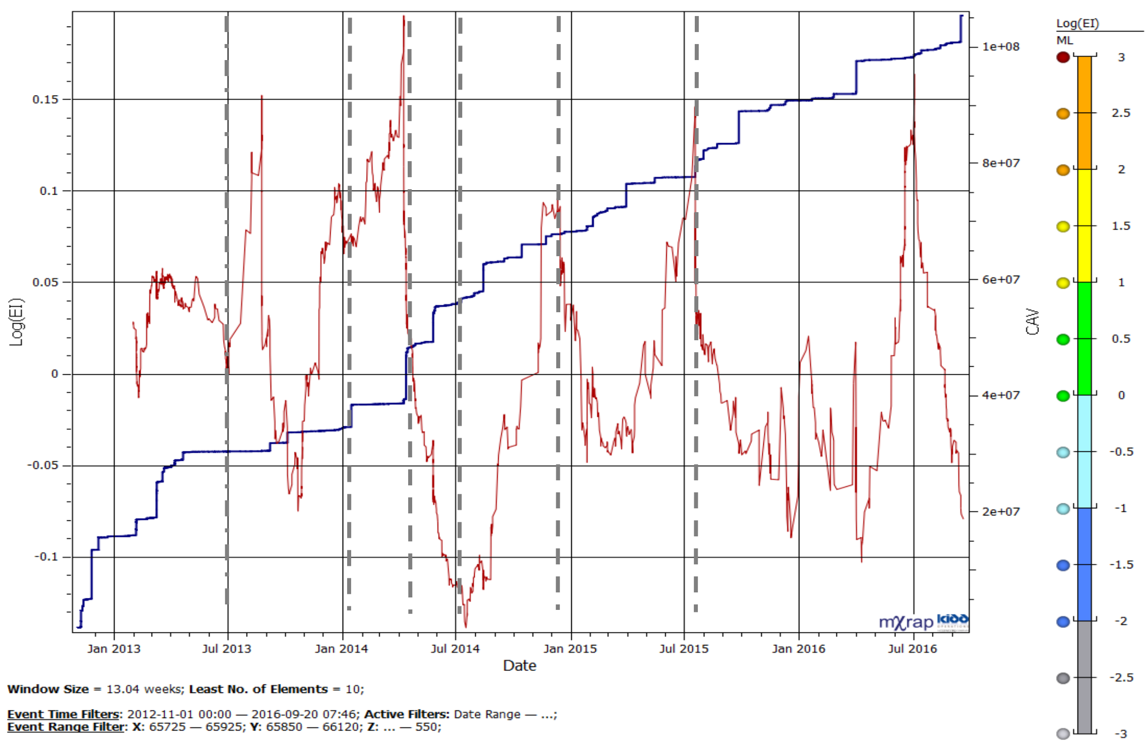

Figure 40: Area 1; Energy Index Log(EI) and Cumulative Apparent Volume (CAV) chart.

The Log(EI) / CAV chart indicates five periods where the Energy Index is greater than 0, signifying increased stress in the rock mass.

4.9.2 Area 2

The second area of interest is located in the south east area, between 7400 and 7900 levels. There is a higher concentration of events near the south access drives and crosscuts with a relatively high event density. Seismicity is occurring along the access drives as well as near stope development. There are 14 high magnitude events ($M_L > 0$), as listed in

Table 6. The seismic records for this area represent approximately 18% of events from January 2012 to September 2016. The seismic event distribution and magnitudes depicted in the section views Figure 41(a) and plan view Figure 41(b) are located in the south east stope and access drives of the 7400 to 7800 levels.

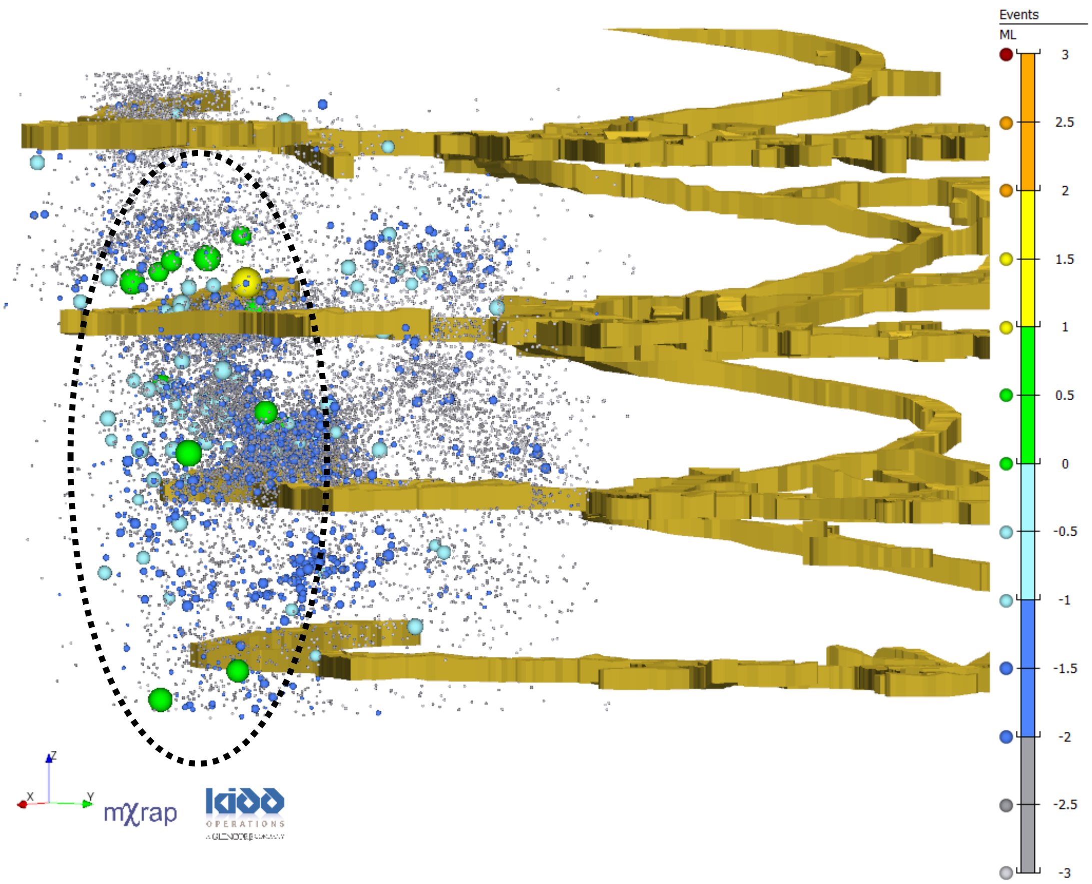

(a)

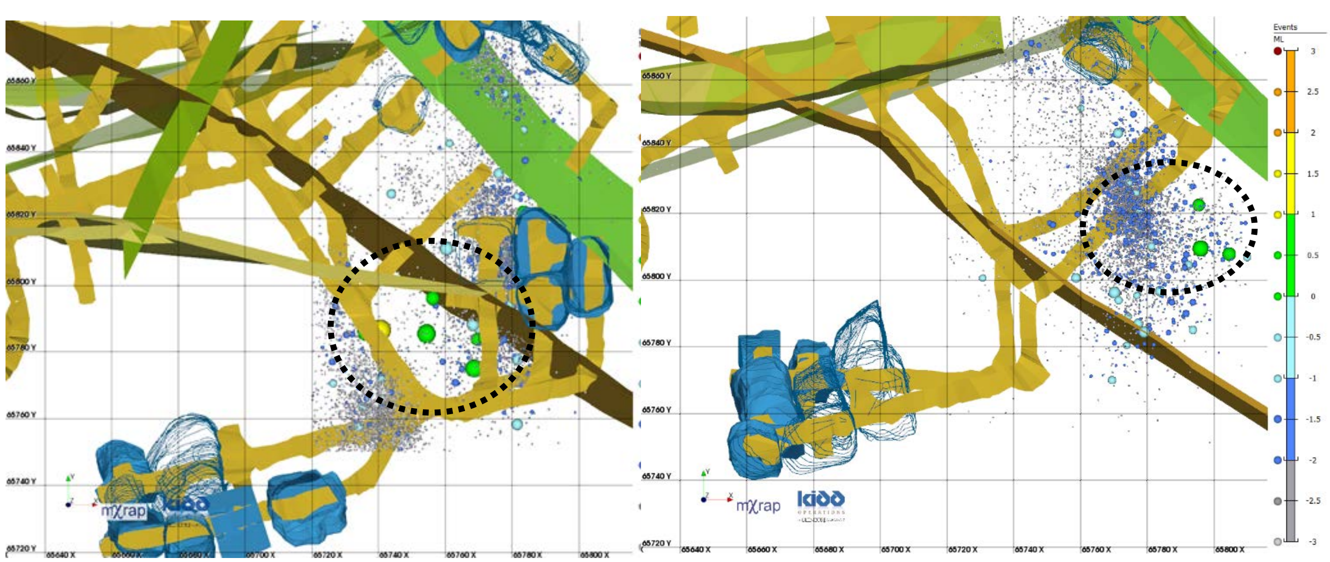

(b)

Figure 41: Area 2, 7400 to 7800 Levels, Seismic event distribution; (a) Section View, looking North West, (b) Plan Views, 7400-7500 L (left) and 7700-7800 L (right), with faults and mined stopes.

4.9.2.1 Frequency-Magnitude and S:P Energy Ratio

The Frequency-Magnitude relation of the Area 2, shown in Figure 42(a), displays strong bi-modal characteristics. The smaller events, $M_L < 0$ have a steep b-value of 1.26 indicates a significant portion of stress driven fracturing events. The larger events, $M_L > 0$, have a flatter b-value of 0.84, indicating shear related, structurally controlled mechanism, also indicated in Table 6 and displayed in Figure 42(b): 8 of 14 large events have an S:P Energy Ratio >10, which is typical of shear related seismic source mechanism.

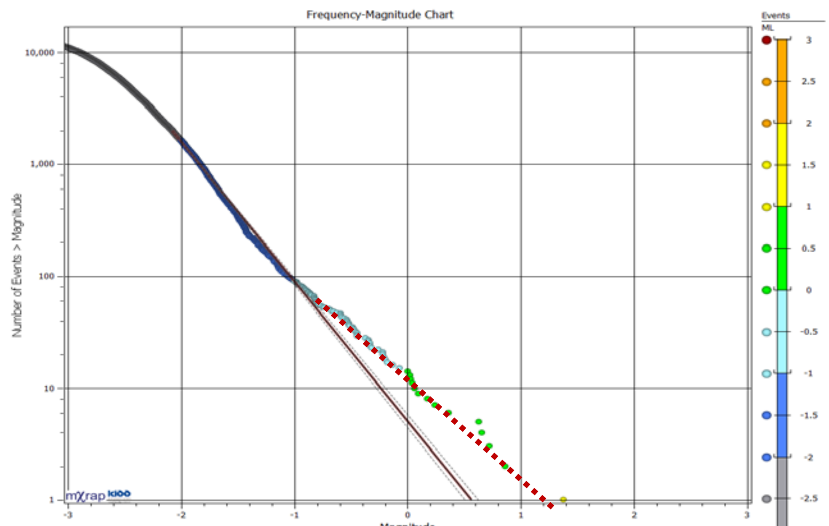

(a) b = 1.25 ± 0.03; m_{min} = -2.09; No. of Events at M_L-2.3 = 3760

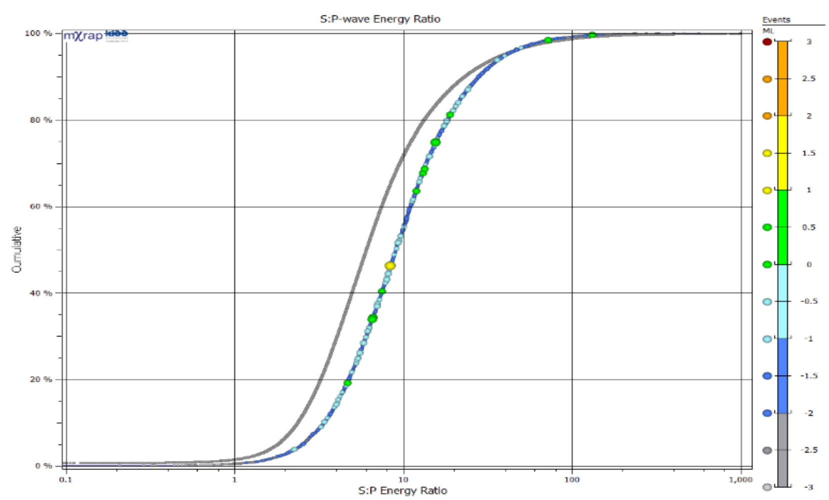

(b)

Figure 42: Area 2: (a) Frequency - Magnitude chart; (b) S:P Energy Ratio.

4.9.2.2 Magnitude-Time History

The Magnitude-Time History of Area 2, shown in Figure 43, shows increased event rates within time periods corresponding with the increased Apparent Stress (Figure 47). The correlation is typically seen at blast times. The high magnitude events generally correspond with the timing of inferred blasts, with the exception of a high magnitude event in early 2015, recorded during a period of reduced seismic activity. Three discrete groupings of seismic behaviour Figure 43 are subdivided and examined further:

a) January 2013 to June 2014 (Figure 44); the event rate in this period indicates periods of large scale blasting with stope development. Two discrete high magnitude events occur, one in December 2013 and one in June 2014;

b) July 2014 to September 2015 (Figure 45); the reduced event rate in this period is indicative of reduced mining activity within Area 2, however, high magnitude events occur without the typical rate of leading lower magnitude events; and

c) September 2015 to September 2016 (Figure 46); two data behaviours are observed – one period of cumulative events and gradually increasing CAV until May 2016; followed by an increase in event rates, indicating resumed large scale blasting, and corresponding high magnitude events.

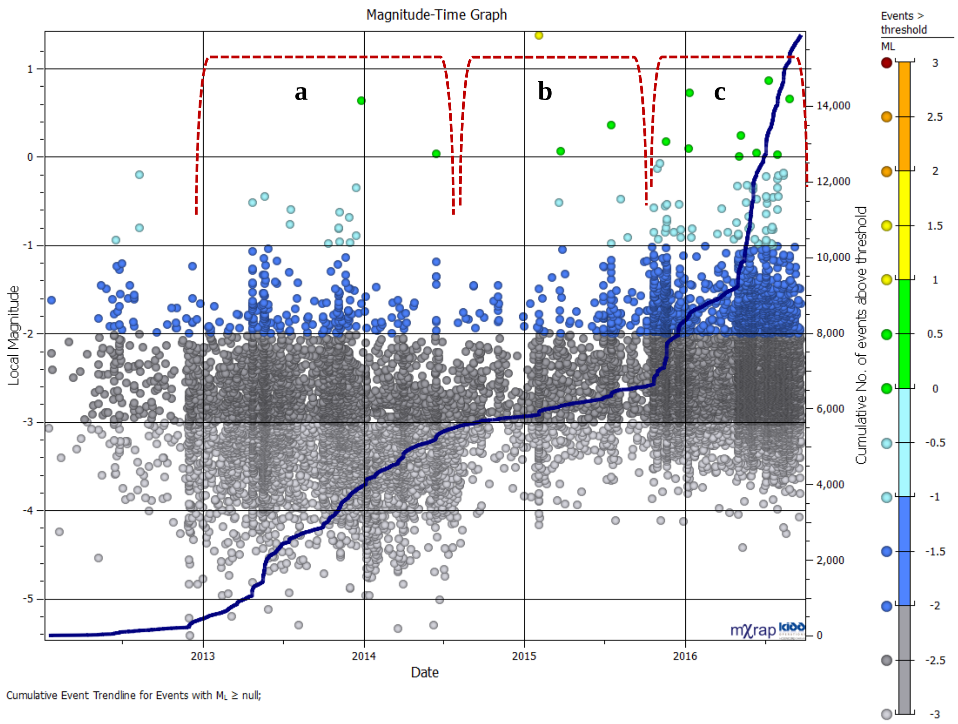

Figure 43: Magnitude-Time History of Area 2; outlining three review periods.

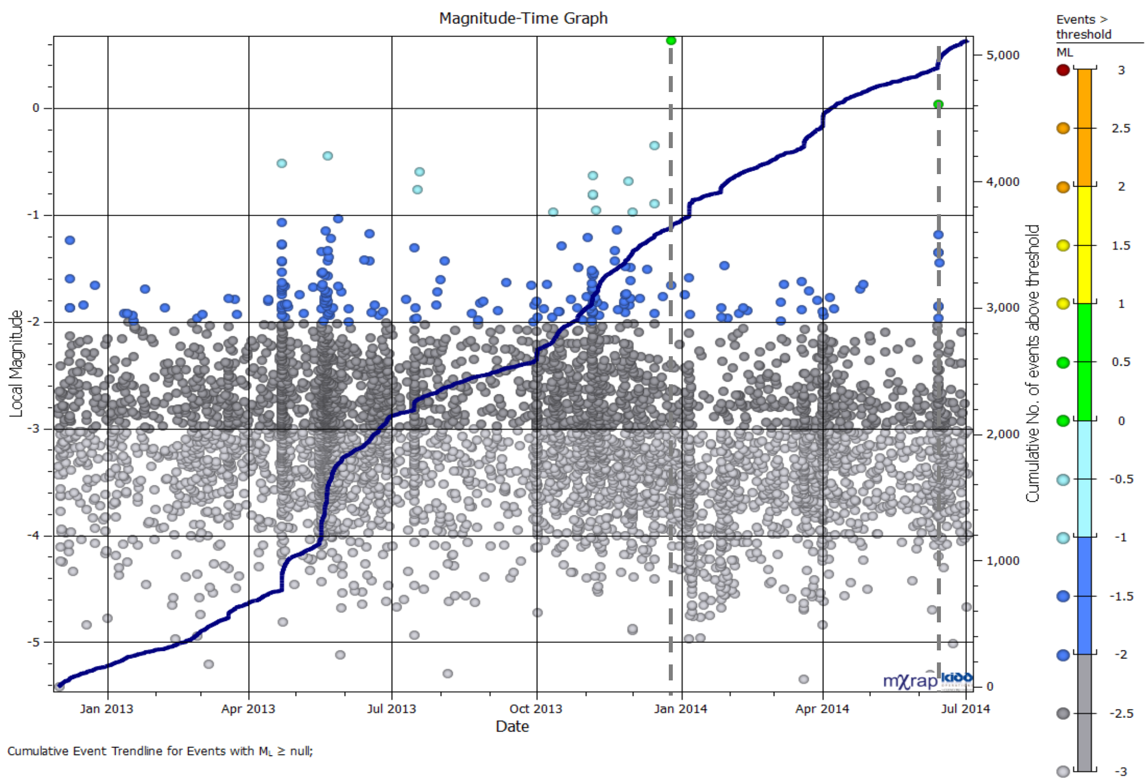

Figure 44: Magnitude-Time History Area 2(a): Dec 2012 to July 2014.

Large blasts are indicated by significant increases in seismic event rates. The first large event of Area 2(a) is not coincident with a mine stope blast, while the second large event appears to occur within a very short time of a stope blast.

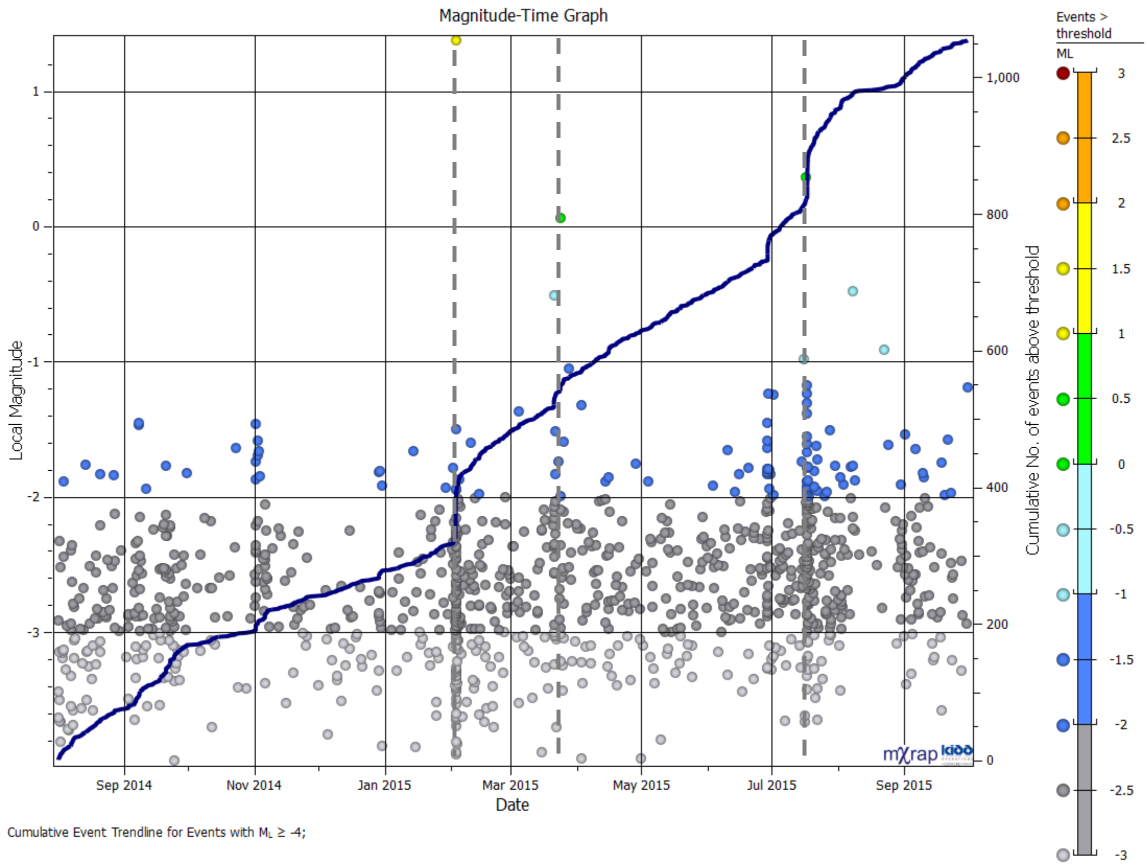

Figure 45: Magnitude-Time History, Area 2(b): August 2014 to September 2015.

This period depicts less mining activity with discrete blasts and relatively little seismic activity in advance of the large events. The first and third large events of Area 2(b) (February and July 2015) are directly following mine stope blasts, however, the second large event (March 2015) occurs a few days after a mine blast.

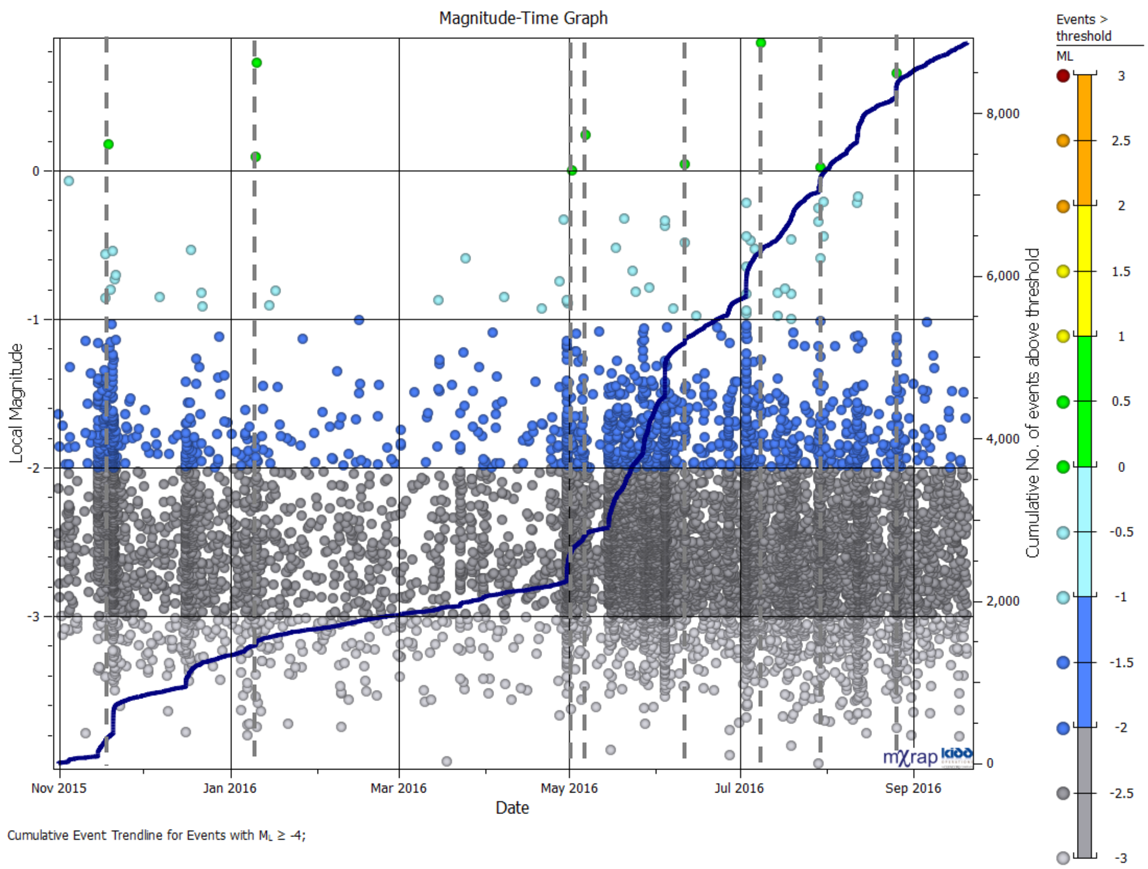

Figure 46: Magnitude-Time History, Area 2(c): November 2015 to September 2016.

Large blasts are observed from November to January 2015 in Area 2(c), then decreased seismic activity followed by a subsequent increase in event rates from May to September 2016. Six of the nine events during this period are strongly shear related with an S:P Energy Ratio > 10. The following lists additional observations of large events for this period:

- The first event, in November 2015, precedes a significant mine blast by several days while events 2, 3, 5, 6, and 7 occur at a time independent of mine stope blasts. Five of the six events have an S:P Energy Ratio greater than 10, indicating shear related events.
- Event 4, 8 and 9 occur directly following mine blasts and two of the three events have a S:P Energy Ratio for 2 of less than 10, indicating stress fracturing.

Area 2(c) shows a correlation between mine blasting and stress driven events and an inverse relation between shearing events and mine blasting.

4.9.2.3 Apparent Stress

High frequency of Apparent Stress occurrences are seen in the later period Area a. The variation in the data from 2012 through to the final months of 2015, indicates different source mechanisms. The chart displayed in Figure 47, indicates occurrences at times of high and low Apparent Stress.

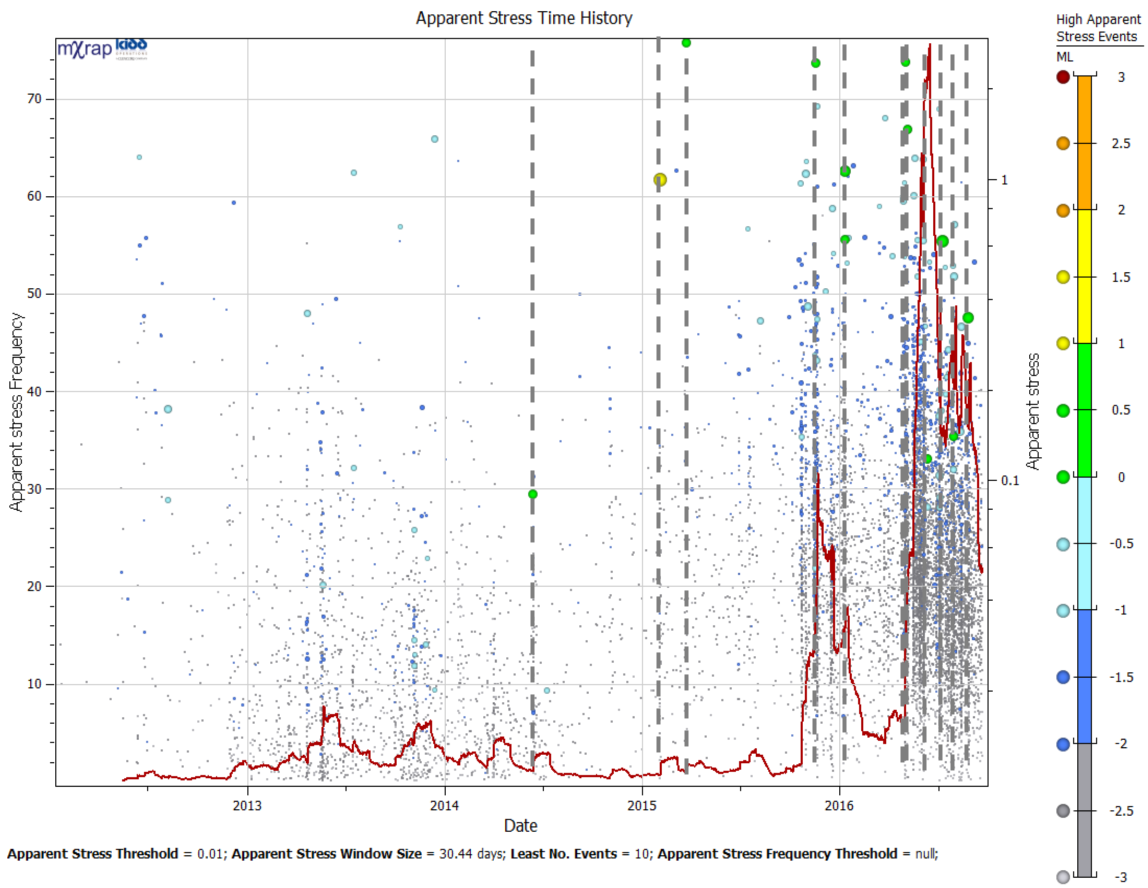

Figure 47: Apparent Stress Frequency Chart of Area 2 data subset.

The following are observations of the Apparent Stress Chart for Area 2:

- The first four large events occur at times of relatively low Apparent Stress Frequency;
- The remaining ten events occur during a period of very high Apparent Stress Frequency.

The Apparent Stress Frequency chart presents a clear indication that large shearing events may occur at times of high Apparent Stress Frequency or low Apparent Stress Frequency.

4.9.2.4 Energy Index and Cumulative Apparent Volume

An Instability Analysis of Area 2 (Energy Index, Cumulative Apparent Volume) is shown in Figure 48. The log(EI) from 2012 to late 2014 is generally below 0, with very little energy variations. The later time period is displays the log(EI) persistently greater than 0, indicating ongoing stress accumulation without significant variations in Cumulative Apparent Volume.

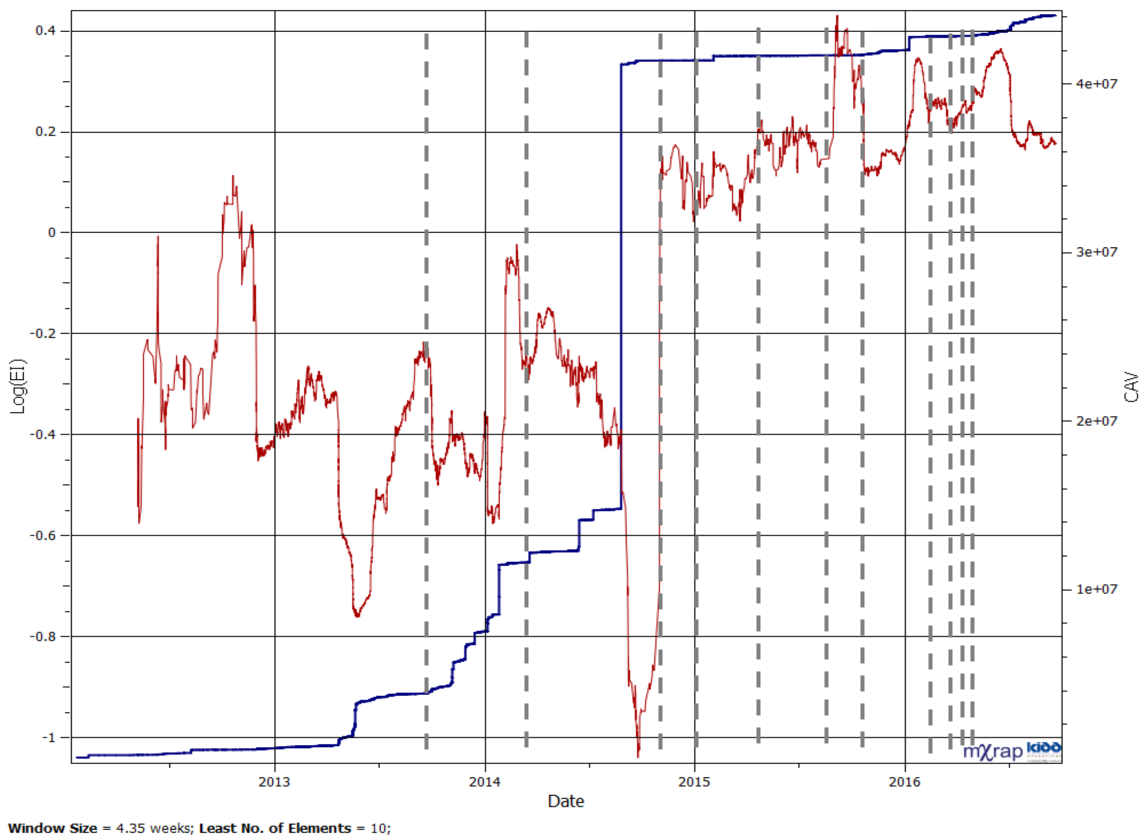

Figure 48: Area 2; Energy Index Log(EI) and Cumulative Apparent Volume (CAV) chart.

The Energy Index and Cumulative Apparent Volume chart for Area 2 does not indicate a strong relation of large events and Energy Index.

4.9.3 Area 3

The third area of interest is located in north abutment of the ore body in the upper levels. The seismic event distribution is depicted in the Section View Figure 49(a) and Plan View in Figure ***49***(b). There is a reduced concentration of events, compared to other areas and many of the smaller and larger events occur at a distance of 50 or more metres from mine development and mine stopes. Closer review of the data may provide a basis for the large events occurring in this area. There are seven occurrences of high magnitude events ($M_L > 0$) and two of these are $M_L > 1$, as listed in

Table 6. The seismic records for this are represent approximately 2% of events from January 2012 to September 2016.

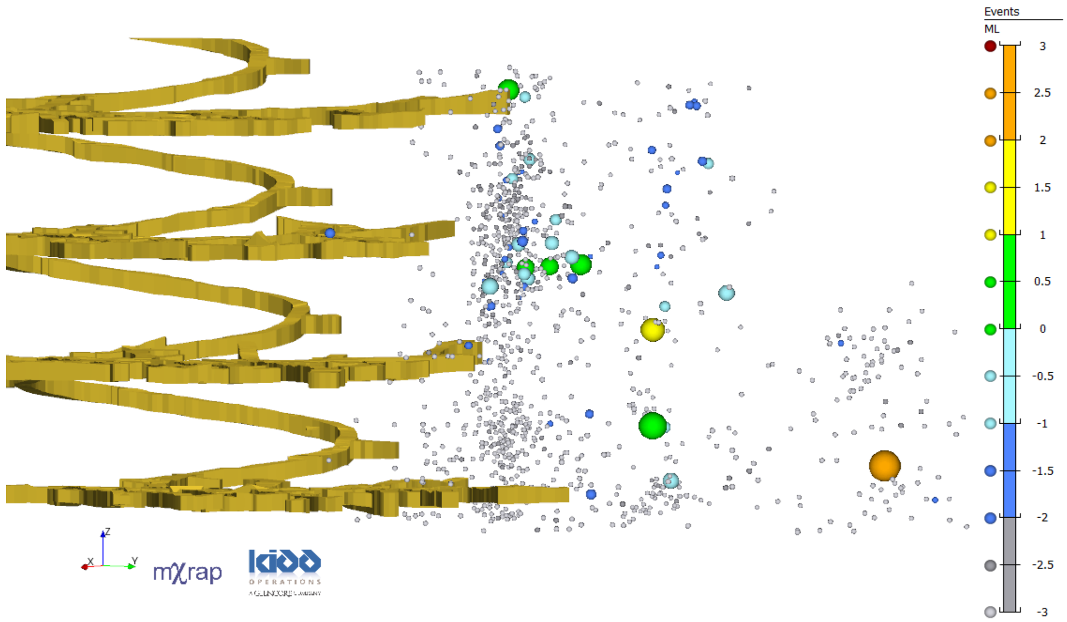

(a)

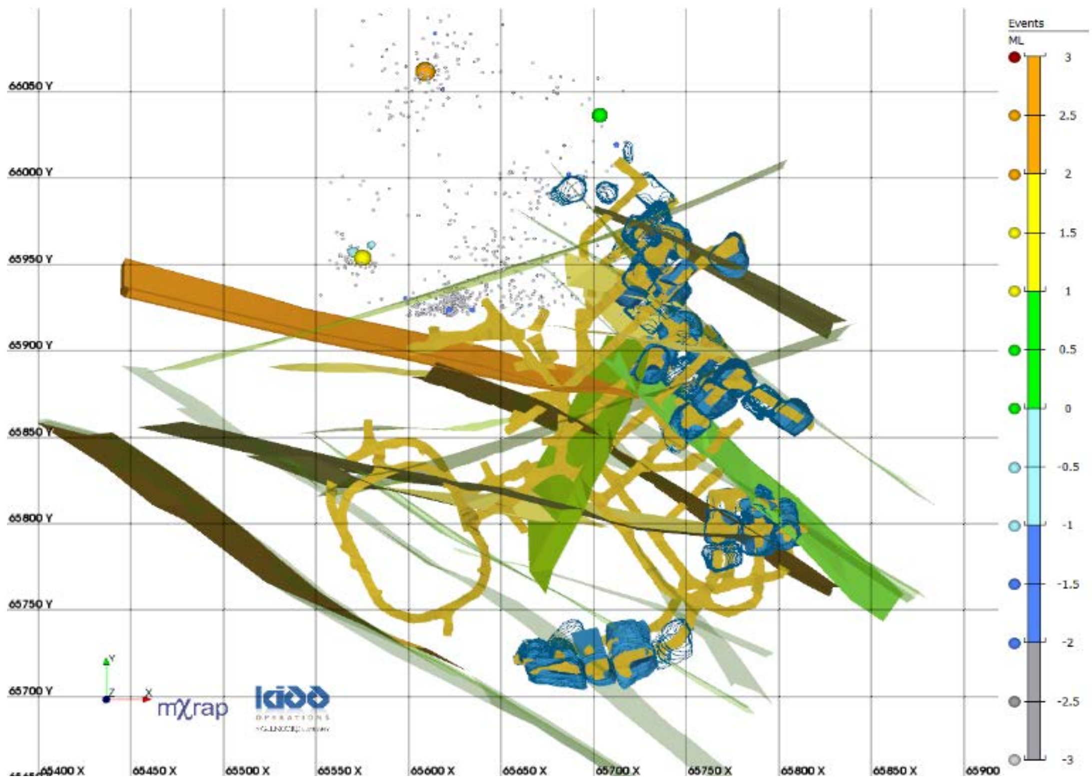

(b)

Figure 49: Area 3, 7000 to 7400 Levels, Seismic event distribution; (a) Section View, looking North West, (b) Plan View, 7300 and 7400 Levels, events; relative location of faults and stopes.

4.9.3.1 *Frequency-Magnitude and S:P Energy Ratio*

The Frequency-Magnitude relation of Area 3 indicates a bi-modal data set, as seen in the graphs of Figure 50. The S:P Energy Ratio indicates that 20% of events, including all of the high magnitude events, are occurring in the shearing region, shown in Figure 50(b), indicating likely fault-slip events.

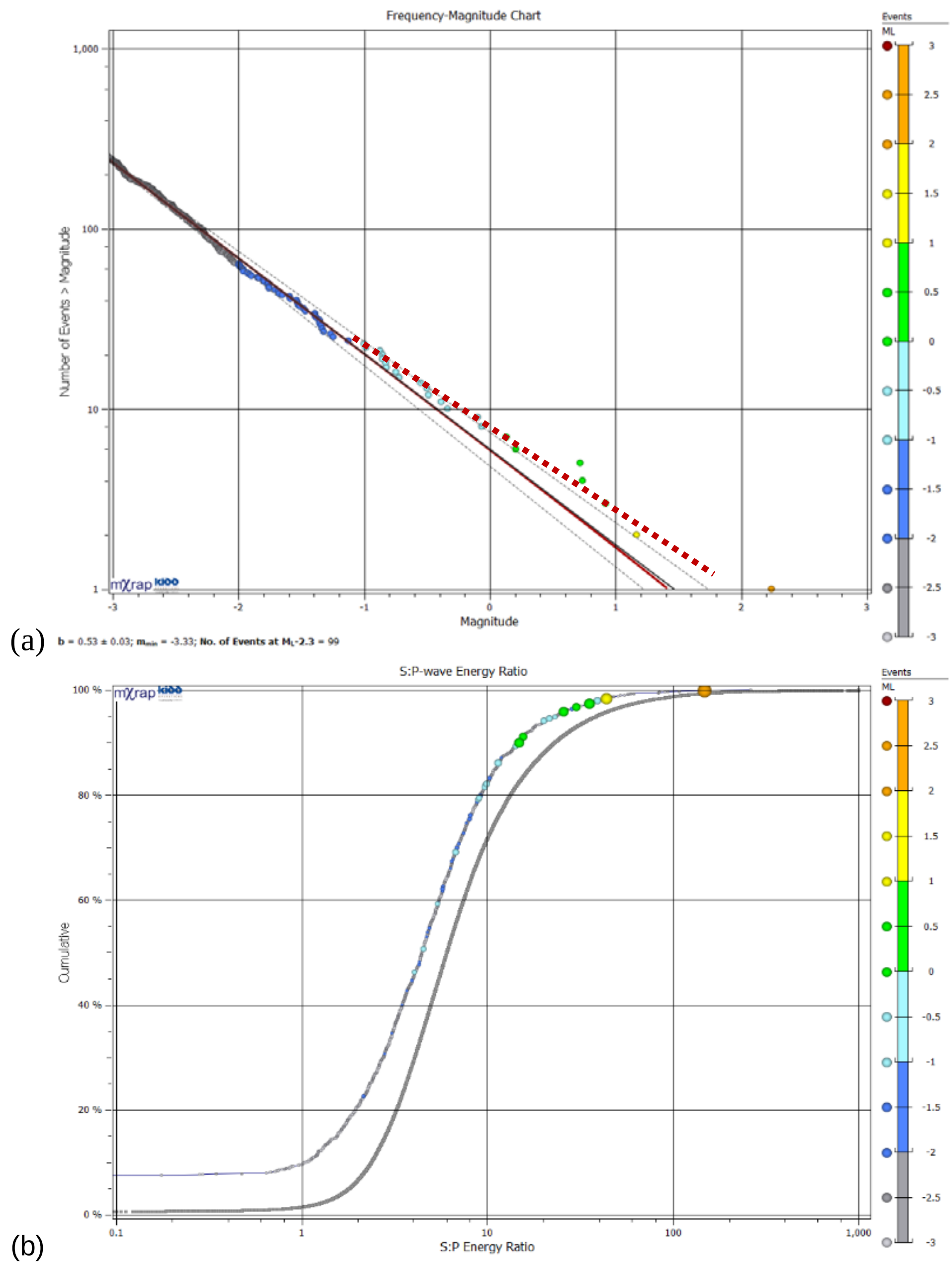

Figure 50: Area 3: (a) Frequency - Magnitude chart; (b) S:P Energy Ratio.

The low overall b-value of 0.53 is quite low, and events larger than M_L -1.0, have a lower b-value of 0.45, as seen with the change of slope, indicating significant shearing source mechanism.

More than 80% of the population has a low S:P energy ratio, with a median S:P < 6 and approximately 16% of the population with an S:P greater than 10.

4.9.3.2 Magnitude-Time History

The Magnitude-Time History of Area 3, seen in Figure 51, shows increased event rates at time periods corresponding with the high magnitude events and with increased Apparent Stress (Figure 52). This data correlation is typical of large blasts, however, the high magnitude events occur in conjunction with the timing of inferred blasts as well as outside of inferred blast times.

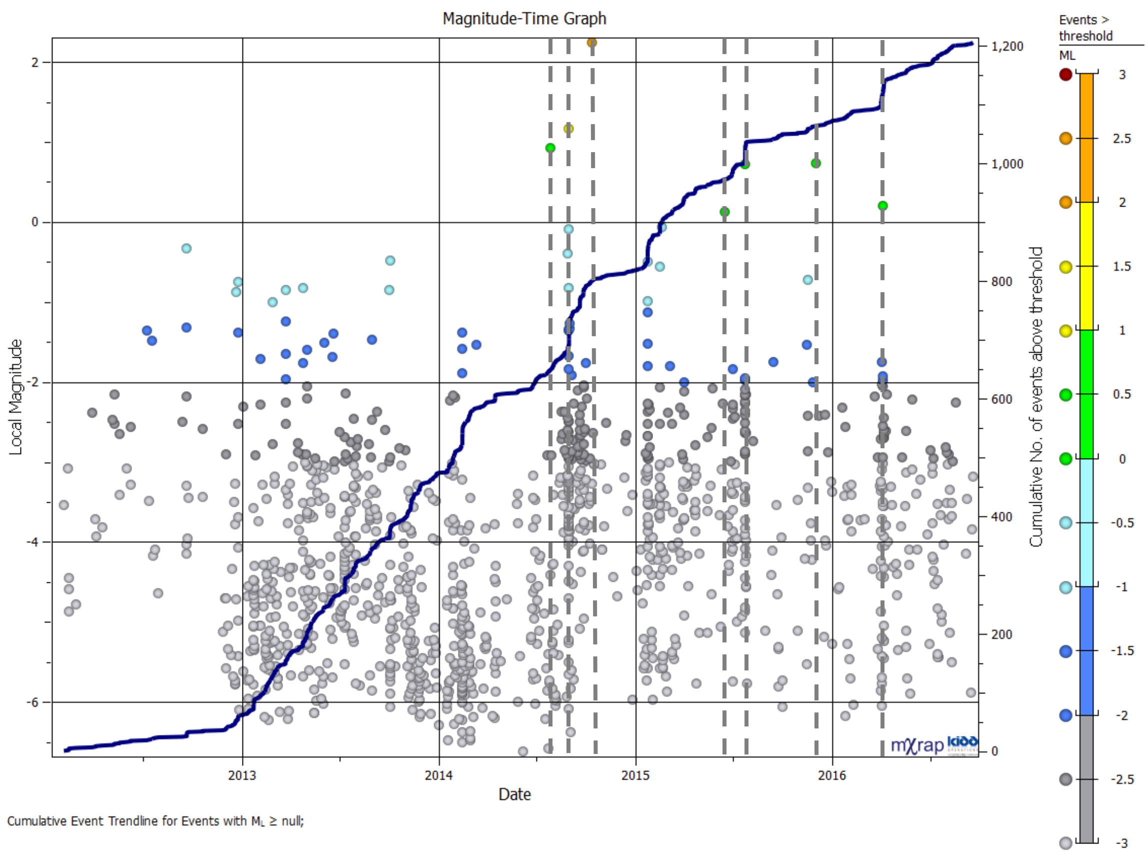

Figure 51: Magnitude-Time History of Area 3 data subset.

The following observations of Area 3 Magnitude-Time History chart (Figure 52) confirm bi-modal data:

- Large events 2, 5, and 7 occur coincident with stope blasts; and
- Events 1, 3, 4, and 6 do not occur directly after stope blast.

4.9.3.3 Apparent Stress

Frequent occurrences of high Apparent Stress with relatively few events are observed in the farfield area of 7000 to 7400 levels. The apparent stress increases sharply at the onset, then reduces sharply, immediately after each high magnitude event; indicating localized stress changes. There is not sufficient data in this area to determine a causal relation.

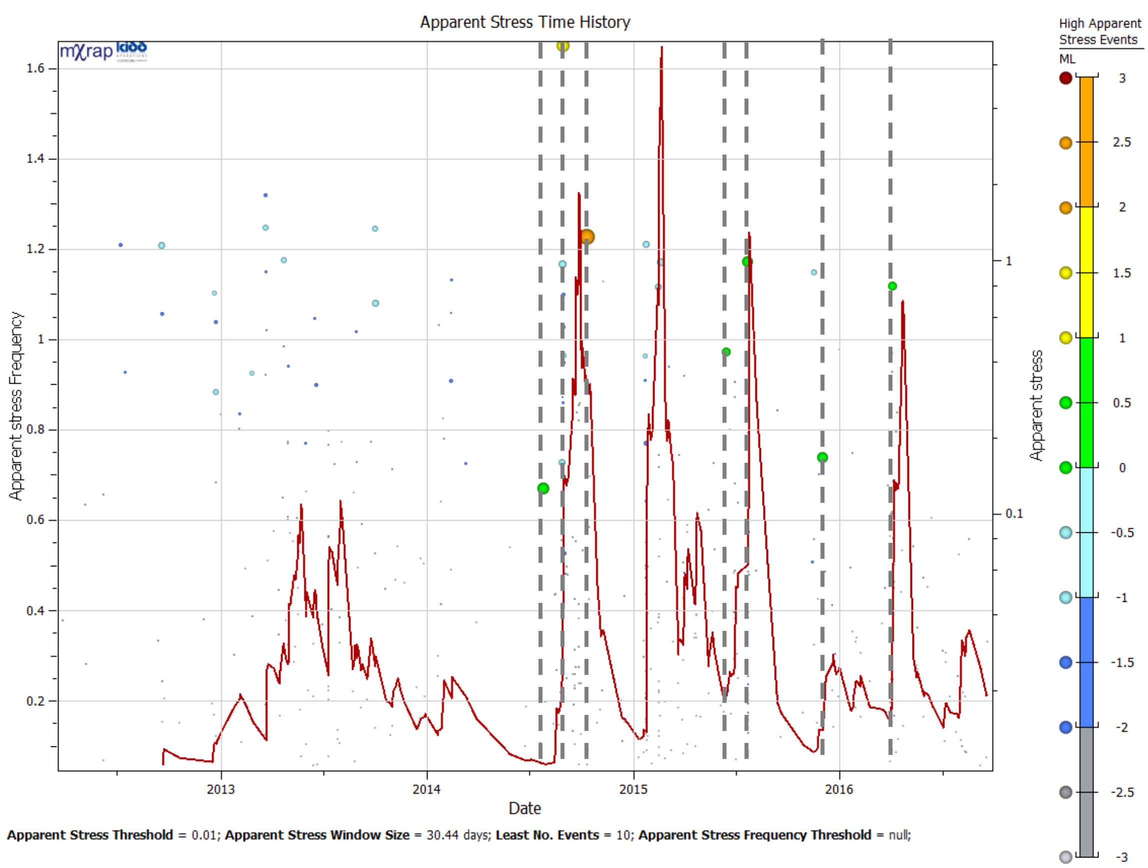

Figure 52: Apparent Stress Frequency Chart of Area 3 data subset.

The following are observations of the Apparent Stress Chart for Area 3:

- There are several increases in Apparent Stress Frequency for Are 3, however, these are much smaller than those seen in Areas 1 and 2;
- Large events 1 to 6 and 7 occur with very low Apparent Stress Frequencies;
- Large event 3 occurs coincident with very high Apparent Frequency; and
- Large events 2 to 6 and 7 are immediately followed by sharp increases in Apparent Stress Frequency.

All of the large events in Area 3 are large shearing events which result in significant stress redistributions in the area, as shown by subsequent spikes in Apparent Stress Frequency. The large events do not occur at times of high stress change, and largely do not occur following mine blasts, as seen in the Magnitude-Time History chart.

4.9.3.4 Energy Index and Cumulative Apparent Volume

The log(EI) from 2012 to late 2014 is generally below 0, with marked variations in energy and a sudden change in mid-2014, corresponding with Apparent Stress Time History (Figure 52). The mid-2014 period indicates a significant change in CAV, and log(EI) is persistently greater than 0, indicating ongoing stress accumulation with relatively little change in Cumulative Apparent Volume.

The graph in Figure 53 identifies the relation between Energy Index and Cumulative Apparent Volume:

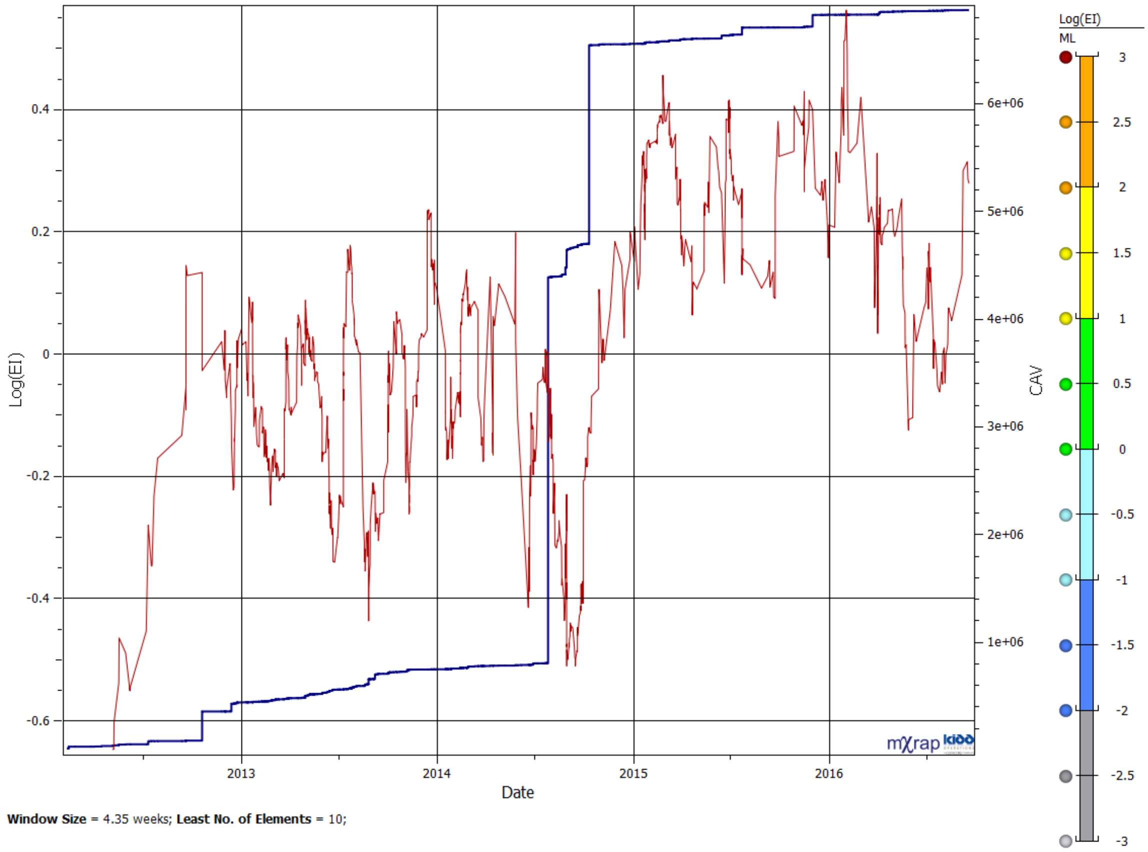

Figure 53: Select time periods in Area 3 exhibiting two distinct behaviours; log(EI) drops with significant step change CAV or log(EI) drops with little to no step change CAV.

The Energy Index and Cumulative Apparent Volume chart for Area 3, similar to Area 2, does not indicate a strong relation of large events and Energy Index.

4.10 Trends and Interactions

The Kidd Mine D seismic system has evolved over time and there are periods where the recorded events vary in minimum sensitivity. There are also periods where a change is seen in the rate of events, either due to an upgrade of the seismic system or a change in the level of mining activity. Overall, the Mine D data is generally well behaved during time period under review, from January 2012 to September 2016.

The examination of seismic events in three distinct areas of the mine, with a focus on the behaviour of high magnitude events, or patterns leading to high magnitude events, was conducted and described in the previous sections. The review successfully identified trends with increased apparent stress and energy variations as pre-cursory seismic activity that may provide seismic risk assessment tools.

High magnitude events, with parameters typical of two distinct mechanisms, are occurring with some consistency in many areas of the mine, as shown in the Magnitude-Time graph in Figure 54. The S:P Energy Ratio suggests that distinct mechanisms are occurring with high magnitude events of Mine D, from 2012 to 2016, plotted in both shearing (40%) and non-shearing behaviour (60%) related to rock mass fracturing or yielding, depicted in the graph of Figure 55.

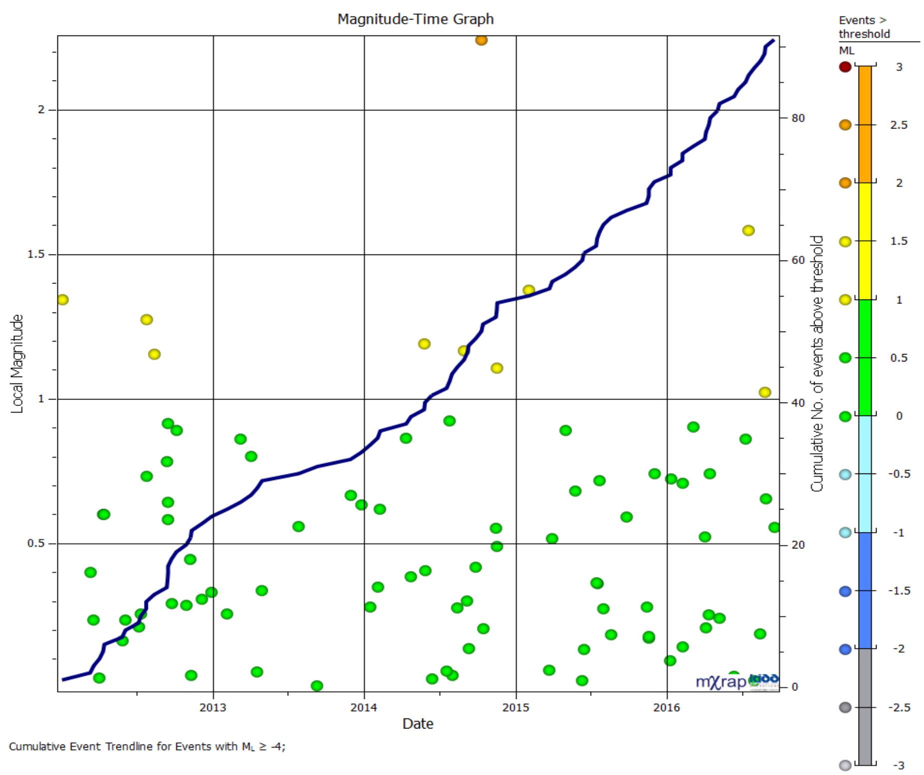

Figure 54: Frequency-Magnitude distribution of Mine D large events (M_L>0) from January 2012 to September 2016.

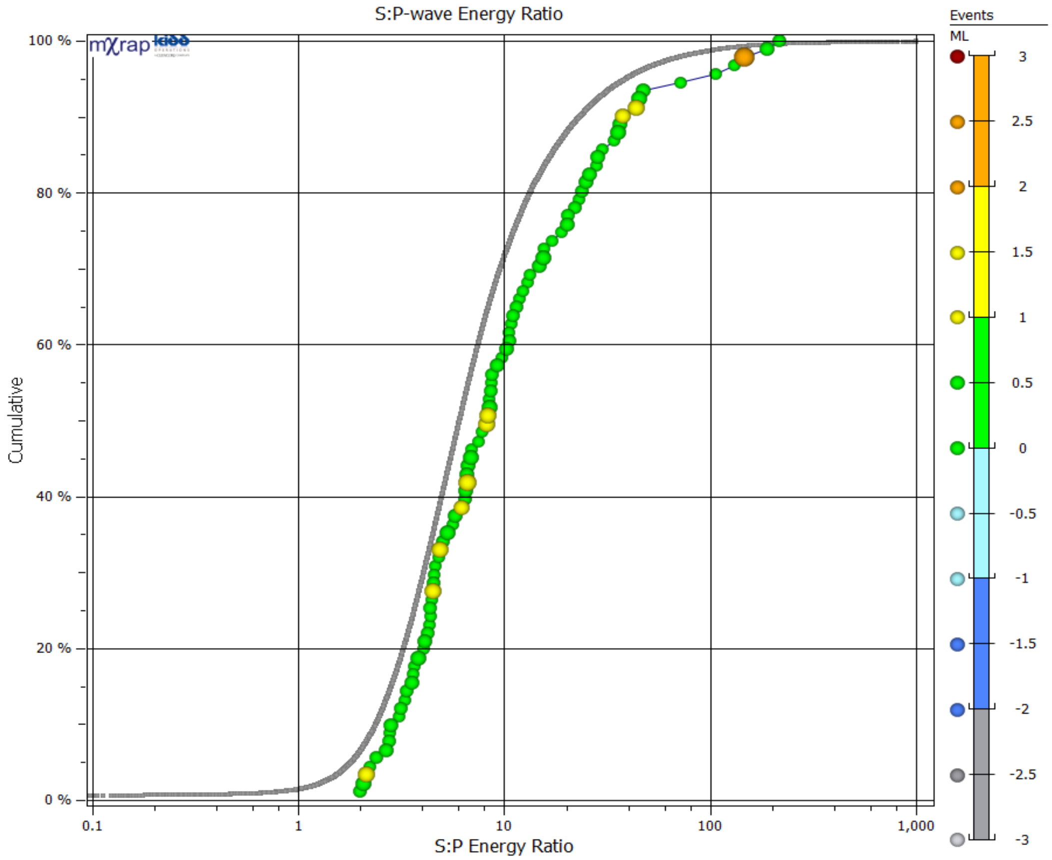

Figure 55: S:P Energy Ratio of Mine D large events (M_L>0) from January 2012 to September 2016.

Of the three areas of interest, Area 2, with a higher density of events as described in section 4.9.2, is more conducive to determining possible trends and examples of the occurrences associated with rock mass fracturing and shearing mechanisms are described in this section.

4.10.1 Rock Mass Fracturing

Events exhibiting rock mass fracturing or yielding behaviour often have a temporal and spatial association with large blasts. These behaviours are indicated by:

- Low S:P Energy Ratio, (less than 10);
- Energy fluctuations recorded with an overall log(EI) increase ahead of the large event; and
- Stresses build prior to a large seismic event, indicated by increasing Apparent Stress.

Stresses are redistributed after a blast and the data reflects this with a reduced Apparent Stress and log(EI), and a less pronounced Cumulative Apparent Volume.

Other high magnitude events include those exhibiting behaviours that are not directly associated with a known structure; and do not have the typical pre-cursory activity associated with large blasts. The event of July 16th, 2015 is an example of this behaviour where there is relatively little precursory seismic activity and no large blasts prior to the high magnitude event. Additional time-history analysis of similar events is needed to determine possible correlation with mining activity in other areas of the mine, or a potential rock mass fracturing due to repeated stress in the same localized area.

The large event in Figure 57(a)(b) and (c), occurred in July, 2015, illustrates an example of a high magnitude event, ML=0.36, with a low S:P ratio of 4.5 and temporally independent of a large mine blast. The location of the events relative to mining development areas is illustrated in the plan view in Figure 58.

Rock mass fracturing and yielding behaviour is seen as gradual stress redistribution and a relatively low event rate preceding the large event, i.e. little precursory seismicity. The seismically quiet period is followed by a high magnitude event followed a day later by the increased event rate indicating mine blasting.

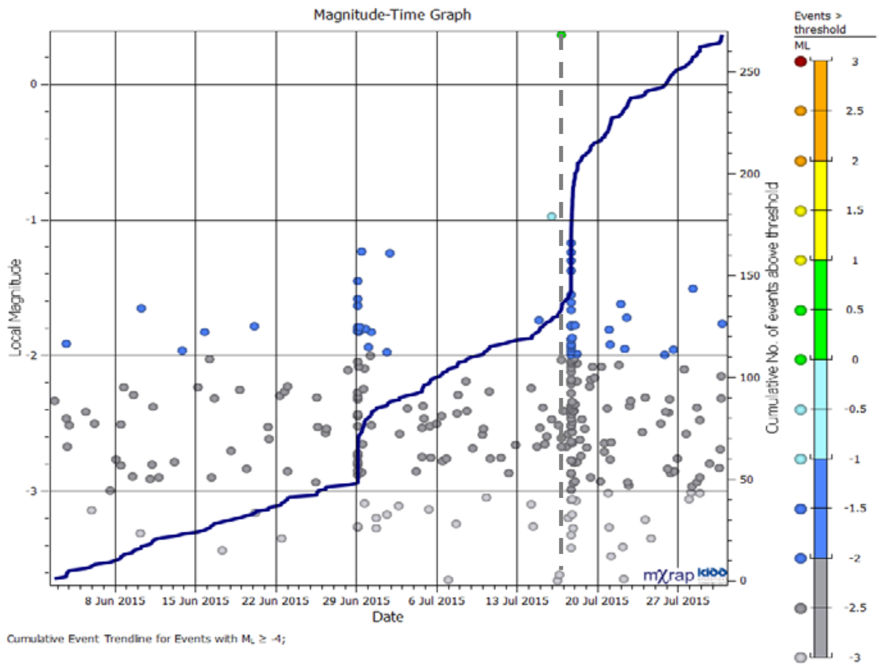
Magnitude-Time Graph
Events > threshold
ML
Local Magnitude
Cumulative No. of events above threshold
Date
8 Jun 2015
15 Jun 2015
22 Jun 2015
29 Jun 2015
6 Jul 2015
13 Jul 2015
20 Jul 2015
27 Jul 2015
Cumulative Event Trendline for Events with $M_L \geq -4$;

(a)

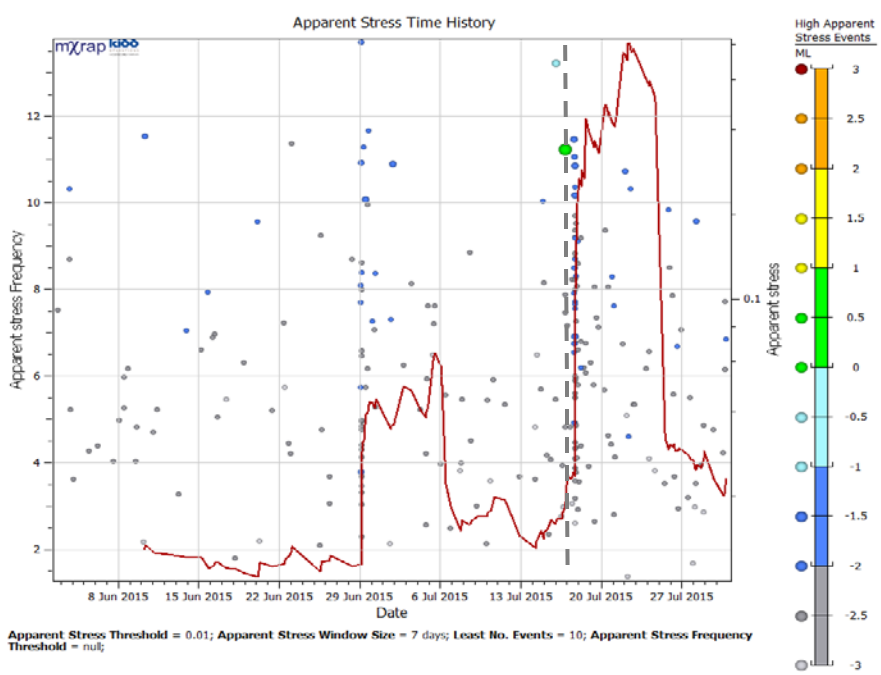
Apparent Stress Time History
High Apparent Stress Events
ML
Apparent stress Frequency
Apparent stress
Date
8 Jun 2015
15 Jun 2015
22 Jun 2015
29 Jun 2015
6 Jul 2015
13 Jul 2015
20 Jul 2015
27 Jul 2015
Apparent Stress Threshold = 0.01; Apparent Stress Window Size = 7 days; Least No. Events = 10; Apparent Stress Frequency Threshold = null;

(b)

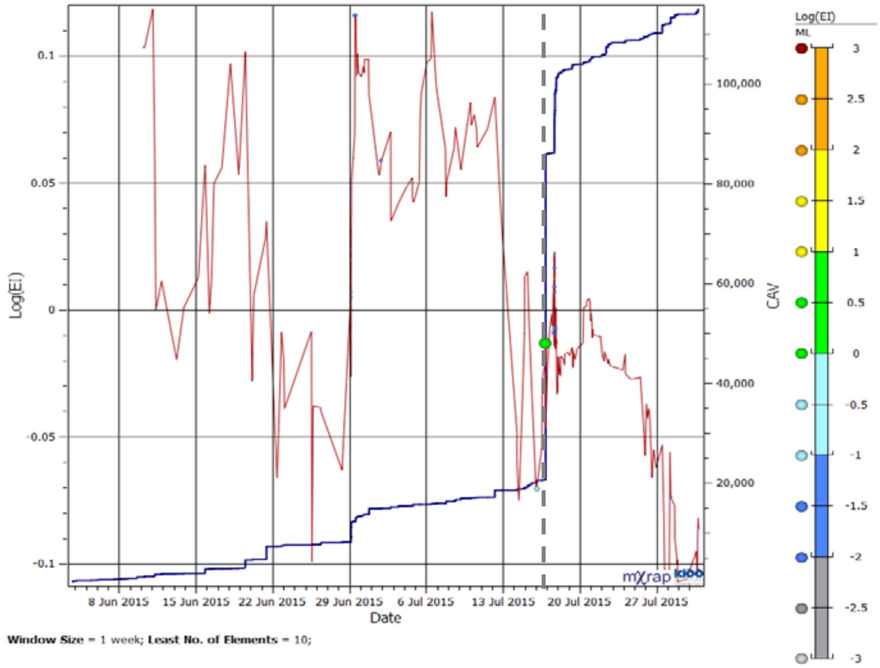

(c)

Figure 56: Area 2, July 16 2015: (a) Magnitude-Time History; (b) Apparent Stress Time-History; and (c) Energy Index graph.

The Apparent Stress Time History graph, Figure 56(b), also indicates relatively little precursory seismicity and low apparent stress frequency before the large event. The Log(EI) graph indicates reduced energy immediately preceding the large event and remain at or below 0 following the event. This provides an indication of the reduced stresses, therefore rock mass fracturing or yielding behaviour.

The location of the large event is approximately 20 m laterally from mine access development to mining development areas is illustrated in the plan view in Figure 57.

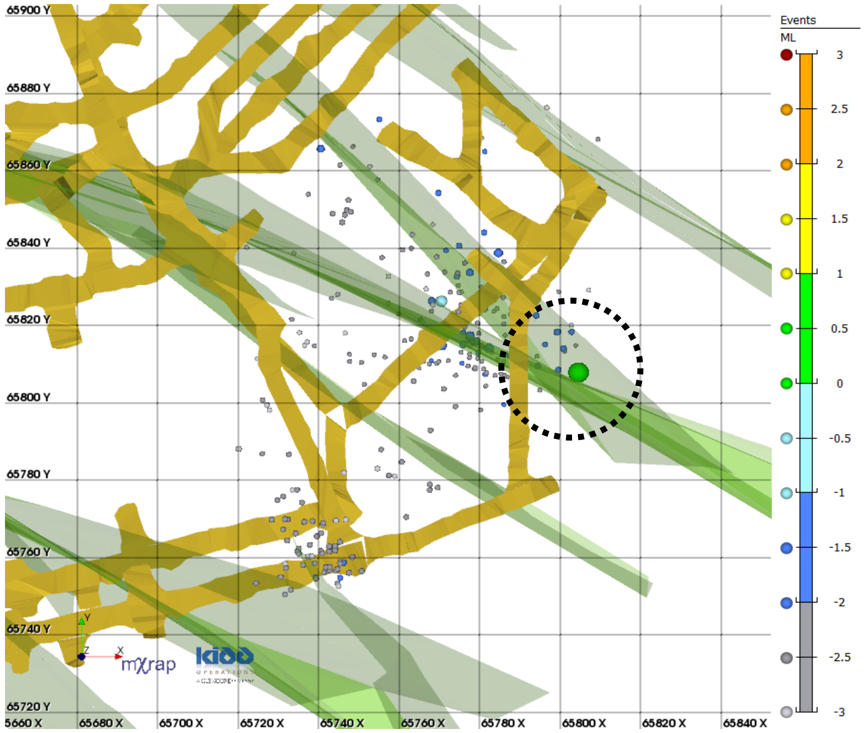

Figure 57: Area 2, 7700-7800 Level, July 2015 large event, plan view.

Multiple high magnitude events are located near the access drives, away from large stope blasts and, while many are in close proximity to mapped faults, many are not directly associated with known structure. The stress increases seen preceding the high magnitude events is seen with both the shear related events and non-shear related events.

4.10.1 Shearing

Events exhibiting shearing or fault slip on existing geological structure are indicated by high magnitudes, primarily located in the abutments, along access drives and outside of the direct influence of the large stope blasts. A significant number of persistent cross cutting faults are mapped throughout the mine and a significant number of events (40%) are located near these structures, indicating a strong relation with shearing mechanism (Figure 58).

High magnitude events associated with shearing or fault slip typically exhibit:

- High S:P Energy Ratio, (greater than 10);
- Sharp log(EI) increase before the occurrence of the large event; and
- Sharp Apparent Stress increase before the large event.

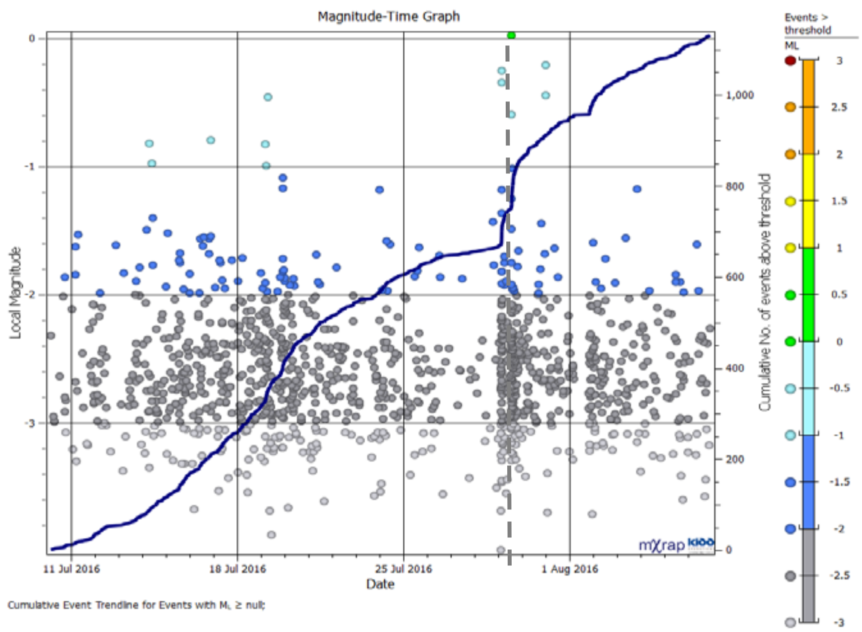

(a)

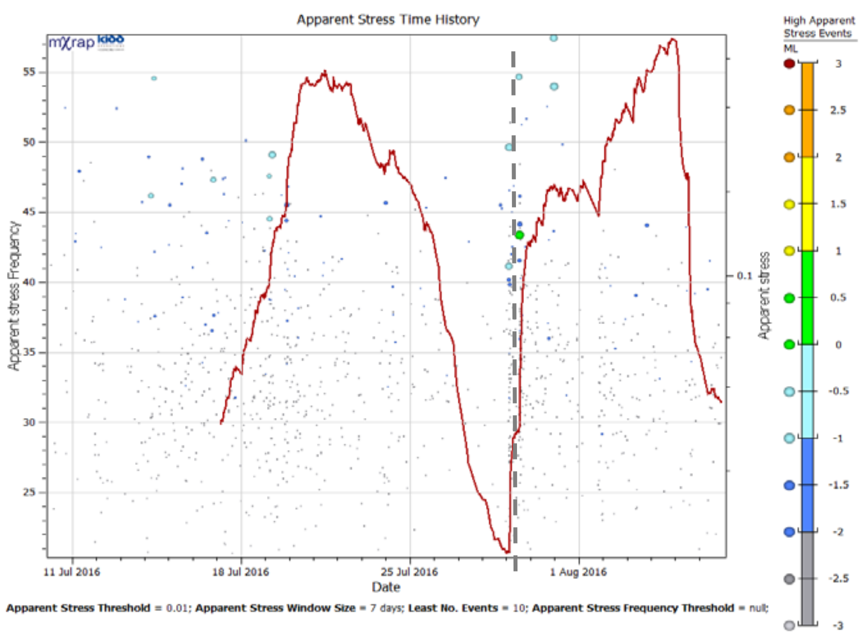

(b)

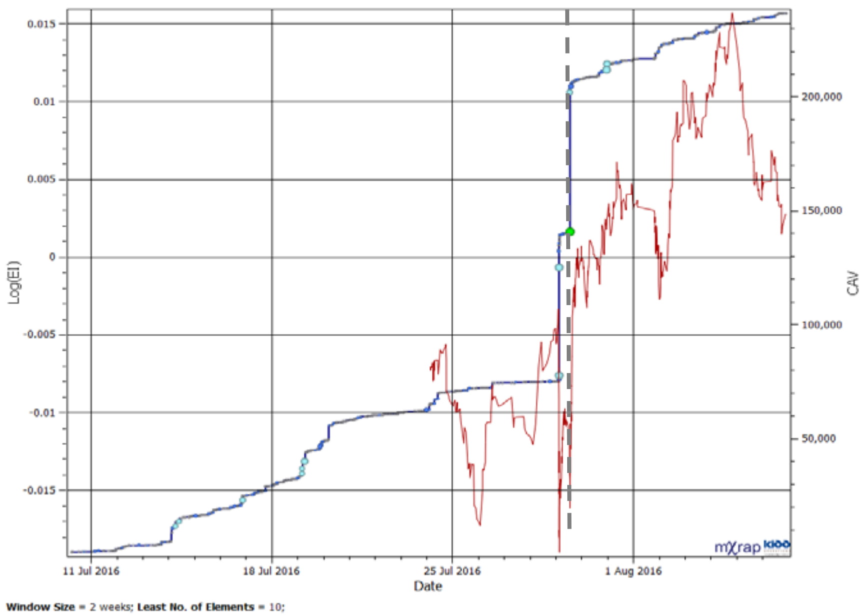

(c)

Figure 58: Area 2, 7500-7700 Level, July2016 large event (a) Magnitude-Time Graph; (b) Apparent Stress Time-History; and (c) Energy Index graph.

Apparent Stress frequency and the log(EI) increase significantly leading up to the large event, as seen in Figure 58 (a) and (b), indicating stresses are building. The location of the events is approximately 20 m laterally from the level development, illustrated in the plan view of Figure *59*, and approximately the same elevation as 7500 Level.

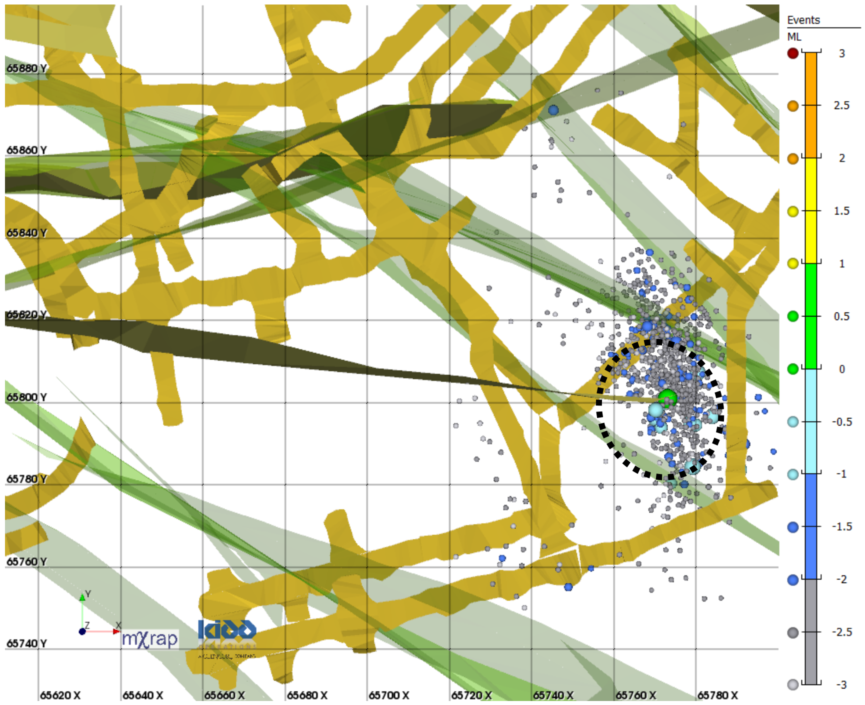

Figure 59: Area 2, 7500-7700 Level, July2016 large event, plan view.

4.10.2 Spatial Trends

The three spatial groups reviewed include 27 large seismic events. Areas 1 and 3 are abutments to the Mine D stoping, and Area 2 is a large pillar between two mining zones (Figure 35). The large events in Areas 1 and 2 are more concentrated, with all large events occurring within 50 to 100 metres of each other. The large events of Area 3 are spatially dispersed across three levels and several occurrences are more than 100 metres from each other.

The large events are also investigated with respect to their proximity to existing mine excavations. Each large event is identified as being within 50 metres of mine development, or more than 50 metres from mine development (

Table 6). Twelve of the 27 large events are rock mass fracturing or yielding events (low S:P energy ratio), while 15 of the 27 large events are shearing events (high S:P energy ratio). With regards to proximity to mining, 6 of the 12 yielding large events are within 50 metres of mine development, while 6 of the 12 yielding large events are more than 50 metres from mine development. The data suggests that the location of the yielding large events are independent of the location of mine development.

For the 15 large shearing events, 13 of the large events are within 50 metres of mine development, while only 2 of the 15 large shearing events are located more than 50 metres from mine development. The data suggests that large shearing events are more likely to occur near mine development.

4.10.3 Temporal Blasting Trends

The timing of large events with respect to mine blasts can be investigated with magnitude time history charts. All of the 27 large events were investigated to identify if they occurred within 24 hours of a significant mine blast, with the results presented in

Table 6. For the 12 large yielding events, 5 of the events occurred within 24 hours of a mine blast, while 7 of the events did not occur within 24 hours of a mine blast. Based on these 12 large events, there is no relation between the occurrence of mine blasts and the occurrence of large yielding events.

For the 15 large shearing events, 6 of the large shearing events occurred within 24 hours of a mine blast, while 9 of the large shearing events did not occur within 24 hours of a mine blast. Based on these 15 events, there is no relation between the occurrence of mine blasts and the occurrence of large shearing events.

4.10.4 Interaction Between the Three Areas

Past work (Wang *et al.*, 2009) at deep mines identified interaction between seismic sources in the mine. For example, when one area suffered a large event, large events occurred in other areas shortly afterwards. For each large event, the other areas were checked for the occurrence of large events in the following 7 days. In only two cases, was a large event in one area followed by a large event in another area (Table 7).

Table 7: Possible interactions between large events in different areas of Mine D

Preceding Event		**Subsequent Event**	
Area 3	Oct/11/2014 ML=2.24	Area 1	Oct/14/2014 ML=0.21
Area 2	Jul/16/2015 ML=0.36	Area 3	Jul/23/2015 ML=-0.72

For the 27 large events in three areas in Mine D, there are no obvious trends of large events in one area triggering or inducing large events in another area.

5.0 SUMMARY

As the mine development reaches greater depths, the maturing mine experiences increased gravitational stresses, reduced confinement at the excavation boundaries and possibly greater interactions with increased potential for crack propagation and fault slip along existing geological structures. The database reviewed has an atypically low event rate relative to the depth of mining and the number of events in discrete areas does not exhibit obvious trends. A holistic review of the events, within relevant time periods, in conjunction with excavation locations and geometries does, however, provide clues to assist with determining hazards and associated risks.

5.1 Identifying Variations in Rock Mass Stress with Seismic Data

The dominant seismic indicators for Areas 1 to 3 of Mine D are the stress and energy variations and cumulative apparent volume. The review, conducted in context of a temporal and spatial occurrence of events, primarily seeking indicators of rock mass instability, identified a correlation with apparent stress and with energy variations. The number of events recorded is lower than the data density typical of deep mine seismic systems; and as such, trends are not easily observed. However, a spatial review of the time-history graphs of apparent stress as well as energy fluctuations and cumulative apparent volume are considered key to assessing indicators of changing stresses and subsequent rock mass response as excavations are developed.

Generally, the Kidd Mine D seismic data indicates that large events are predominantly in a few areas and occur in both shear and yielding mechanisms. The locations are in mine abutments and in pillars between mining zones. There are very few large events occurring near open stopes. Relatively few of the large events are shearing events.

Increasing Apparent Stress consistently matches occurrences of increasing log(EI) with a steadily increasing Cumulative Apparent Volume indicating stress accumulation. Occurrences with a significant drop in log(EI) and a sharp increase in CAV typically indicate rock mass yielding, potentially leading to instability.

The log(EI) / Cumulative Apparent Volume relation is readily associated with inferred blast time periods and rock mass fracturing, while Apparent Stress provides a tool to infer stress changes in the rock mass. The log(EI) / Cumulative Apparent Volume and the Apparent Stress changes can be associated with the five regions of strain softening (introduced in Section 2) and the sequential rock mass response conditions, ranging from small events with low apparent stress, large events with distinct rock mass response related to high or low apparent stress and smaller events indicating residual strength or possible failure.

The rock in the pillars and stope abutments is capable of supporting loads in a yielded state and the seismic data review focused on searching for primary indicators of yielding with high moment associated with low apparent stress in areas surrounding the pillars and stope abutments. An indication of relaxation in the rock mass is also associated with reduced stresses and reduced risk of discrete rockburst events as mining development advances.

5.1.1 Source Mechanisms

There is no single source parameter analysis that will suit all situations and the apparent stress and energy index analysis should be used as one of several tools, currently in use throughout the industry, developed to assist with mine design decisions. The application of Apparent Stress and log(EI)/Cumulative Apparent Volume analysis must be confirmed by a back analysis over a reasonable time period. Confirmation of shearing or non-shearing seismic source mechanism can also be obtained with the S:P Energy Ratio. The frequency of high apparent stress during mining is often associated with the frequency of high magnitude events that can be expected in the short term future mining. With sufficient data and additional back-analysis of a single population, the probability of large events can be estimated from b-value and the a/b factor obtained from the frequency-magnitude relation graph.

5.1.2 Large Events

The preceding events, typically within one magnitude of the large events, does not occur consistently, however, a repeatable pattern of early onset stress increases can be seen in most instances. Where stresses continued to increase sharply, there have been second large events within a short time period. The subsequent stress redistribution following large events is also consistent.

5.1.3 Event Location and Source Interactions

The analysis approach was developed to identify the potential interaction of spatially distinct areas. The method established the high magnitude events and identified groupings and relative location with distinct parameters associated with the high magnitude events. Mining activity generally appears to be spatially restricted, with little interaction seen between mining areas at the same time.

5.2 Seismic Analysis to Identify Seismic Risk

Ongoing holistic analysis applied throughout the mine life, in general, includes seismicity review, identification of geological structure and stress redistribution around advancing development. Additional review of high magnitude events with identification of pre-cursory, stress driven behaviour could assist with identifying future hazard areas of typical and atypical seismic response. These combined analyses, monitored and updated continually, will provide a basis for proactive mine design decisions to reduce risks associated with high stresses that is typical in deep hard rock mining. The seismic record analysis will assist with developing an understanding of the expected frequency of high magnitude, mining induced, potentially damaging events and hazard areas.

A prescriptive review of the data including the spatial grouping of events, the apparent stress and energy variations with a magnitude time-history analysis represents a robust approach with useful outcomes that can be applied to mine design decisions. Such an analysis methodology can assist with hazard and risk assessment of future development areas and additional case studies with larger data sets may provide better definition of the shear mechanisms in locations where there are no known structures.

The inherent variability of the seismic systems and the resulting data collected requires an initial assessment of the seismic dataset for a given mine site to ensure that there is sufficient quality and quantity to conduct an analysis. Initial review should include the use of established industry tools to determine reliability and to assess the data quality with relations of Frequency-Magnitude, Magnitude-Time history and Energy-Moment. With a reliable data set, the subsequent analyses are ore likely to provide useful results.

5.3 Future Work

A holistic analysis, encompassing operational data, with additional systematic temporal and spatial review of the different mining areas will assist with understanding possible correlations with mining activities or with geological structure. An assessment of apparent stress and energy variations can provide indicators of localized rock mass response as excavations are developed, to form the basis to better understand the potential hazards during future development.

Additional investigation in areas with undetermined or contradictory mechanism may provide an interesting review in areas with sufficient data to identify correlations.

Applying a systematic spatial and temporal analysis to an inventory of large events or highly seismic areas with different mine data sets will likely produce different results due to the unique nature of ore placement, mining methods and sequences at different mine sites, ultimately resulting in unique seismic response. Additional studies will provide an understanding of areas that undergo more frequent seismicity or frequent large events. Subsequent trend analyses would provide hazard assessment tools to identify areas that have undergone fracturing and relaxation and reduced risk of rockbursting as well as the high hazard areas. This approach can be used to reconcile engineering design and future ground support decisions.

REFERENCES

Alcott, J., Kaiser, P., Simser, B., and Peterson, D. (1998) Micro-seismic risk assessment: Integration of micro-seismic data into the ground control decision making process. 100th CIM/AGM, Montreal, Quebec, Canada.

Andrieux, P.P. Hudyma, M.R., O'Connor, C.P., Li, H., Cotesta, L., and Brummer, R.K. (2008) Calibration of large-scale three-dimensional non-linear models of underground mines using microseismicity data. Proceedings of the First International FLAC/DEM Symposium, Itasca Consulting Group Inc., Minneapolis, August 2008. Retrieved Feb 1, 2017, from <https://www.researchgate.net/>.

Brace, W.F., Paulding, B.W. and Scholz, C. (1966) Dilatancy in the fracture of Crystalline rocks. Journal of Geophysical Research, Vol. 71, pp.3939-3953.

Brady, B.H.G., and Brown, E.T., (2006) Rock mechanics for underground mining. Third Edition, Springer 2006. Chapter 10, pp. 270-311.

Brown, L., and Hudyma, M. (2017) Identification of stress change within a rock mass through apparent stress of local seismic events. Rock Mechanics and Rock Engineering, Vol .50, No. 1, pp. 81-88.

Castro, L.A.M., McCreath, D.R., and Kaiser, P.K. (1995) Rock mass strength determination from breakouts in tunnels and boreholes. 8th Congress ISRM Conference Paper, pp. 531-536.

Castro, L.A.M., Grabinski, M.W., and McCreath, D.R. (1997) Damage initiation through extension fracturing in a moderately jointed brittle rock mass. International Journal of Rock Mechanics & Mining Science Vol. 34, No. 3-4, 1997, Vol 34, No. 3-4, Paper No. 110.

Choy, G.L., and McGarr, A., (2002) Strike-slip earthquakes in the oceanic lithosphere: observations of exceptionally high apparent stress. US Geological Survey, Denver, CO, US Geological Survey, Menlo Park, CA, USA, Geophysics Journal International, pp. 506–523.

Choy, G.L., and Kirby, S.H., (2004) Apparent stress, fault maturity and seismic hazard for normal-fault earthquakes at subduction zones. US Geological Survey, Denver, CO, US Geological Survey, Menlo Park, CA, USA, Geophysics Journal International, July 27, 2004, pp. 991-1012.

Cichowicz, A., Green, R.W.E., Brink, A.v.Z, Grobler, P. and Mountfort, P.I. (1990) The space and time variation of micro-event parameters occurring in front of an active stope. In Proceedings of Rockbursts and Seismicity in Mines, Minneapolis. (Editor: C. Fairhurst). Rotterdam: A.A. Balkema. pp. 171-175.

Cotesta, L., O'Connor, C.P., Brummer, R.K., and Punkkinen, A.R. (2014) Numerical modelling and scientific visualization – integration of Geomechanics into modern mine design. Proceedings of the Seventh International Conference on Deep and High Stress Mining 2014, (Editor: Y Potvin and M Hudyma), Australian Centre for Geomechanics, Perth, 16 September, 2014, pp.377-394.

Counter, D.B. (2014) Kidd Mine - dealing with issues of deep and high stress mining – past, present and future. Proceedings of the Seventh International Conference on Deep and High Stress Mining 2014, (Editors: Y Potvin and M Hudyma) Australian Centre for Geomechanics, Perth, 16 September, 2014, pp.3-22.

Counter, D.B. (2009) Xstrata Copper Kidd Creek Mine Geotechnical Mine Design Package and 2008 Annual Mine Stability Review. Version 2008-1, January 31, 2009.

Counter, D.B., Ferrari, H., Leonard, D., Toner, J., Fiset, R., Watt, R., Farrell, R., Simser, B., Carlsisle, S., and Andrieux, P. (2009a) Xstrata Copper – Kidd Mine Ground Inspection Report, No. 7100 090106, January 9, 2009.

Counter, D.B., Leonard, D., Ferrari, H., Mcneil, G., Fiset, R., Davis, J., Murphy, J.P., Cooper, G., Watt, R., and Farrell, R. (2009b) Xstrata Copper – Kidd Mine Ground Inspection Report, No. 7500 090615, June 17, 2009.

Diederichs, M.S., (1999) Instability of Hard Rockmasses: The Role of Tensile Damage and Relaxation. A thesis presented to the University of Waterloo in fulfillment of the thesis requirement for the degree of Doctor of Philosophy in Civil Engineering, Waterloo, Ontario, Canada, 1999.

Diederichs, M.S., (2003) Rock fracture and collapse under low confinement conditions. Rock Mechanics and Rock Engineering, Vol.36, No. 5, pp.339–381.

Diederichs, M.S. and Kaiser, P.K. (2004) Tensile strength and abutment relaxation as failure control mechanisms in underground excavations. International Journal of Rock Mechanics and Mining Sciences, Vol. 36, pp.69-96.

Diederichs, M.S., (2007) The 2003 Canadian Geotechnical Colloquium: Mechanistic interpretation and practical application of damage and spalling prediction criteria for deep tunnelling. Canadian Geotechnical Journal Vol 44, pp.1082-1116.

Disley, N.V., (2014) Seismic risk and hazard management at Kidd Mine. Proceedings of the Seventh International Conference on Deep and High Stress Mining 2014, (Editor: Y Potvin and M Hudyma), Australian Centre for Geomechanics, Perth, 16 September, 2014, pp.107-121.

Earthquakes Canada (2017) Natural Ressources Canada Earthquakes database. <http://www.earthquakescanada.nrcan.gc.ca/index-en.php>, accessed February 4, 2017.

Falmagne, V., (2001) Quantification of rock mass degradation using microseismic monitoring and applications for mine design. Doctor of Philosophy thesis, Queens University, Kingston, Ontario.

Gibowicz, S.J., and Lasocki, S., (2001) Seismicity induced by mining: ten years later. Advances in Geophysics Vol. 44, Academic Press, (Editors: R. Dmowska and B. Saltzman), pp.39-181.

Glazer, S.N. (1997) Applied mine seismology: A Vaal Reefs perspective. In Proceedings of Rockbursts and Seismicity in Mines, Krakow, (Editors: S. Gibowicz and S. Lasocki), pp. 227-231.

Hanks, T.C. and Kanamori, H. (1979) A moment magnitude scale. Journal of Geophysical Research, Vol. 84, pp. 2348-2350.

Harris, P., and Wesseloo, J., (2015) Mine Seismicity Risk Analysis Program, Australian Centre for Geomechanics, ACG mXrap, version 4.1.9.1.

Hoek, E., and Brown, E.T., (1980) Underground excavations in rock. Chapter 6: Strength of Rock and Rock Masses, The Institution of Mining and Metallurgy, London, England, pp. 131-182.

Hoek, E., Kaiser, P.K and Bawden, W.F., (2000) Support of Underground Excavations in Hard Rock, Mining Research Directorate and Universities Research Incentive Fund, Published by A.A. Balkema, Rotterdam, Netherlands, Ch.10, pp. 121-136.

Hudyma, M., (2004) Mining-induced seismicity in underground, mechanised, hardrock mines; results of a world-wide survey. Australian Centre for Geomechanics, 2004.

Hudyma, M., (2010) Applied mine seismology concepts and techniques. Technical Notes for ENG-5356 – Mine Seismic Monitoring Systems, Laurentian University, January 2010.

Hudyma, M., Potvin, Y., and Allison, D., (2008) Seismic monitoring of the Northparkes Lift 2 block cave – part 2 production caving. The Journal of the South African Institute of Mining and Metallurgy, Volume 108, July 2008. pp. 421-430.

Kaiser, P.K., Diederichs, M.S., Martin, C. D., Sharp, J. and Steiner, W., (2000) Underground works in hard rock tunnelling and mining. International Society for Rock Mechanics, ISRM International Symposium, 19-24 November, Melbourne, Australia, pp. 841-926.

Król, M. (1998) Application of seismic moment tensor and spectral analysis of seismic waves to study seismic events at the Polkowice-Sieroszowice copper mine. (Ph.D. thesis) Institute of Geophysics, Polish Academy of Sciences, Warsaw (in Polish).

Lunder, P.J., Pakalnis, R.C., and Vongpaisal, S., (1994) Development of pillar design guidelines for hard rock mining operations. Presented at the 16th CIM District 6 meeting, Vancouver B.C., October 1994, pp.148-156.

Martin, C.D., (1997) Seventeenth Canadian Geotechnical Colloquium: The effect of cohesion loss and stress path on brittle rock strength. Canadian Geotechnical Journal, May 6, 1997, Vol. 34, pp. 698-725.

Martin C.D., Kaiser P.K., and McCreath D.R., (1999) Hoek-Brown parameters for predicting the depth of brittle failure around tunnels. Canadian Geotechnical Journal, Vol. 36, pp.136-251.

Martin, C.D. and Maybee, W.G., (2000) The strength of hard-rock pillars. International Journal of Rock Mechanics & Mining Sciences, Vol. 37, pp.1239-1246.

McGarr, A., (2001) Control of strong ground motion of mining-induced earthquakes by the strength of the seismogenic rock mass. Rockbursts and Seismicity in Mines, RaSiM5, (Editors: G. van Aswegen, R.J. Durrheim, W.D. Ortlepp), South African Institute of Mining and Metallurgy, 2001. pp. 69-73.

Mendecki, A.J., and van Aswegen, G. (2001) Seismic monitoring in mines: selected terms and definitions. Rockburst and Seismicity in Mines, RaSim5, (Editors: G. van Aswegen, R.J. Durrheim, W.D. Ortlepp), South African Institute of Mining and Metallurgy, 2001. pp. 563-569.

Mendecki, A.J., Lynch, R.A., and Malovichko, D.A. (2007) Routine Seismic Monitoring in Mines. VNIMI Seminar on Seismic Monitoring in Mines, September 14. 2007.

Mikula, P., Heal, D., and Hudyma, M. (2008) Generic seismic risk management plan for underground hardrock mines. Australian Centre for Geomechanics, Nedlands, WA.

Nuttli, O. W. (1973) The Mississippi Valley earthquakes of 1811 and 1812: Intensities, ground motion, and magnitudes. Bulletin Seismological Society of America, 63, pp. 227-248.

Qin, J., and Qian, X. (2006) On temporal and spatial distribution of seismic apparent stresses in Yunnan Area. Earthquake Administration of Yunnan Province, Kumming, China, ACTA Seismologica Sinica, Vol. 19, No.3, May 2006, pp. 233-242.

Ortlepp, W.D. (1997) Rock fracture and rockbursts, an illustrative study. The South African Institute of Mining and Metallurgy, Monograph Series M9, Johannesburg, 1997.

Ortlepp, W.D., Murphy, S., and van Aswegen G. (2007) The mechanism of a rockburst – an informative study. Challenges in Deep and High Stress Mining, Australian Centre for Geomechanics, Perth, pp. 461-467.

Richter, C.F. (1935) An instrumental earthquake magnitude scale. Bulletin of the Seismological Society of America, Vol. 25, pp. 1-32.

Senatorski, P. (2007) Apparent stress scaling and statistical trends. Physics of the Earth and Planetary Processes, Sciencedirect.com, Retrieved February 22, 2014, pp. 230-244.

Spottiswoode, S.M., Linzer, L.M., and Majiet, S. (2008) Energy and stiffness of mine models and seismicity. SHIRMS Volume 1, Australian Centre for Geomechanics, Perth, 19 September, 2008, pp. 693-707.

Starfield, A., and Fairhurst, C. (1968) How high-speed computers advance the design of practical mine pillar systems. Engineering Mining Journal, Vol. 169, No.5, pp.78-84.

Urbancic, T.I., Feigner, B. and Young, R.P. (1992) Influence of source region properties on scaling relations for M<0 events. Pure and Applied Geophysics, Vol. 139, No. 3/4, pp.721-739.

Wang, G., Kaiser, P.K., and Vasak, P. (2009) Modeling of mining-induced seismicity migration. Proceedings of 3rd CANUS Rock Mechanics Symposium, (Editors: M. Diederichs and G. Grasselli), Toronto.

Wyss, M. and Brune, J.N. (1968) Seismic moment, stress and source dimensions for earthquakes in the California-Nevada region. Journal of Geophysical Research, Vol. 73, pp. 4681-4694